Use of Waste/Recycled Material as Insulation in Road Construction

by

Seyedeh Negar Tavafzadeh Haghi

A thesis submitted in partial fulfillment of the requirements for the degree of

Doctor of Philosophy
in
Transportation Engineering

Civil and Environmental Engineering
University of Alberta

ABSTRACT

Pavements in cold regions are prone to frost damages during winter as a result of prolong sever below zero temperature. Frost heave can negatively affect the performance and ride quality of the road. At the end of the frost season, when thawing begins in the sublayers, pore water pressure builds up in the subgrade soil. This reduces the resilient modulus of the subgrade considerably and degrades the structural integrity of the pavement. Reducing the depth of frost penetration into the pavement structure can enable design engineers to decrease the thickness of the base/subbase layers; hence, reduce the use of natural aggregate and advance towards a more economical and sustainable design. Insulating the pavement foundation is one strategy to reduce heat loss from the pavement structure and maintain pavement subgrade temperatures above freezing during the winter months.

While the number of test roads that are designed and constructed for in-situ measurement and evaluation of pavement performance are limited, there is a lack of knowledge on the effect of using new and recycled material on pavement. This research is designed to conduct a state-of-the-art investigation on the effect of using waste/recycled materials for insulation. As part of the research, controlled tests were performed at the full-scale test road of University of Alberta's Integrated Road Research Facility (IRRF), located in Edmonton, Alberta, Canada. The IRRF test road has three monitoring sections with insulation made of bottom ash (100 cm) and two different thicknesses of polystyrene boards (5 cm and 10 cm), and a control section (CS) with no insulation. The sections are fully instrumented across the depths of the pavement.

In this research, the effects of using insulation layers on the thermal regime of the pavement is investigated and the effectiveness of each insulation layer is quantified. The thermal and moisture regime of the pavement structure over time are used to divide a year into freezing, thawing and non-freeze- thaw periods. The thermal and moisture variation in different seasons can affect the loading characteristics of the pavement layers over time. In an attempt to quantify the impact of seasonal changes (fluctuation of different layers modulus) on the overall strength of the pavement, Falling Weight Deflectometer (FWD) tests were carried out on the IRRF test road and the results are compared with the temperature and moisture regime in the pavement.

The time history data collected from field FWD tests is used to identify the characteristic response of different sections. The structural behavior of each section is evaluated and the long term performance of each section is quantified in terms of fatigue cracking occurrence on the pavement using the elasto-plastic and stress-strain theories.

To investigate the cost effectiveness of using insulation materials, the capital construction cost of the insulated roads, along with substituting the subgrade material with high quality granular base course (GBC) material is calculated. Recommendations are provided for optimum thickness of insulation material based on the distance and frost depth of the road from the location of the insulation material sources

An essential part of this research is the creation of a finite element model for a better prediction of temperature changes in the insulated pavement system. The model has been calibrated using field data collected in this research. In order to develop a predictive model, it is necessary to incorporate laboratory test results on material characteristics in different well-controlled environmental conditions. The model is constructed in the Geo-Studio software.

Based on this research, it can be concluded that, bottom ash as a waste material can be used as an insulation layer in road construction. Bottom Ah, can effectively decease the frost penetration, while it provides a favorable load bearing capacity and pavement performance during the critical thaw weakening season.

PREFACE

This dissertation is the original work carried out by the author and presented in a paper format. In all the papers, I am the principal investigator and responsible for the experimental field study, laboratory testing, data analysis, and manuscript writing. Chapter 3 has been published in "N. Tavafzadeh, S. Nassiri, M.H. Shafie and A. Bayat, 2014. Using Field Data to Evaluate Bottom Ash as Pavement Insulation Layer. Transportation Research Record: Journal of the Transportation Research Board 2433: 39-47." Chapter 4 has been published in "N. Tavafzadeh, L. Hashemian and A. Bayat, 2018. The Effect of Insulation Layers on Pavement Strength during Non-Freeze-Thaw Season. International Journal of Pavement Research and Technology. 19.6 (2018): 543-552." Chapter 5 has been published as "N. Tavafzadeh, L.Hashemian and A.Bayat, The Effect of Seasonal Variation on Load Bearing Capacity of Pavements Comprised of Insulation Layers. 2016. Transportation Research Record: Journal of the Transportation Research Board 2579 (2016): 87-95." Chapter 6 is accepted for publication in "N. Tavafzadeh, L. Hashemian and A. Bayat. 2018, Seasonal Response and Damage Evaluation of Pavements Comprised of Insulation Layers. International Journal of Pavement Research and Technology." Chapter 7 is accepted for publication in "N. Tavafzadeh, M. Ahmadian N. M., L. Hashemian and A. Bayat. 2019, ASCE's Journal of Construction Engineering and Management."

DEDICATION

To

The joy of my life, Alborz

To

My great supporters: baba, maman, Nasim & Ali

Table of Contents

LIST OF TABLES

LIST OF FIGURES

1. INTRODUCTION

The acceptable design of a pavement system in a layered format depends on a couple of complex tasks which normally should be performed iteratively. Two main parts of these iterative tasks are applying a computational model to incorporate the external environmental effects over the design life of the pavement system and, secondly, quantifying the effect of these changes on the performance of each pavement layer (Zapata and Houston, 2008). Environmental conditions such as precipitation, variation in ambient temperature, and depth to the water level cause seasonal variation in the moisture content of the unbound layers, which leads to fluctuation in resilient modulus of different layers of the pavement (Models, 2000). Fluctuation in moisture content of unbound material and as a result, changes in effective stress (Krahn and Fredlund, 1972), has a significant effect on the resilient modulus, stability and permanent deformation (Carlos et al., 2011). Damage due to freezing occurs when frost penetrates the subgrade soil, increases matric suction in the freezing zone. Then, water moves toward the freezing front and ice lenses form. Ice lenses in fine soils continuously expand by attracting moisture from the underlying shallow water table, resulting in frost heave at the pavement surface (Dore and Zubeck, 2009). Frost heave can negatively affect the performance and ride quality of the road. When thawing occurs in the following spring, ice lenses melt, causing an increase in water content of subgrade soil, which cannot be discharges out of the pavement system rapidly. Consequently, the strength of the subgrade soil decreases, leading to structural damage, differential settlements and damage to the pavement structure when exposed to heavy traffic loads (Dore and Zubeck, 2009). These issues become critical for roads in cold regions where increased freeze-thaw cycles are expected in the future as a result of climate change. Frost heave and associated thaw-weakening in subgrade soils and unbound pavement materials are complex engineering problems that have been studied for several years (Qi et al., 2008).

One strategy for minimizing seasonal effects on subgrade is using insulation layers to protect frost-susceptible subgrade from being influenced by frost. An insulation layer controls the heat transfer between the ambient air and the pavement layers and delays thawing and/or freezing (Yang et al., 2005). The insulation layers minimize the seasonal fluctuation in resilient modulus of subgrade by reducing the frost penetration. They also decrease the risk of thaw weakening

during early spring. If the insulation layers provide an adequate load bearing capacity for the pavement and do not create and decrease the risk of moisture accumulation in the system, using them will result in reducing the depth of frost penetration into the pavement structure. Limiting the frost depth in pavements enables design engineers to moderate the base/subbase layers' thicknesses. Decreasing the thickness of structural layers, which are comprise of high quality crushed aggregate, leads to limiting the depletion of natural aggregate resources and results in more economical and sustainable design strategies. The minimum required thickness of insulation material is controlled by the thermal properties of the all pavements layers and the climate (Dore and Zubeck, 2009). In an attempt for construction of a more sustainable and environmental friendly road, waste/recycle material has been introduced to be used as insulation layer in cold region.

Since the 1990s, several materials were introduced and evaluated as insulation layers, including sawdust, tire chips, and plastic (Dore et al 1995). Polystyrene boards are one of the most well-known insulation materials that have had a long history of application since 1965 (Myhre 1994). Some recycled materials have recently been introduced as thermal resistive layers. These materials can be a sustainable and cost-effective option while still providing the same benefits as conventional insulation layers.

The main objective of this dissertation is to investigate effect of using insulation material on thermal and mechanical performance of the pavement. Chapters of this research is devided as follow:

- Investigation thermal performance of insulation layers

The first step of the research was to investigate the thermal performance of the insulation layers using the field data. At chapter 3, the temperature within depth of a test road is monitored to explore the effect of using insulation material in temperature distribution and frost depth of insulated pavement and to compare those values with the conventional pavements.

- Evaluating effect of using insulation layers on seasonal variation in structural performance of pavement

This section of the study is focused on improving our understanding of environmental interaction with pavement systems to better predict the changes in pavement performance over time. Effect

of using insulation layer on overall structural capacity of the pavement, also its influence on the seasonal variation of the subgrade modulus were investigated in chapter 4 and 5. The goal is achieved via using FWD data and investigating the moisture and temperature data collected from the test road.

- ❖ Investigate the long-term performance of using insulation material in terms of risk of fatigue cracking occurrence on the pavement

At this stage of research FWD time history data was used to evaluate and compare effect of using insulation layers on viscoelastic behavior along with estimation of number of load repetition could be applied on the insulated pavements until the fatigue cracking occurs. This objective is followed on chapter 6, where finally the fatigue performance of insulated pavement is compared to the conventional sections.

- ❖ Optimizing the insulation layer thickness required for improving the environmental and structural performance of the pavement

Thickness of insulation layers should be carefully selected since, although increasing the thickness provides more thermal advantages, it negatively affects the load bearing capacity and increases the risk of differential icing. The design engineers should be able to evaluate and quantify the effect of insulation layers on the performance of the road. In this way, optimizing the thickness of insulation layers to maximize their benefits and minimize the disadvantages is vital. This goal is fulfilled in Chapter 7 via investigated the cost effectiveness of using insulation layer by optimizing the thickness based on thermal and structural performance

- ❖ Perform simulations of moisture and temperature variations for the different sections of IRRF test road with the EICM and Geo-Studio modeling software (TEMP/W and VADOSE/W moduli).

Providing a predictive model to accurately simulate the temperature and moisture distribution within depth of a pavement in case of using insulation layer and validating the result of EICM, as commonly used software, is one of the important parts of this research.

1.1. REFERENCE

ARA, Inc., (2004). ERES Consultant Division. "*Guide for Mechanistic–Empirical Design of New*

and Rehabilitated Pavement Structures". Final report, NCHRP Project 1-37A. Transportation Research Board of the National Academies, Washington, D.C. http://www.trb.org/mepdg/guide.htm.

Cary, C.and Zapata C.E.. (2011), "*Resilient Modulus for Unsaturated Unbound Materials*", Road Materials and Pavement Design, (12.3), 615-638

Doré, G., and Zubeck, H. K. (2009). "*Cold Regions Pavement Engineering"*. 1st ed. New York: McGraw-Hill Professional.

Dore, G., Konrad, J. M., Roy, M., and Rioux, N. (1995). "*Use of alternative materials in pavement frost protection: Material characteristics and performance modeling*". *Transportation research record*, (1481), 63-74.

Krahn, J., and Fredlund D.(1972), "*On Total, Matric and Osmotic Suction*", The Emergence of Unsaturated Soil Mechanics, 35.

Myhre, O. (1994). "*Bearing Capacity and Performance of Pavement Structures Insulated with Polystyrene Boads*." In 4th International Conference, Bearing Capacity of Roads and AirfieldsFHWA, U of Minnesota, Army Corps of Engineers, NRC Canada, FAA (Vol. 2).

Yang, S. R., Huang, W. H., & Tai, Y. T (2005), "*Variation of Resilient Modulus with Soil Suction for Compacted Subgrade Soils*". Transportation Research Record: Journal of the Transportation Research Board, (1913), 99-106.

Qi, Jilin, Wei Ma, and Chunxia Song (2008), "*Influence of Freeze–Thaw on Engineering Properties of a Silty Soil*", Cold Regions Science and Technology, 53(3), 397-404.

Zapata, Ce, and Wn Houston. (2008). "*Calibration and Validation of the Enhanced Integrated Climatic Model for Pavement Design*", Vol. 602). Transportation Research Board.

2. BACKGROUND

The concept of using insulation material in the road system is suggested by (Oosterbaan and Leonards, 1965) and the first full-scale field test road using insulation material was built in Iowa, Michigan, and Minnesota. Then, for the first time, frost penetration depths beneath small concrete slabs, which included an insulating layer of cellular glass, were measured at a test road in Winnipeg (Young, 1965). The next generation of insulation layers were plastic foam boards, which were verified to be effective in both decreasing the frost depth and extenuating the induced heave (Dore and Zubeck, 2009). During one year data monitoring, elevation measurements conducted at Wolf Creek Pass in Colorado indicated that a 5-cm Extruded polystyrene layer section experienced 14 cm less frost heave compared to the previous winter when no insulation layer was used (Eaton et al., 1994). In 1972, a roadway near Chitina, Alaska was built with 5 cm and 10 cm Extruded polystyrene layers to prevent settlement (Esch, 1972). This road was monitored for approximately three years, and the results indicated that both insulated sections were effective in preventing frost penetration. The settlement in the adjacent conventional Control Section was eight times greater than the 5 cm Extruded polystyrene section and 11 times greater than the 10 cm Extruded polystyrene section (Esch, 1972). Insulating a test road section in Alaska showed that 5-cm and 10-cm thick polystyrene insulation layers could noticeably reduce the thaw depth from 61 cm to 20 and 10 cm, respectively. Additionally, settlement data collected during the Alaskan study from July 1971 through September 1972 presented up to 9 cm less settlement in the insulated sections when compared to the normal sections (Esch, 1972). Gandahl investigated the frost resistance performance of the polystyrene boards in insulated sections of a road and showed that the water content of the underlying layers as well as the thickness and thermal property of the polystyrene considerably influence the pavement frost related damage protection. Longitudinal frost heave measurements collected from a test road in north Sweden indicated less heave in the insulated sections compared to the non-insulated sections (Gadahl, 1982). Results from a recent case study performed in Edmonton, Alberta showed the impact of a 5-cm thick Extruded polystyrene Highload 40 extruded polystyrene insulation board in reducing frost penetration into the subgrade by 40 percent compared to the non-insulated section. Field measurements of the frost line's

advancement over time agreed with geothermal modeling predictions (Tatarniuk and Lewycky, 2011).

Several researchers have evaluated and compared the performance of different recycled thermal resistant materials as insulation layers. Bottom ash, which is a byproduct of coal combustion when burnt in the boiler furnace of electric power plants, has recently been introduced as an insulation material in pavement applications. Bottom ash is mainly composed of silica, alumina, and iron and is utilized in highway construction, primarily in cold-mixed asphalt, embankments, and base courses. In 2012, approximately 52 percent of Alberta's power was generated via burning coal. In addition to this, approximately 650,000 m^3 of bottom ash and fly ash are produced annually through the province's power generation process (Alberta Recycling, 2013). Alberta's rate of ash production is high enough to raise concerns that insufficient disposal space will be available in ash lagoons by 2015. The use of bottom ash in road embankments to mitigate frost damage is a new concept (Alberta Recycling, 2013). Few studies have investigated the ability of bottom ash mixed with the subgrade and base materials in limiting frost depth. A study conducted in the City of Helsinki, Finland over the course of three winters revealed that frost depth in bottom ash sections was 40 to 60 percent of that in gravel sections. This study showed that carefully compacted ash is not susceptible to frost due to its low permeability and hardening (Havulianen, 1987). Huang (1990) showed that mechanically- and chemically-stabilized bottom ash can be considered a high-quality base material for highway applications. Experimental results concluded that most bottom ashes met several performance criteria, such as physical appearance, gradation, and soundness, which make them suitable for pavement construction (Huang 1990). The application of bottom ash on top of saturated silt could effectively mitigate frost heave and transverse cracking in western Canada. In a study conducted by Nixon and Lewycky (2011) in Edmonton, Alberta, pavement sections comprising a 500-mm gravel base course and a 1100-mm bottom ash insulation layer showed a maximum frost depth of 1.5 m, with no frost reaching the underlying silt layer, while it was predicted that the frost would reach up to 2.4 m below the surface in the conventional section (Nixon and Lewycky, 2011).

While using the insulation layers in pavement has a long history of application, incorporating their effects in pavement design is still unexplored. Over time, many different methods were developed to integrate the effect of environmental factors on pavement. Recently, the pavement design

methods have evolved from AASHTO 1993 design guide, which is a pure empirical approach, to advanced mechanistic design procedures, Mechanistic-Empirical Design Guide (MEPDG), which correlate the pavement structural responses from traffic loads under different environmental conditions to pavement distresses. Therefore, diurnal and seasonal fluctuations in the moisture and temperature profiles in the pavement structure brought by changes in ambient temperature, ground water table, precipitation/infiltration, freeze-thaw cycles, and other external factors are modelled in a very comprehensive manner by a climatic model called the Enhanced Integrated Climatic Model (EICM) (Zapata et al., 2007). The EICM is a one-dimensional coupled heat and moisture flow program that simulates changes in the behavior and characteristics of pavement and subgrade materials in conjunction with climate condition over several years of operation (MEPDG Design Guide, 2004). It can generate patterns of rainfall, solar radiation, cloud cover, wind speed, and air temperature to simulate the upper boundary conditions of a pavement-soil system. The program calculates the temperature, suction and pore pressure without loading effects, moisture content, and resilient modulus for each node in the profile for the entire analysis period, as well as frost, infiltration and drainage behavior (Birgisson et al., 2000).

The direct measurement of the moisture and temperature profiles in pavement via pavement instrumentation can be very beneficial to the development and verification of the EICM in the case of using different insulation materials and under different environmental conditions. However, it should be noted that there is no model defined until now to properly account for the existance of an insulation layer. The comparison of the field data and EICM results indicates that the EICM provides acceptable predictions of temperature profiles in pavement systems [(Ahmed et al. 2005) and (Quintero 2007). However, the studies performed in Ohio and New Jersey revealed that the EICM is not able to properly simulate the fluctuations in water content within depths of the pavement [(Ahmed et al. 2005) and (Liang et al. 2006)]. The need for a trustworthy model for calculating the moisture and temperature change in the pavement is particularly critical, when the freeze/thaw cycle moisture level fluctuation can lead to sever structural performance drop, especially during spring.

2.1. REFERENCE

Ahmed, Z., Marukic, I., Zaghloul, S., & Vitillo, N. (2005). Validation of enhanced integrated climatic model predictions with New Jersey seasonal monitoring data. *Transportation*

Research Record: Journal of the Transportation Research Board, (1913), 148-161.

"Alberta Recycling." http://www.albertarecycling.ca/RecyclingMain.aspx?id=84 Accessed Jan. 1, 2013.

ARA, Inc., (2004). ERES Consultant Division. Guide for Mechanistic–Empirical Design of New and Rehabilitated Pavement Structures. *Final report, NCHRP Project 1-37A. Transportation Research Board of the National Academies*, Washington, D.C. http://www.trb.org/mepdg/guide.htm.

Birgisson, B., Ovik, J., & Newcomb, D. (2000). Analytical predictions of seasonal variations in flexible pavements: Minnesota Road Research Project site. *Transportation Research Record: Journal of the Transportation Research Board*, (1730), 81-90.

Cary, C. E., & Zapata, C. E. (2011), Resilient Modulus for Unsaturated Unbound Materials", *Road Materials and Pavement Design,* (12.3), 615-638Dore, G., Konrad, J. M., Roy, M., & Rioux, N. (1995). Use of alternative materials in pavement frost protection: Material characteristics and performance modeling. *Transportation research record*, (1481), 63-74.

Doré, G., and Zubeck, H. K. (2009). Cold Regions Pavement Engineering. 1st ed. *New York: McGraw-Hill Professional*.

Dysli, M., Lunardini, V., & Stenberg, L. (1997). Related effects on frost action: Freezing and solar radiation indices. *Ground freezing*, *97*, 3-23.

Eaton, R. A., Roberts, R. J., & Humphrey, D. N. (1994). Gravel Road Test Sections Insulated with Scrap Tire Chips: Construction and the First Year's Results (No. CRREL-SR-94-21). *Cold Regions Research And Engineering Lab Hanover Nh*.

Esch, D.C. (1972). Control of Permafrost Degradation Beneath a Roadway by Subgrade Insulation *, Alaska Highway Department*. Juneau, Alaska.

Gandahl, R. (1982). The Use of Plastic Foam Insulation in Roads. In *4th Canadian Permafrost Conference, Calgary, Alberta , March 2*, 570–76. Calgary, Alberta, march 1981.

Havukainen, J. (1987). The Utilization of Coal ash in Earth Works. *Edited by A.K.M Rainbow, 245. Nottingham, England,* September 7-11, 1987: Elsevier.

Huang, W. H. (1990). The Use of Bottom Ash in Highway Embankment and Pavement Construction, ProQuest Dissertations and Theses. *Purdue University. Available*: http://login.ezproxy.library.ualberta.ca/login?url=http://search.proquest.com/docview/303864838?accountid=14474

Krahn, J., and Fredlund D. G. (1972), On Total, Matric and Osmotic Suction, *The Emergence of Unsaturated Soil Mechanics*, 35.

Liang, R., Al-Akhras K., and Rabab'ah S. (2006). Field Monitoring of Moisture Variations Under Flexible Pavement. *Transportation Research Record* 1967 (1): 160–72. doi:10.3141/1967-16.

Models, Moisture-summary O F Predictive. (2000). Guide for Mechanistic-Empirical Design Moisture-Summary of Predictive Models," June.

Myhre, O. (1994). Bearing Capacity and Performance of Pavement Structures Insulated with Polystyrene Boards. *In 4th International Conference, Bearing Capacity of Roads and*

AirfieldsFHWA, U of Minnesota, Army Corps of Engineers, NRC Canada, FAA (Vol. 2). Nixon, D., Eng, P., & Lewycky, E. D. (2011). Edmonton Experience with Bottom ash and Other Insulating Materials for Mitigation of Frost Heave Induced Damage. In *Annual Conference of the Transportation Association of Canada , Edmonton, Alberta, September 11-14*. Edmonton, Alberta.Oosterbaan, M. D., and Leonards G. A. (1965). Use of Insulating Layer to Attenuate Frost Action in Highway Pavements. Highway Research Record (101).

Qi, J., Ma, W., & Song, C. (2008), Influence of Freeze–Thaw on Engineering Properties of a Silty Soil, *Cold Regions Science and Technology*, 53(3), 397-404.Quintero, N. (2007). "Validation of the Enhanced Integrated Climatic Model (EICM) for the Ohio SHRP Test Road at U.S. 23." *M.S. Thesis Submitted to the Russ College of Engineering and Technology of Ohio University*,November.

Tatarniuk, C., Lewycky, D. (2011). A Case Study on the Performance of High Load Polystyrene as Roadway Insulation in Edmonton , Alberta , Canada. In *2011 Conference and Exhibition of the Transportation Association of Canada, September 11, Edmonton, Alberta*. Edmonton, Alberta.

Tavafzadeh, N., Nassiri, S., Shafiee, M., & Bayat, A. (2014). Using Field Data to Evaluate Bottom ash as Pavement Insulation Layer. *Transportation Research Record: Journal of the Transportation Research Board*, (2433), 39-47.

Young, F. D. (1965). Experimental foamed plastic base course. *Highway Research Record*, (101).

Yang, Shu-Rong, Wei-Hsing Huang, and Yu-Tsung Tai. (2005), Variation of Resilient Modulus with Soil Suction for Compacted Subgrade Soils. *Transportation Research Record: Journal of the Transportation Research Board,* (1913), 99-106.

Zapata, C. E., Andrei, D., Witczak, M. W., & Houston, W. N. (2007). Incorporation of Environmental Effects in Pavement Design. *Road Materials and Pavement Design* 8 (4): 667–93. doi:10.1080/14680629.2007.9690094.Zapata, Ce, and Houston W.. (2008). Calibration and Validation of the Enhanced Integrated Climatic Model for Pavement Design. (Vol. 602) *Transportation Research Record*

3. INVESTIGATION THERMAL PERFORMANCE OF INSULATION LAYERS

This section has been published as N.Tavafzadeh, S.Nassiri, M.H.Shafie and A.Bayat, "Using Field Data to Evaluate Bottom Ash as Pavement Insulation Layer," Transportation Research Record: Journal of the Transportation Research Board 2433 (2014): 39-47

3.1. ABSTRACT

A common problem in cold regions is the penetration of frost into susceptible subgrade soils. This study investigates the application of bottom ash in comparison to polystyrene extruded polystyrene boards as an insulation layer at a test road in Edmonton, Alberta. The adjacent normal section is used as the Control Section. All sections were instrumented with thermistors and Time Domain Reflectometers (TDR).

Temperature variations in the base and subgrade layers, frost depth, frozen and thawing periods were analyzed for each section based on the field data available from October 2012 to June 2013. R-Values were calculated each layer considering its thickness and thermal properties, and were used for justifying and comparing the temperature trends. R-values were established at 0.13, 0.50, 1.4 and 14.3 m^2.°C/W for the Asphalt Concrete, Gravel Base Course, bottom ash and polystyrene Board, respectively.

The base layer in the polystyrene section experienced higher temperatures in the summer and lower temperatures in the winter in relation to the bottom ash and Control Sections. Based on temperature measurements at depths 1.61 to 3.27 m, the subgrade in the polystyrene section showed the lowest variation in temperature with respect to time and depth, followed by the bottom ash and then the Control Section. This behavior indicates that the insulation layers obstructed the heat transfer between the surface and the lower layers. The use of polystyrene boards and bottom ash as insulation materials decreased the frost depth by at least 40 and 28 percent, respectively compared to the Control Section.

Key word: insulation layer, bottom ash, Polystyrene, frost depth, freezing index

3.2. INTRODUCTION

Pavement in cold regions is prone to frost heave during the winter as a result of severe temperature drops and deep frost in the pavement sublayers. Frost heave can negatively impact the performance and riding quality of the road. At the end of frost season, when thawing begins in the sublayers, pore water pressure builds up in the subgrade soil. This reduces the resilient modulus of the subgrade considerably and degrades the structural adequacy of the pavement. Reducing the depth of frost penetration into the pavement structure can enable design engineers to moderate the base/subbase layers' thicknesses; hence, limit the depletion of natural aggregate resources and advance towards more economical and sustainable design strategies. Insulating the pavement foundation is one strategy to alleviate heat loss from the pavement structure and maintain pavement subgrade temperatures above freezing during the winter months (Doré and Zubeck, 2009).

Several researchers have evaluated and compared the performance of different economical and recycled thermal resistant materials as insulation layers. Bottom ash, one material that can be used as an insulating layer, is a byproduct of coal combustion when burnt in the boiler furnace of electric power plants. Bottom ash is mainly composed of silica, alumina, and iron, and is utilized in highway construction primarily in cold-mixed asphalt, embankments, and base courses. Few studies have investigated the ability of bottom ash in the subgrade and base material in limiting frost depth. A study conducted in the City of Helsinki, Finland over the course of three winters revealed that frost depth in bottom ash sections was 40 to 60 percent of that in gravel sections. This study showed that carefully compacted ash is not susceptible to frost due to its low permeability and hardening (Havukainen, 1987). Huang (1990) showed that mechanically- and chemically-stabilized bottom ash can be considered a high-quality base material for highway applications. Based on experimental results, it was concluded that most bottom ashes met several performance criteria, such as physical appearance, gradation, and soundness, which make them suitable for pavement construction. The application of bottom ash on top of saturated silt could effectively mitigate frost heave and transverse cracking in western Canada. In a study conducted by Nixon and Lewycky (2001) in Edmonton, Alberta pavement sections comprising a 500-mm gravel base course and a 1100-mm bottom ash insulation layer showed a maximum frost depth of 1.5 m, with no frost reaching to the underlying silt layer.

Plastic foam boards have been widely used as heat insulation layers in several countries to extenuate frost penetration into the pavement foundation. Previous studies have shown that using a 5 cm Extruded polystyrene insulation layer can reduce frost heave. Elevation measurements conducted at Wolf Creek Pass in Colorado indicated that Extruded polystyrene sections experienced 14 cm less frost heave compared to the previous winter when no insulation layer was used (Eaton et al., 1994). Insulating a test road section in Alaska showed that 5-cm and 10-cm thick Extruded polystyrene insulation layers could noticeably reduce the thaw depth from 61 cm to 20 and 10 cm, respectively. Additionally, settlement data collected during this study from July 1971 through September 1972 presented up to 9 cm less settlement in the insulated sections when compared to the normal sections (Esch, 1972). Gandahl (1982) investigated the frost resistance capacity of the polystyrene insulated sections and showed that the water content of the underlying layers , as well as the thickness and thermal conductivity of the polystyrene, play a significant role in the frost resistance capacity of the insulation layer. Longitudinal frost heave measurements collected from a test road in north Sweden indicated less heave in the insulated sections compared to the non-insulated sections (Gandahl, 1982). Results from a recent case study performed in Edmonton, Alberta showed the impact of a 5-cm thick Extruded polystyrene Highload 40 extruded polystyrene insulation board in reducing frost penetration into the subgrade by 40 percent compared to the non-insulated section. Field measurements of the frost line's advancement over time agreed with geothermal modeling predictions (Tatarniuk and Lewycky, 2011).

Edmonton is located in freeze-dry climatic conditions, where the average freezing index based on 30 years of historic weather data is 1365°C.days (Environment Canada, 2013). Freezing index is the accumulation of daily average temperate of below 0°C (Steurer, 1989). Frost penetration leading to frost heave and spring weakening is a yearly challenge faced by the local highway agency. As reviewed above, pavement insulation layers have been used to prevent deep frost penetration into the subgrade of a few projects in Alberta. This study investigates the field performance of bottom ash as an insulation layer at the University of Alberta's Integrated Road Research Facility (IRRF)'s test road in Edmonton. Bottom ash is an industry byproduct readily available in Alberta in comparison to the costly polystyrene boards that are commonly used as insulation layers. For this project, both bottom and ash polystyrene boards were used as insulation layers beneath the base course of the test road. The effectiveness of the bottom ash layer in

protecting the subgrade from freezing and thawing was compared to an adjacent, non-insulated Control Section and the polystyrene section. The three test sections were instrumented with thermistors and Time Domain Reflectometers (TDR) at various depths throughout the pavement structures. Temperature records from October 2012 to June 2013 in the three sections were analyzed in this study. Temperature variations in the base and subgrade layers, frost depth, frozen period, and thawing (recovery) period were established for each section in comparison to the Control Section. As a result, the most effective layer in alleviating the effects of freeze and thaw in the subgrade was identified.

3.3. DESCRIPTION OF TEST ROAD

The IRRF's test road facility is a new access to the Edmonton Waste Management Center (EWMC), located on the eastern edge of Edmonton, approximately 15 km from downtown. Construction of the IRRF's test road started in May 2012, with Stage 1 paving completed in August 2012. The test road comprises two lanes, and is approximately 500 m long. Based on the data collected from weigh-in-motion (WIM) systems during the spring of 2016, the road carries about 2,000 vehicles per lane each day. During the monitoring period for this study, the pavement structure for the test road comprised 160 mm of Hot Mix Asphalt (HMA) placed on 450 mm of Granular Base Course (GBC).

In the northern section, the test road includes two successive test sections consisting of different insulation layers placed immediately underneath the GBC. Figure 3-1 shows pictures of the placement of the bottom ash layer and the polystyrene boards.

Figure 3-2 illustrate a schematic plan view of the test sections. To facilitate a smooth transition from the untreated ground to the polystyrene section and to avoid deferential icing, a 20-m long section was constructed from Stationing 130+340 to +360, where a thin (50-mm) layer of polystyrene board was placed under the GBC. The adjacent section comprises a 100-mm layer of polystyrene boards, starting at Stationing 130+340 and ending at 130+320. This section is followed by bottom ash section, which stretches from Stationing 130+320 to +300 and includes a 1000-mm layer of bottom ash. As illustrated in Figure 3-2, the insulation layers extend underneath the shoulders. Another section of the road, approximately 50 m east of the insulated sections, as shown in the figure, was instrumented at Stationing 130+250 to serve as the Control Section.

Figure 3-1: Placement of the (left) Bottom ash and polystyrene boards (right)

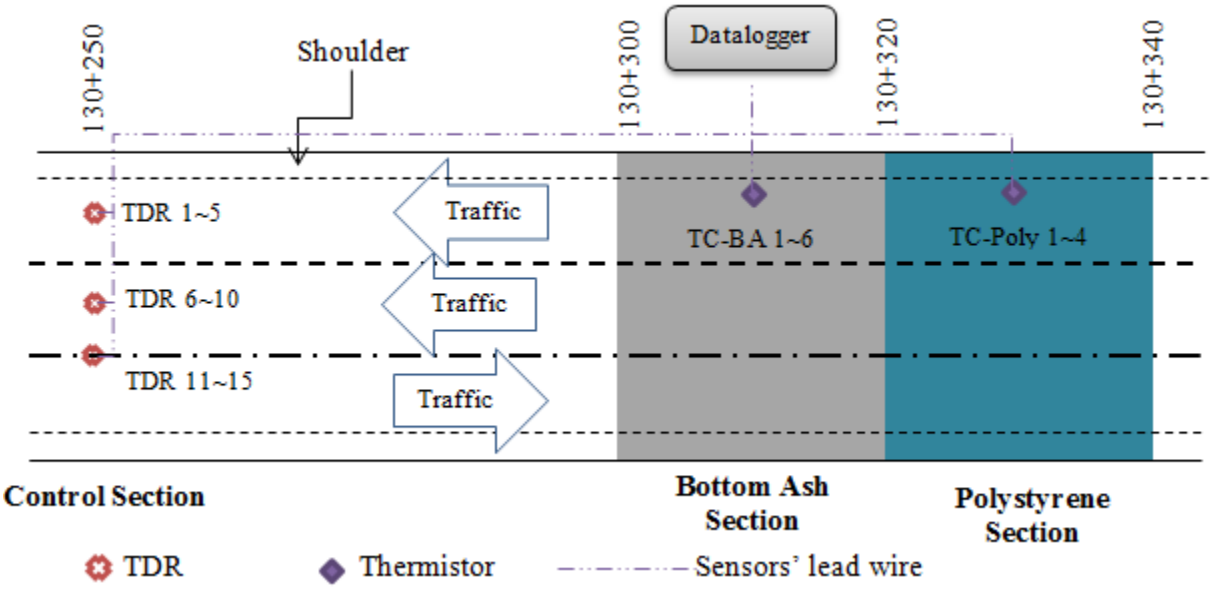

Figure 3-2: Plan view of the test sections

3.4. MATERIALS

During the monitoring period, the pavement structure comprised 160 mm of HMA placed in August 2012. Thermal properties of the pavement materials are provided in Table 3-1, k is thermal conductivity: "Thermal conductivity represents the capacity of a material to transport heat by conduction" (Dore and Zubeck, 2009). Cp is heat capacity: "represents the ability of soils or materials to accumulate heat" (Dore and Zubeck, 2009). R isthermal resistivity (R-value = D/k), where D is the layer thickness The R-value for the 160-mm HMA layer was established as 0.13 m^2.°C/W.

Sieve analysis in accordance with ASTM C 136-06 (2006) revealed that the subgrade soil and the base material were Clayey Sand (SC) and Well-Graded Gravel (GW) based on the Unified Soil Classification System (USCS). Figure 3-3 shows the particle distribution for the subgrade and base materials. The R-value of the 450-mm GBC was calculated as 0.50 m^2.°C/W, based on typical k for this material.

Table 3-1: Typical Thermal Properties of the Materials Used in the Study.

Material	c_p (kJ/kg.°C)	k (W/m.°C)	D (mm)	R-value (m^2.°C/W)	Source
Asphalt concrete	0.92	1.21	160	0.13	Tompson et al. (1988)
GBC	0.71	0.9	450	0.50	
Subgrade soil	0.71	0.6	-	-	
Bottom ash	0.8	0.7	1000	1.43	Klein et al. (2003)
Styrofoam board	1.25	0.007	100	14.29	Dow Construction webpage (2013)

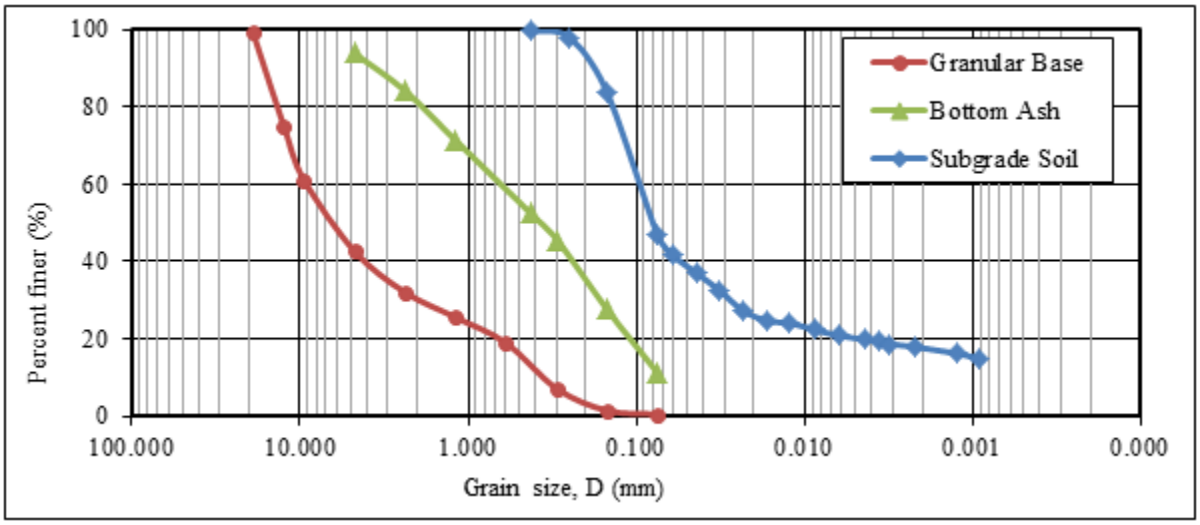

Figure 3-3: Grain size distribution for the bottom ash used in the project.

Bottom ash and polystyrene foam boards were used as insulation materials in the project. Characterizing thermal properties of the different materials in the laboratory is within the future scope of the project. However, for this study, a typical value available in literature for thermal properties of the bottom ash was used. The bottom ash was free of large lumps that could break

down under ordinary compaction equipment. Moreover, the bottom ash did not contain impurities, such as clay particles, and the amount of non-combusted coal particles was less than 5 percent of the material by weight. Also, the natural moisture content of the bottom ash was maintained at less than 35 percent during the compaction process, which was finalized in one day (July 31, 2012). The GBC was placed on the same day and the road was paved on August 1, 2012. The results of sieve analysis on samples of the bottom ash are provided in Figure 3-4. Typical thermal properties for the bottom ash are reported in Table 3-1 and were used to calculate an R-value of 1.43 m^2.°C/W.

Closed cell Styrofoam Highload 100 extruded polystyrene foam boards produced by Dow Chemical Company were used for this study. They have a compressive strength of 690 kPa and a minimum flexural strength of 585 kPa and an R-value of 14.29 m^2.°C/W based on the manufacturer's data sheet.

3.5. INSTRUMENTATION AND DATA COLLECTION

To monitor frost penetration and compare the effectiveness of bottom ash in relation to the polystyrene and Control Sections, all three sections were instrumented with 109AM-L thermistors and CS650 TDRs from Campbell Scientific Canada. The as-built depth and stationing for the instrumentation in each section is presented schematically in Figure 3-4. The spatial location of the instrumentation was provided previously in Figure 3-2. The Control Section consists of a total of 15 TDRs, which were installed in three groups of five: As illustrated in Figure 3-2, two of the TDR groups were installed in the middle of each lane (TDR 1~5 and TDR6~10) and the last group was installed at centerline location at Stationing 130 + 250 (TDR 11~15). Only the temperature data measured by the thermistor in the TDRs was used in this study. Variation in the moisture content in different layers will be the scope of future studies. Thermistors in all of the insulation sections were installed approximately 0.5 m from the inner edge of the shoulder in the southbound lane. The total number of thermistors in the bottom ash and polystyrene sections is six (TC-BA 1~6) and four (TC-Poly 1~4), respectively. As seen in the Figure 3-4, sensors were installed as deep as 2.5, 3.3 and 3.2 m in the Control, bottom ash and polystyrene sections, respectively to capture moisture and temperature change within depth of the pavement. Installing the sensors at those depths required drilling in the exiting ground with an auger (Figure 3-5, left).

All of the sensors were wired to a CR1000 datalogger from Campbell Scientific Canada. The datalogger, located at Stationing 130+310, was programmed to collect the data from all of the sensors at 15-minute intervals (Figure 3-2 and Figure 3-5, right). The datalogger was equipped with a spread spectrum Model RF401 radio used to communicate with an antenna Model L14221 installed on an on-site trailer. Through remote desktop access, the data is retrieved at the University of Alberta from the on-site computer.

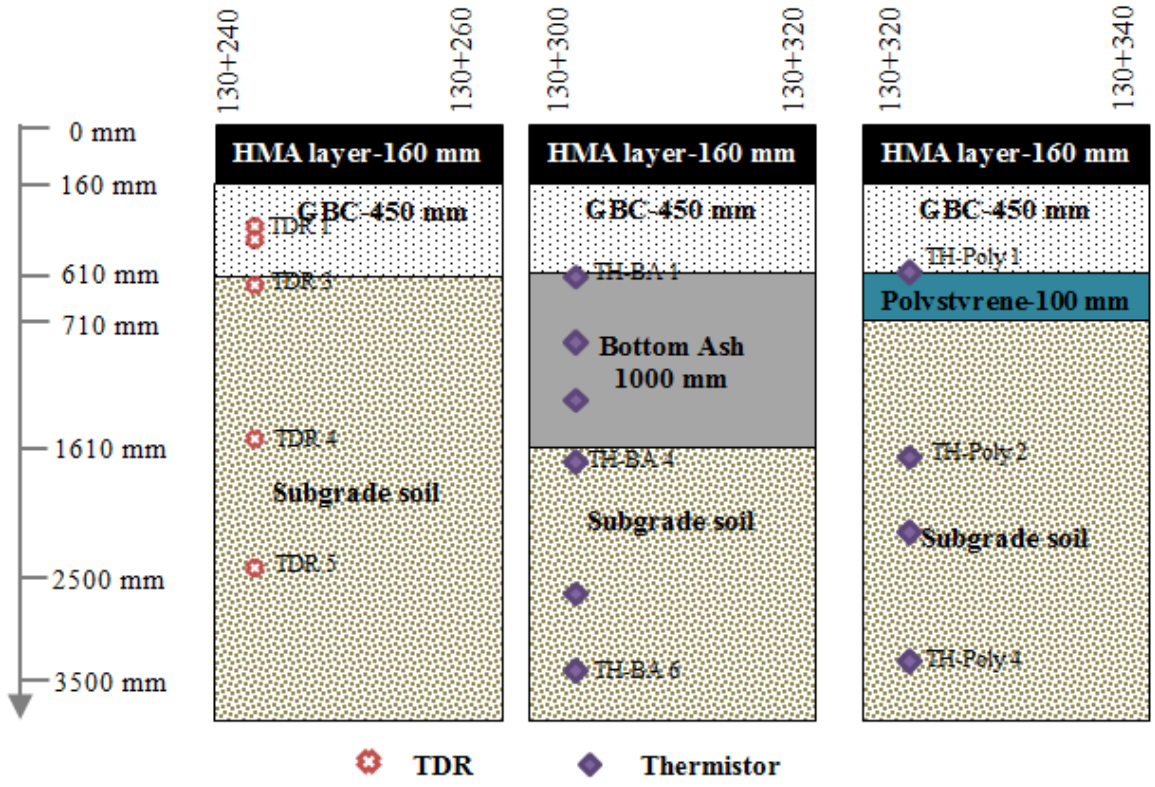

Figure 3-4: As-built depth of thermistors and moisture probes

3.6. ANALYSIS OF DATA

3.6.1. Temperature Change with Time

Climatic data was collected from the EWMC's closest weather station located ~700 m from the test road. Maximum and minimum average daily temperatures were -25.6 ˚C and 23.2 ˚C during the monitoring period (October 2012 to July 2013), and the Freezing Index was established at -1317.5˚C-days.

Figure 3-5: Installing the deep sensors using an auger (left); sensors' lead conveyed to the datalogger box in a trench (right)

Figure 3-6 (a) plots the average daily temperature data measured at the bottom of the base layer for all three sections together with the daily ambient temperature. The as-built depths of the sensors, as seen in Figure 3-4, are 0.65, 0.63 and 0.55 m in the Control, bottom ash, and polystyrene sections, respectively. The discontinuity in the data from November 6, 2012 to December 5, 2012 and from December 20, 2012 to January 9, 2013 was due to technical issues with the data collection system. Figure 3-6 (a) illustrates that the base temperature in all of the sections followed the trend of ambient temperature.

A general trend is noted in Figure 3-6 (a) for temperature variation in the base for all of the sections. Between October and February, the Control Section had the warmest base, while the polystyrene section, with the highest R-value (14.29 m^2.°C/W), had the coldest base, followed by the bottom ash section, with R-value of 1.43 m^2.°C/W. This trend was reversed between April and July, when the polystyrene showed the highest temperature records, followed by the bottom ash and then the Control Section. Further, the base temperature for the polystyrene section was 32˚C on the hottest day (June 30th) of the monitoring period. On January 31st, the base temperature for the polystyrene section was the lowest of all sections at -14˚C. The difference between maximum and minimum temperatures in the base layer of the polystyrene section was 45.7 °C, while this value was 33 and 35°C in the bottom ash and Control Section, respectively.

This phenomenon indicates that the insulation layers blocked the heat exchange between the base and the subgrade layers, when compared to the Control Section. Therefore, when the ambient

temperature was low, the base layer in the insulated sections experienced lower temperatures compared to the Control Section. This is the result of accumulated cold within the layers above the insulation layer. In contrast, when the ambient temperature is high, heat is trapped in the base, and the temperature of the base above the insulation layers will be higher compared to the Control Section (Doré and Zubeck, 2009). On the other hand, compared to the polystyrene boards, the bottom ash layer did not affect the base layer's temperature. This behaviour can be due to the fact that the R-value of the bottom ash layer is 10 times less than the polystyrene layer, also the bottom ash layer stretches one meter below the GBC compared to the polystyrene layer.

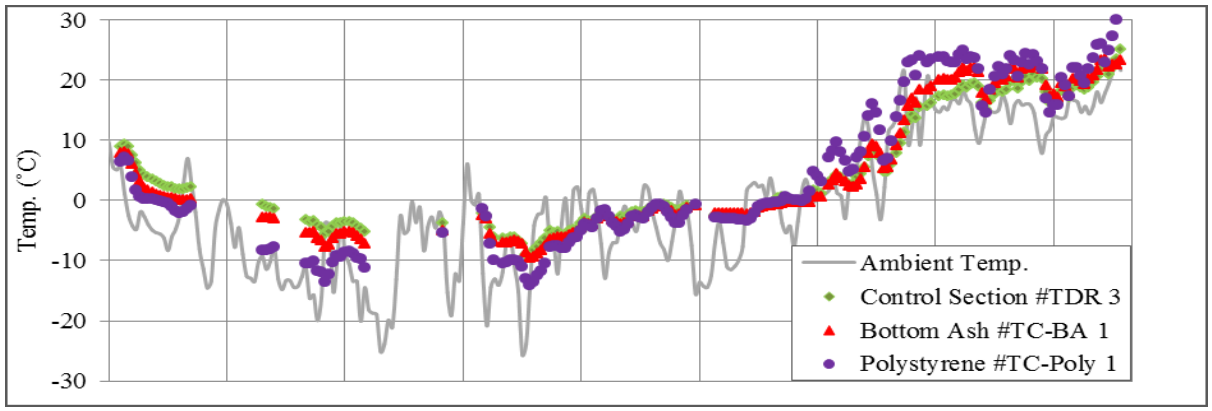

(a)

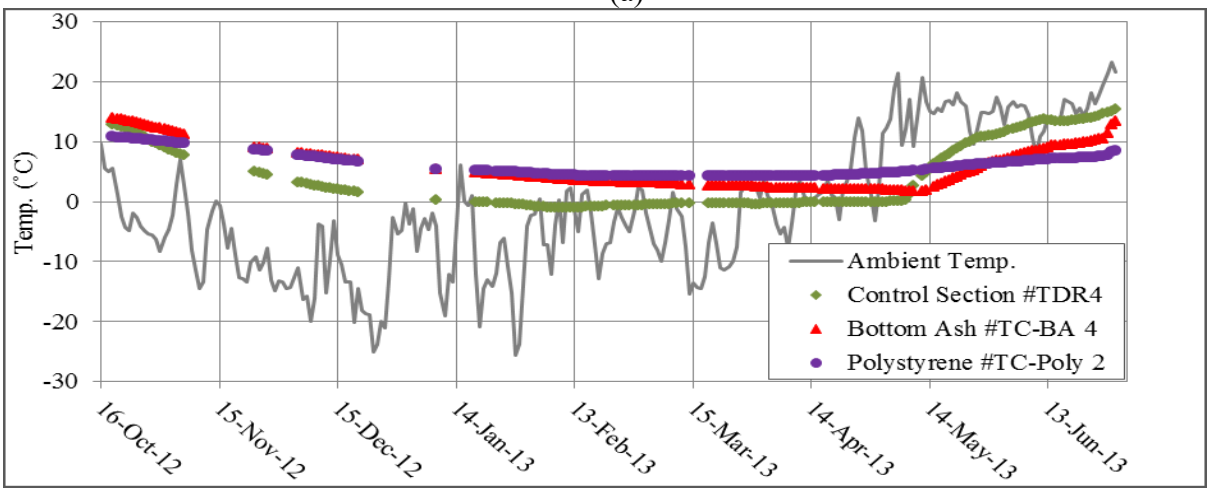

(b)

Figure 3-6: Average daily ambient temperature (a) in the base, (b) in the subgrade

Within the subgrade layer, temperature measurements were available in all sections at a depth of approximately 1.6 m below the asphalt surface. The as-built depths of the sensors are 1.61, 1.71 and 1.76 m in the Control, bottom ash, and polystyrene sections, respectively. According to Figure

3-6 (b), at this depth, subgrade temperature in the bottom ash and polystyrene sections did not drop below zero during the monitoring period; whereas, the subgrade of the Control Section froze at this depth in January and remained frozen until the beginning of May.

3.6.2. Temperature Distribution Across the Pavement Depth

Figure 3-7 presents the temperature data at monthly intervals in all three sections from mid-October 2012 to the end of June 2013. As discussed previously, changes in the temperature of the base layer can be an indicator of how effectively the insulation layer has blocked heat transfer between the base and subgrade layers. Minimum temperature was experienced in the base on January 31th and was recorded at -9.5, -9.5 and -14.0˚C in the Control, bottom ash, and polystyrene sections, respectively. Maximum temperature records in the base for the Control, bottom ash, and polystyrene sections were 25.2, 23.5 and 31.7 ˚C on June 30th, respectively. Based on temperature difference between the lowest and highest records, the polystyrene (45.8˚C) performed more effectively than the bottom ash (33.0˚C) as an insulation layer. The Control Section's temperature difference was 34.6˚C, which is slightly more than that of the bottom ash.

The deepest sensors were installed at 2.5, 3.3 and 3.2 m in the Control, bottom ash, and polystyrene sections. Comparing the changes in the temperature measured by the deepest sensor for all sections indicates that the Control Section showed maximum temperature variation from October 2012 to July 2013. This temperature variation is 12˚C for the Control Section; while it is 10 and 4˚C for bottom ash and polystyrene sections, respectively. Figure 3-7 (a) indicates that the temperature is distributed linearly across the depth in the Control Section in all months, except for the thawing months of Aril and May. However, for the insulated sections, temperature distribution is interrupted at the insulation layer depth.

To compare the variation in temperature of the subgrade for all the three sections, the temperature gradient was calculated by dividing the temperature difference between the shallowest and deepest sensors in the subgrade of each section by their distance. In the Control Section, the temperature gradient in the subgrade varied from -5.1˚C/m on June 30st to 3.9˚C/m on December 15th, while this range was -3.7 to 1.6 and -1.2 to 1.2˚C/m in the bottom ash and polystyrene sections, respectively. When compared to the Control Section, these lower temperature gradients illustrate

how effectively the insulation layers prevented heat transfer between layers located above and underneath the insulation layer.

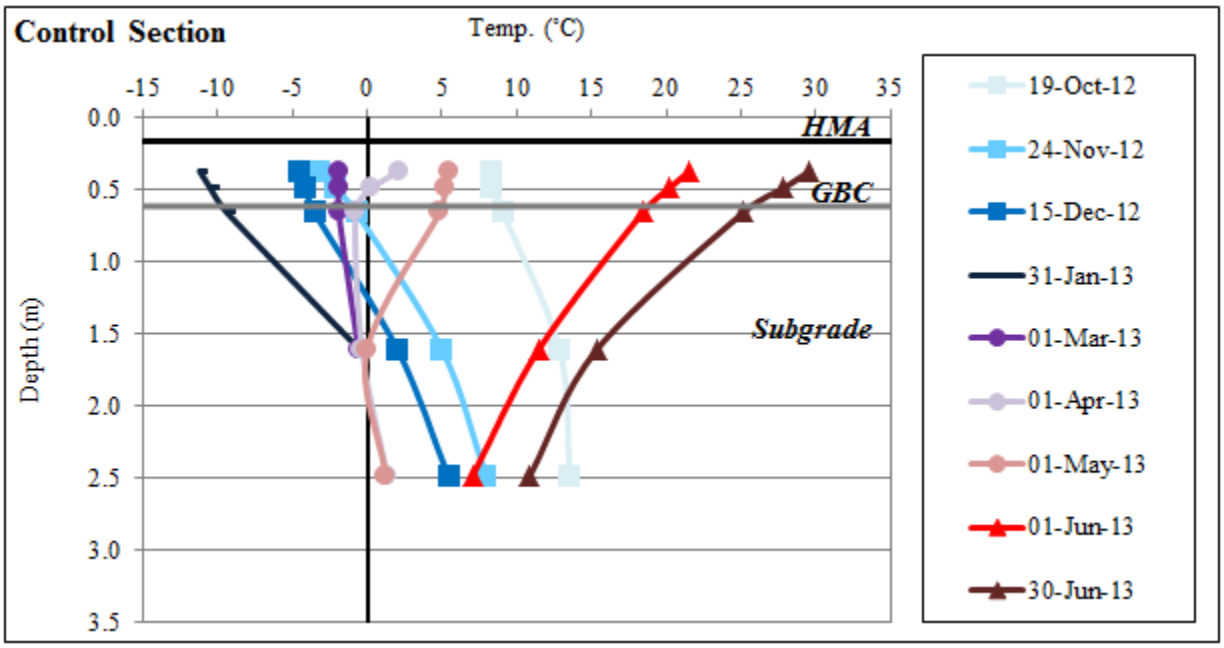

(a)

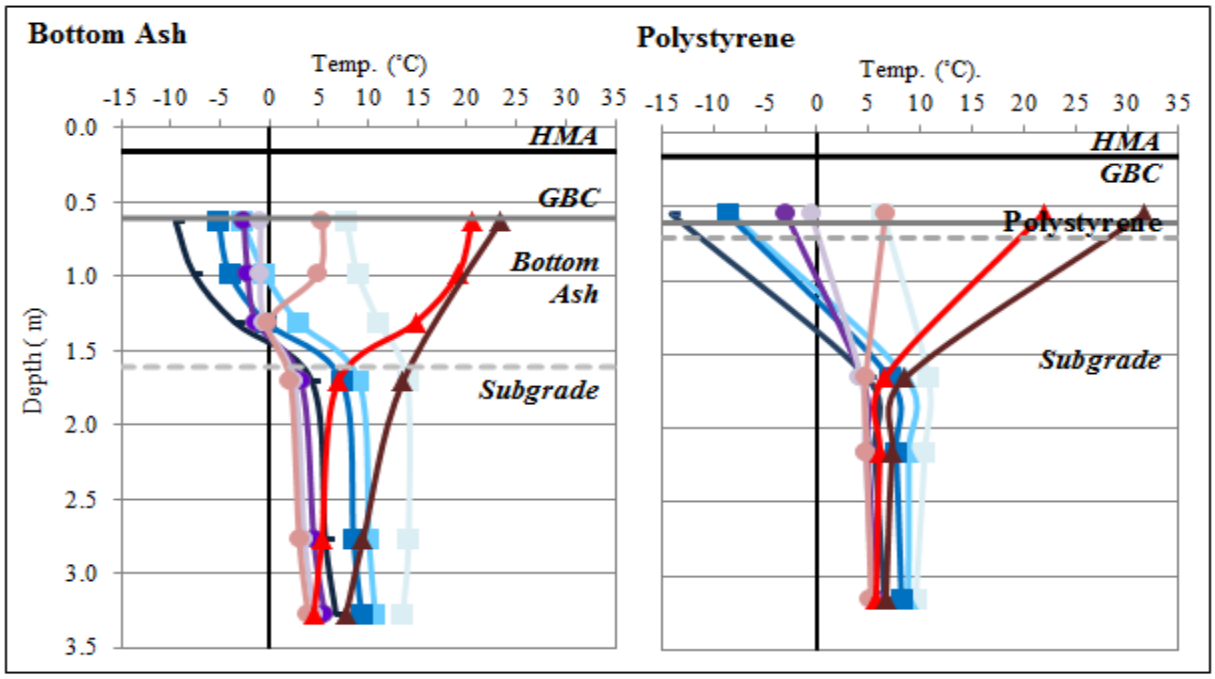

(b) (c)

Figure 3-7: Temperature distribution across the depth at monthly intervals for (a) Control Section, (b) bottom ash and (c) Polystyrene sections from mid-October 2012 to end of June 2013

The Temperature-change rate over time for all three sensor depths in the subgrade of all three sections was determined by taking an average of the temperature difference between two successive days provided in Figure 3-7 divided by their time difference. The average temperature-change rate at the deepest depths in the subgrade for each section is used herein for comparison. The annual average temperature-change rate at the deepest locations was 0.11, 0.07 and 0.03˚C/day for the Control, bottom ash, and polystyrene sections, respectively. This rate reveals how quickly the heat transferred from the surface to the subgrade. Therefore, the polystyrene layer's considerably lower rate indicates that it performed better as an insulation layer.

3.6.3. Frost Depth

Figure 3-8 demonstrates a comparative frost depth chart for all sections. The figure shows that the maximum frost depth for the Control Section was approximately 2.0 m. The frost remained in the subgrade of this section from mid-November to mid-April (Figure 3-7).

The subgrade layer in the bottom ash section did not freeze at any depth, and the frost depth was limited to 1.7 m, which is within the bottom ash layer. Frost at this depth started in mid-December and had fully recovered by mid-April. Based on the data from the thermistor directly underneath the polystyrene (1.7 m below the surface), the subgrade temperature did not drop below zero at any depth during the monitoring period.

Due to lack of thermistors between depths 0.6 and 1.7 m under the polystyrene layer (the two thermistors were accidentally cut by the electric contractor during the final stages of construction), the absolute frost depth for this section cannot be established. Therefore, the minimum possible frost depth can be directly underneath the polystyrene layer as it is expected that the temperature after this layer in the subgrade remains nearly constant. Considering a linear relation between the temperature measured by the two thermistors at depths 0.6 and 1.7 m provides the maximum possible frost depth of 1.2 m (Figure 3-8).

The frost depth criteria indicates that the polystyrene layer performed more effectively than the bottom ash layer, which decreased the frost depth by 0.5 m in comparison to the Control Section.

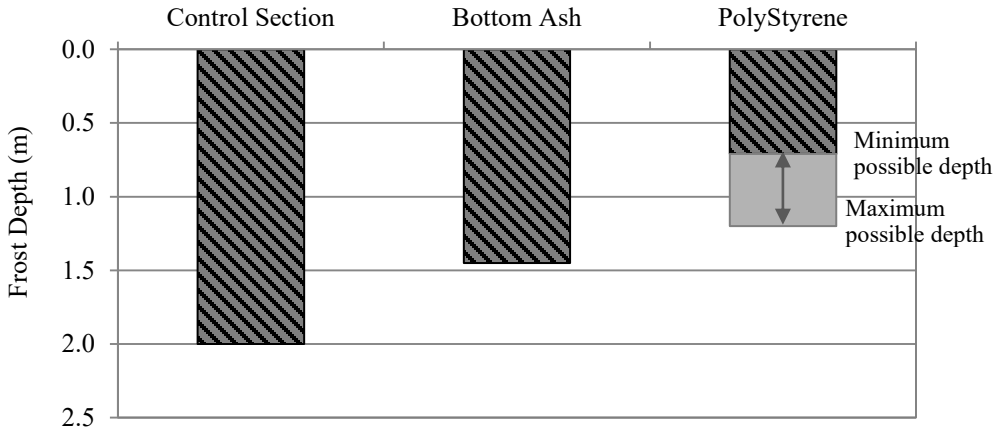

Figure 3-8: Maximum frost depth in the three test sections.

3.7. CONCLUSIONS

The temperature data from instrumentation installed at different depths of three successive test sections and the climatic data collected from the EWMC weather station were applied to investigate the performance of bottom ash and polystyrene boards as insulation layers. Both layers were easily placed and compacted (in the case of the bottom ash layer) prior to placement and compaction of the granular base layer. Typical thermal properties for the bottom ash were obtained from literature to explain the trends in the recorded temperature. The following statements can be concluded from the study:

1- The effect of the insulation layer on temperature distribution within the base layer was evident only in the polystyrene section, whose R-value is 10 times higher than that of the bottom ash (14.3 versus 1.4 m^2.°C/W). The temperature difference in the base layer of the polystyrene section on the hottest and coldest days was approximately 46˚C, while it was 33 and 35˚C in the bottom ash and Control Section, implying that the polystyrene layer blocked the heat exchange between the base and the underlying layers more effectively than the bottom ash.

2- The polystyrene and bottom ash sections showed considerably lower average temperature-change rates in the subgrade, 0.03 and 0.07˚C/day, respectively throughout the monitoring period compared to the Control Section, which showed a variation of 0.11˚C/day. This behavior indicates that the bottom ash and polystyrene effectively blocked the heat transfer between the environment and the pavement under layers.

3- Higher R-value of the polystyrene boards (14.3 versus 1.4 m^2.°C/W for the bottom ash) resulted in this section outperforming the bottom ash layer as insulation by decreasing the frost depth by at least 40 percent in comparison to the Control Section. The bottom ash displayed a 28-percent reduction in frost depth. The subgrade temperature in the bottom ash and polystyrene sections never dropped below zero; however, frost penetrated 1.4 m in the subgrade of the Control Section, which remained frozen for four months.

Based on the above observations one can conclude that bottom ash was effective in reducing frost penetration into the subgrade. Over the course of the monitoring period, both test sections performed well and there has been no evidence of any distresses at the pavement surface to date. Future studies will focus on investigating the sufficiency of the structural capacity of the pavement section containing the bottom ash layer and also characterizing thermal properties of this material.

3.8. REFERENCES

ASTM Standard C136-06 (2006). Standard Test Method for Sieve Analysis of Fine and Coarse Aggregates. ASTM International, West Conshohocken, PA.

Doré, G., and Zubeck, H. K. (2009). *Cold Regions Pavement Engineering*. 1st ed. New York: McGraw-Hill Professional.

Dow Building Solutions. http://dow-styrofoam.custhelp.com/app/answers/detail/a_id/721. Accessed Jul. 1, 2013.

Eaton, R. A., Roberts, R. J., & Humphrey, D. N. (1994) Gravel Road Test Sections Insulated with Scrap Tire Chips: Construction and First Year's Results. (No. CRREL-SR-94-21), *Cold Regions Research and Engineering Lab Hanover NH*.Environment Canada. http://weather.gc.ca/canada_e.html, Accessed Jan. 1, 2013.

Esch, D. C. (1972) *Control of Permafrost Degradation beneath a Roadway by Subgrade Insulation*. Alaska Department of Transportation and Public Facilities, Juneau, Alaska.

Gandahl, R. U. N. E. (1982). The use of plastic foam insulation in roads. In *Proceedings of the 4th Canadian Permafrost Conference,* Calgary, Alberta, 570-576.

Havukainen, J. (1987) The Utilization of Coal ash in Earth Works. Reclamation, Treatment and Utilization of Coal Mining Wastes, p.245.

Huang, W. (1990) The Use of bottom ash in Highway Embankment and Pavement Construction, PhD, Purdue University.

Klein, R., N. Nestle, R. Niessner, and T. Baumann. (2003) Numerical Modeling of the Generation and Transport of Heat in a Bottom Ash Monofill. Journal of Hazardous Materials, Vol. 100, No. 1–3, 147–162.

Nixon, D., Eng, P., & Lewycky, E. D. (2011). Edmonton Experience with Bottom ash and Other Insulating Materials for Mitigation of Frost Heave Induced Damage. In *Annual Conference of the Transportation Association of Canada , Edmonton, Alberta, September 11-14*. Edmonton, Alberta.Steurer, P. M. (1989) Methods used to create an estimate of the 100-year return period of the air-freezing index. Frost-protected shallow foundation development program—Phase II final report: Appendix A. Rep. Prepared for the Society of the Plastics Industry, NAHB Research Center, Upper Marlboro, MD, 7 pp.

Tatarniuk, D., and C., Lewycky. (2011) A Case Study on the Performance of High Load Polystyrene as Roadway Insulation in Edmonton, Alberta. Presented at the Conference and Exhibition of the Transportation Association of Canada, Edmonton, Alberta.

Tompson, M.R., Dempsey, B.J., Hill, H., and Vogel, J. (1988) Characterizing Temperature Effects for Pavement Analysis and Design. Transportation Research Record, No. 1121, Journal of the Transportation Board of the National Academy, Washington, D.C., 14–22.

4. EVALUATING EFFECT OF USING INSULATION LAYERS ON SEASONAL STRUCTURAL PERFORMANCE OF PAVEMENT

This section has been published as N.Tavafzadeh, L.Hashemian and A.Bayat, "The Effect of Insulation Layers on Pavement Strength during Non-Freeze-Thaw Season," International Journal of Pavement Research and Technology, 19.6 (2018): 543-552.

4.1. ABSTARCT

This chapter examines the effect of integrating insulation layers, including bottom ash and polystyrene, on pavement strength using Falling Weight Deflectometer testing data conducted on an instrumented test road in Edmonton, Alberta, Canada. For this purpose, effective modulus and structural number of insulated sections were compared to a conventional control section in non-freeze-thaw season. The durations of pavement freezing, recovering and fully recovered (non-freeze-thaw) periods were established by monitoring the moisture variations in different pavement layers. The results indicated that using insulation layers generally reduces pavement strength, and this reduction is more pronounced in the insulated section with thicker polystyrene.

Key words: Insulation Layer, Bottom Ash, Polystyrene, Non-Freeze-Thaw, FWD, Structural Capacity, Effective Modulus, Structural Number

4.2. INTRODUCTION:

Prolonged low temperatures during winter in cold regions can result in the creation of ice lenses in frost-susceptible subgrade soils. Ice lenses in fine soils continuously expand by attracting moisture from the underlying shallow water table, resulting in frost heave at the pavement surface (Dore and Zubeck, 2009). Surface heave alters the road profile and can negatively affect the road's ride quality, especially if the heave is differential and uneven. Additionally, excessive melted water from the ice lenses causes buildup of pore water pressure in the subgrade and subsequently decreases the load bearing capacity of the unbound layers during spring thaw, which weakens the entire pavement structure. As mentioned in the *Mechanistic-Empirical Pavement Design Guide* (MEPDG) (2004), during the freezing period when the moisture in the soil is frozen, the modulus of the subgrade may rise to 13,800 MPa for fine grain material, while during the thaw period, the subgrade becomes considerably weaker than the normal (unfrozen) condition. Weak subgrade

support results in higher deflections that cause accumulation of fatigue in the pavement, which leads to different types of cracks, including alligator cracking. When melted snow or rain seep into the pavement through cracks, modulus of the base and subgrade layer decrease. This causes local deficiency in load bearing capacity of pavement and ultimately leads to the formation of potholes (Dore and Zubeck, 2009). Using insulation layers is one strategy for alleviating the abovementioned problems in cold regions, as they decrease the frost penetration and prevent thaw settlement of the pavement's under-layers during the spring season (Dore and Zubeck, 2009).

Polystyrene has been used as an insulation material since 1967 (Penner 1967). In 1972, a roadway near Chitina, Alaska was built with 5 cm and 10 cm Extruded polystyrene layers to prevent settlement (Esch 1972). This road was monitored for approximately three years, and the results indicated that both insulated sections were effective in preventing frost penetration. The settlement in the adjacent conventional control section was eight times greater than the 5 cm Extruded polystyrene section and 11 times greater than the 10 cm Extruded polystyrene section (Esch 1972). The 2013 study at the University of Alberta's Integrated Road Research Facility (IRRF)'s test road in Edmonton, Alberta, Canada, showed that an insulation layer of polystyrene with 10 cm thickness can reduce the frost depth by at least 40 percent when compared to uninsulated roadway (Tavafzadeh et al. 2014).

Some recycled materials have recently been introduced as thermal-resistive layers. These materials can be a sustainable and cost-effective option while still providing the same benefits as conventional insulation layers. Bottom ash, a waste material produced from the incineration of coal in power plants, has recently been presented as an option for the construction of road embankments. In 2012, approximately 52 percent of Alberta's power was generated via burning coal. In addition to this, as mentioned on the Alberta Utility Commission webpage (2014), approximately 650,000 m^3 of bottom ash and fly ash is produced annually through the province's power generation process (Alberta Recycling, 2013). Alberta's rate of ash production is high enough to raise concerns that sufficient disposal space will not be available in ash lagoons by 2015. The use of bottom ash in road embankments to mitigate frost damage is a new concept. A project in Helsinki, Finland, showed a 40 to 60 percent decrease of frost depth in a roadway constructed with bottom ash insulation sections compared to traditional gravel sections during three years of monitoring (Havukainen 1987). Two different studies conducted in Edmonton, Canada, in 2001

and 2013 illustrated that bottom ash was able to keep the frost from penetrating into the subgrade and the frost depth was limited to the bottom ash layer (Tavafzadeh et al. 2014), (Nixon and Lewycky 2011).

Despite all abovementioned advantages of using insulation layers in reducing the penetration of frost depth into the subgrade, evaluating the effect of insulation layers on the structural capacity of the insulated pavement in comparison to a conventional one during the non-freeze-thaw season, is vital. The thickness of insulation layers should be carefully selected since, although increasing the thickness provides more thermal advantages, it negatively affects the load bearing capacity and increases the risk of differential icing. The design engineers should be able to evaluate and quantify the effect of insulation layers on the performance of the road.

The objective of this study is to compare the strength of the sections containing insulation layers with the conventional section before the freeze season, when subgrade has fully recovered from the previous thaw and the excess water from the melted ice has drained. Two different insulation materials were investigated at a test road constructed at the University of Alberta's IRRF in Edmonton, Alberta. Edmonton, with a freezing index of 1,365°C.days based on 30 years of historic data extracted from the Environment Canada webpage (2014), is considered to have freeze-dry climatic conditions (Environment Canada 2013). Hence, the road in this area may be affected by ground freezing damages. The insulated sections in the IRRF's test road included bottom ash and two different thicknesses of polystyrene board. For the purpose of this project, three different periods of freeze, recovery and non-freeze-thaw season based on moisture data collected from the test road were determined. July, September and October were chosen as the representatives of the non- freeze-thaw period when the subgrade layers of all sections were stable and load bearing capacity was unaffected by possible thaw weakening or frost action. Then, the Falling Weight Deflectometer (FWD) tests were conducted along the IRRF's test road to evaluate and compare the strength of the different sections. The Effective Modulus of Pavement (E_p) and Structural Number (SN) are calculated based on the American Association of State Highway and Transportation Officials (AASHTO) method and evaluated for comparing the structural capacity changes that resulted from using the insulation layer.

4.3. TEST ROAD DESIGN AND CONSTRUCTION

The IRRF's test road facility was constructed to provide access to the Edmonton Waste Management Center (EWMC). Based on the data collected from weigh-in-motion (WIM) systems during the spring of 2016, the road carries about 2,000 vehicles per lane each day. It is worth mention that at the time of this study, the road was not open to traffic yet. The road itself consists of two lanes approximately 500 m in length. Construction of the IRRF's test road was performed in two stages. The first stage began in May 2012 and was completed in August 2012 with the placement of the hot mix asphalt (HMA) layer with a total thickness of 16 cm. The second stage was completed in August 2013 with the addition of 9 cm HMA on top of the paved road.

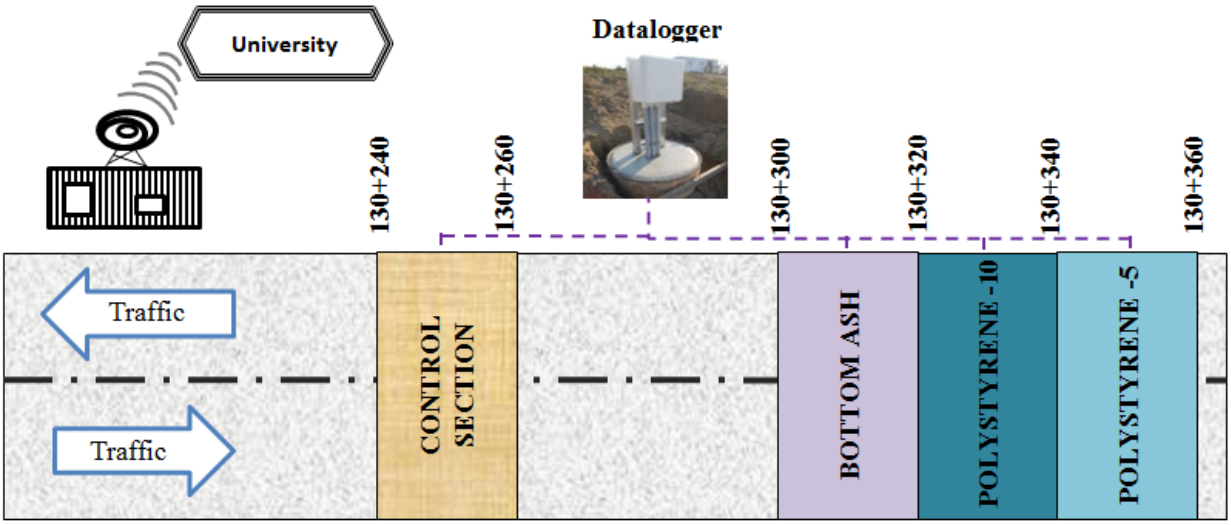

Figure 4-1: Plan view of the test sections

Figure 4-1 shows a schematic plan view of the test road. Two different materials were used as insulation layers in this project: bottom ash and polystyrene. Each insulated section and the control sections (CS) are roughly 20 m in length. The insulated sections stretched from Stationing 130+300 to 130+360, with the first section consisting of bottom ash (B.ash), followed by 10-cm polystyrene (Poly-10), and 5-cm polystyrene (Poly-5).

4.3.1. Materials and Construction

The subgrade soil possessed a maximum particle size of 0.5 mm, liquid limit of 25 percent and plastic index (PI) of 9 percent. Based on the Unified Soil Classification System (USCS), the subgrade soil was classified as Clayey Sand (SC). Meanwhile, the GBC layer consisted of crushed

aggregates with a maximum size of 19 mm. Based on USCS, the GBC was classified as Well-Graded Gravel (GW). The grain distribution of the GBC and subgrade material can be found in Table 4-1.

Table 4-1: Grain size distribution of GBC, bottom ash and subgrade soil used in IRRF project.

Subgrade Soil		GBC		B.ash	
Grain Size, D (mm)	**Percent Finer (%)**	**Grain Size, D (mm)**	**Percent Finer (%)**	**Grain Size, D (mm)**	**Percent Finer (%)**
0.250	98.0	19.000	99.15	4.75	93.89
0.150	83.9	12.500	75.17	2.38	84.24
0.075	46.9	9.500	61.23	1.19	71.40
0.044	37.1	4.750	42.73	0.425	52.50
0.032	32.5	2.380	32.08	0.297	45.64
0.023	27.3	1.190	25.61	0.149	27.57
0.012	24.1	0.595	18.93	0.075	11.23
0.009	22.4	0.297	7.09	----	----
0.004	19.9	0.149	1.46	----	----
0.001	15.0	0.075	0.51	----	----

The bottom ash layer was free of large lumps and impurities. Table 4-1 shows the grain size distribution of the bottom ash, which had a maximum particle size of about 5 mm. The amount of non-combusted coal particles was less than five percent of the material weight. To maintain the natural moisture content of bottom ash at less 35 percent, the compaction of this layer and the placement of the GBC were completed on the same day (July 31, 2012). Figure 4-2 (a) illustrates how the bottom ash layer was wrapped in geotextile to avoid mixing with natural soil. Figure 4-2 (b) shows that bottom ash could be easily compacted using ordinary compaction equipment.

This study used closed-cell Styrofoam Highload 100 extruded polystyrene boards provided by Dow Chemical Company. Based on the manufacturer's data sheet, the polystyrene boards had a compressive strength of 690 kPa and a minimum flexural strength of 585 kPa. The thickness of the boards was 5 cm; therefore, Poly-10 comprised two layers of polystyrene board while Poly-5 was constructed using a single layer. Figures 4-3(a) and (b) illustrate how polystyrene boards were placed on the subgrade soil before placement and compaction of the granular base layer. The

subgrade was completely leveled (deviation of less than 10 mm at any place on a 3-m straight edge) before placing the polystyrene boards. To facilitate a smooth transition from the untreated ground to the Poly-10 section and to avoid deferential icing, the Poly-5 section is located between Poly-10 and the rest of the road, which was constructed as a conventional section.

(a) (b)

Figure 4-2: (a) wrapping bottom ash in geotextile; (b) Placement of bottom ash in the test road

(b)

Figure 4-3: (a) Spreading the polystyrene boards (b) Placement of one and two layers of polystyrene boards

Both HMA mixes in this project were prepared based on Marshall Mix design in accordance with the City of Edmonton Transportation (2015) specification provided on their webpage for Designation-1 asphalt concrete mix. These mixes incorporated 20 percent Reclaimed Asphalt

Pavement (RAP) for the bottom 16-cm layer and 10 percent for the top 9-cm layer. The gradation of granular material used in this project is presented in Figure 4-4, and the physical properties of both mixes are presented in Table 4-2.

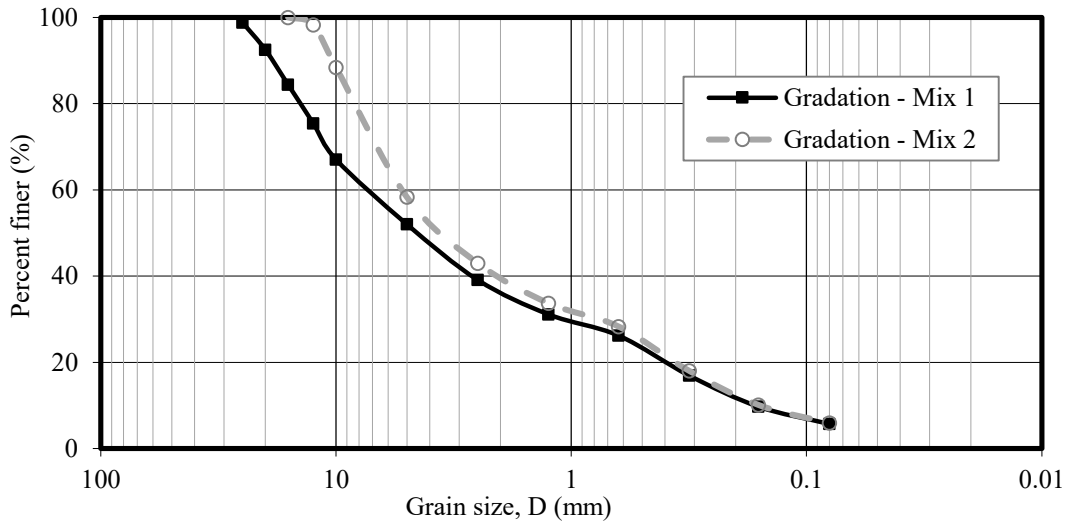

Figure 4-4: Grain size distribution of asphalt granular material used in two different Mixes of HMA

Table 4-2: Physical properties HMA mixes used in the test road

Property	**Asphalt Physical Properties**	
	First Lift	**Second Lift**
Max. Aggregate size (mm)	25	12.5
Binder Grade	PG 58-28	PG 58-28
Reclaimed Asphalt Pavement (RAP) (%)	20	10
Binder Content by Weight of Mix (%)	4.58	5.3
Void in Mineral Aggregate (VMA) (%)	13.1	14.3
Void Filled with Asphalt (VFA) (%)	69.4	74.9
Air Voids (%)	4	3.6
Density (kg/m3)	2355	2344
Marshal Stability (KN)	17.7	16.9
Flow (mm)	2.25	2.5
Theoretical Film Thickness (μm)	6.7	7.1
Tensile Strength Ratio (TSR) (%)	98	81.6

4.3.2. Instrumentation and Data Collection

To investigate temperature changes and moisture variation in different layers, all sections except for Poly-5 were instrumented with 109AM-L thermistors and CS650 Time Domain Reflectometers (TDRs) from Campbell Scientific Canada. Although TDRs are mainly designed for measuring volumetric water content (VWC), a thermistor was placed in the TDR heads to allow temperature measurement. Both temperature and moisture data from TDRs were included in the analysis. Figure 4-5 illustrates the as-built depth of sensors in each section, which are located 0.5 m from the inner edge of the road's shoulder. The TDRs were installed in the CS as deep as 2.5 m below the surface. The location of the deepest thermistors in the B.ash and Poly-10 sections were about 3.3 m from the surface. A total of five sensors were installed in each station.

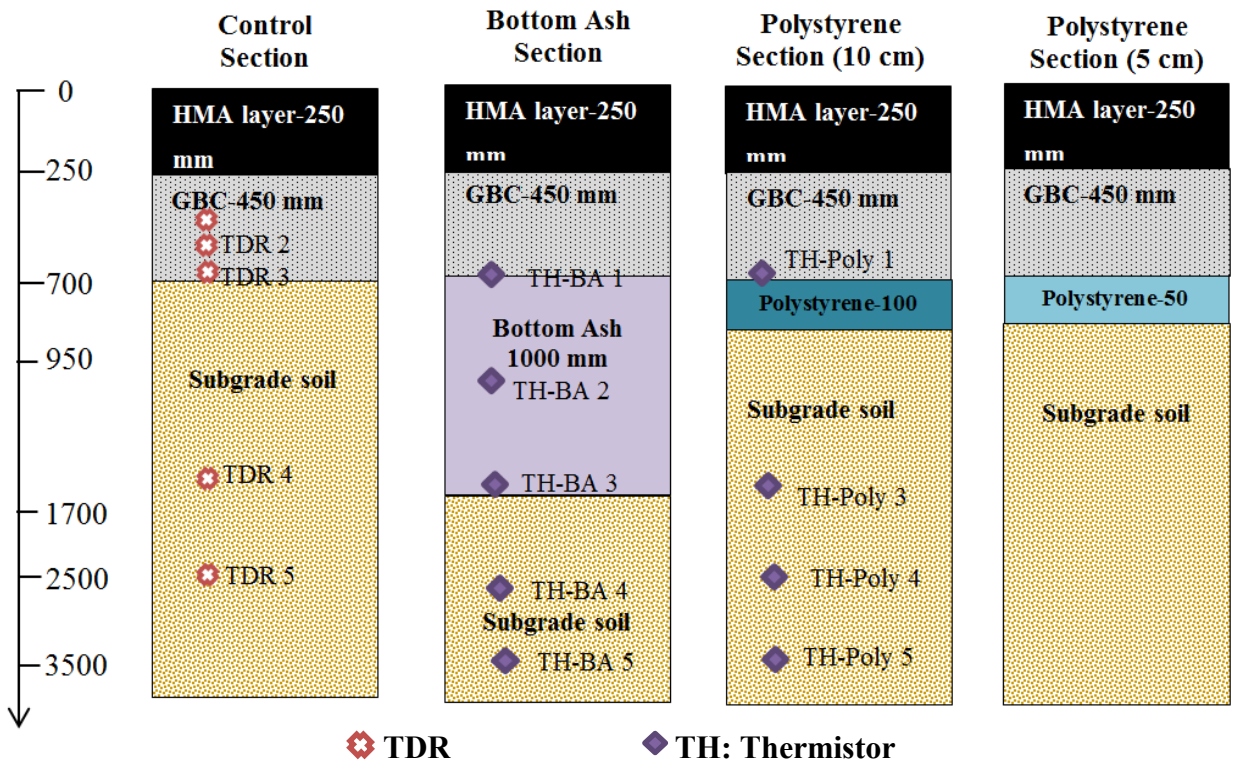

Figure 4-5: Cross sections and as-built depth of thermistors and moisture probes

A CR1000 Datalogger from Campbell Scientific Canada was programmed to collect data from the sensors at 15-minute intervals from the abovementioned sections. The Datalogger was equipped with a spread spectrum Model RF401 radio used to communicate with an antenna Model L14221

installed at an onsite trailer, where a computer transmitted the data regularly to the University of Alberta.

4.4. EVALUATION OF STRUCTURAL CAPACITY

4.4.1. Identifying the Non-Freeze-Thaw Period

The main objective of this study is to investigate the effect of insulation layers on the structural capacity of the pavement during a time when the subgrade is free from the effect of freeze and thaw in all sections. For this purpose, using MEPDG (2004), the whole year was divided into different sections according to the behaviour of unbound material under freezing/thawing conditions that includes frozen, thawed and unfrozen (natural) material. MEPDG outlines three periods of freezing, recovery and non-freeze-thaw, and the recovery period is defined as the required period for the material to recover from the thawed condition to normal, unfrozen condition (MEPDG).

Investigating the temperature data within depths reveals the launch time of both freezing and thawing periods. However, it does not establish the drainage duration of the excess melted ice water. Moisture data can be considered an indicator of identifying and separating three different time periods of frozen, recovering and fully recovered (unfrozen) pavement. To obtain the abovementioned periods in the IRRF's test road, moisture data from TDRs in different depths were used. Figure 4-6 shows the moisture and temperature variations of the CS from October 2013 until October 2014 at three depths of (a) 0.7 m below the surface or the top of the subgrade layer, (b) 1.7 m below the surface or 1.0 m in the subgrade layer, and (c) 2.6 m below the surface or 1.9 m in the subgrade layer. Tavafzadeh et al. (2014) established the frost depth at 2.0 m below the surface, so the three different depths outlined above will correspond to the required depth for investigation of frost action in the subgrade layer.

Evaluating the temperature data in Figure 4-6(a) indicates that the freezing period at the top of the subgrade layer started on November 26, 2013, and the temperature at this depth remained below 0°C until the beginning of April 4, 2014 (129 days), except for a short period of time in March when the temperature rose to about 0°C. As soon as the thawing period starts, the water begins to

drain out of the system. However, as illustrated in Figure 4-6(a), the recovery period ended by May 20, 2014 (46 days).

Investigating the temperature and moisture data of the sensor located 1.7 m below the surface indicates that the frost penetrated into this layer on February 18, 2014, and the water at this depth remained frozen until May 4, 2014 (75 days). The excess water drained out of the system by July 16, 2014, indicating that the recovery period lasted for 73 days.

Figure 4-6(c) shows that the temperature of the subgrade layer 2.6 m below the surface always remains above or at 0°C. However, a 15 percent decrease in VWC during winter and a sharp increase of about 17 percent in VWC during spring are observed. The system will get rid of all excess water by mid-July 2014.

From the above discussion, it can be concluded that frost penetrated the subgrade on November 26, 2013, and remained in place until April 4, 2014, which is approximately four months out of the year or 129 days. When thawing of the subgrade layer started on April 4, 2014, the water began to drain out of the system. Considering the launch time of the thawing period and the time that the water drained out of the system from all different depths (July 16, 2014), the recovering period lasted for about 103 days (Figure 4-7). According to MEPDG (2004), the recovering period is a function of the material properties. For the subgrade soil with the properties presented in Table 4-1, the recommended recovery period is approximately 120 days.

Based on the one year of data monitoring shown in Figure 4-7, the non-freeze-thaw season started in mid-July 2014, when the subgrade had recovered from the thaw effect, and lasted until November 2014. Thus, the non-freeze-thaw (unfrozen) period lasted for about 133 days. In other words, this period is more than one third of a year.

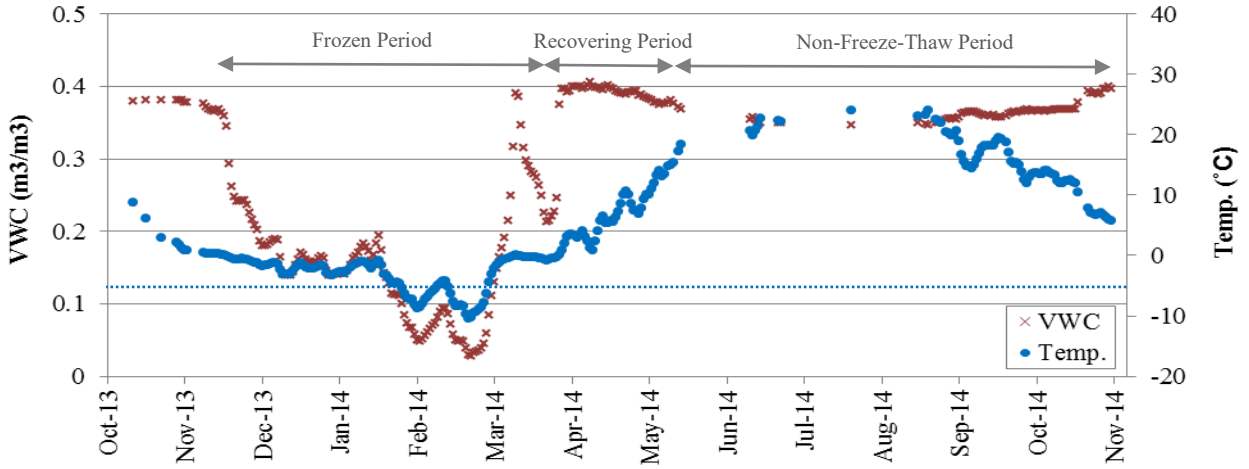

(a) Top of Subgrade (TDR 3)

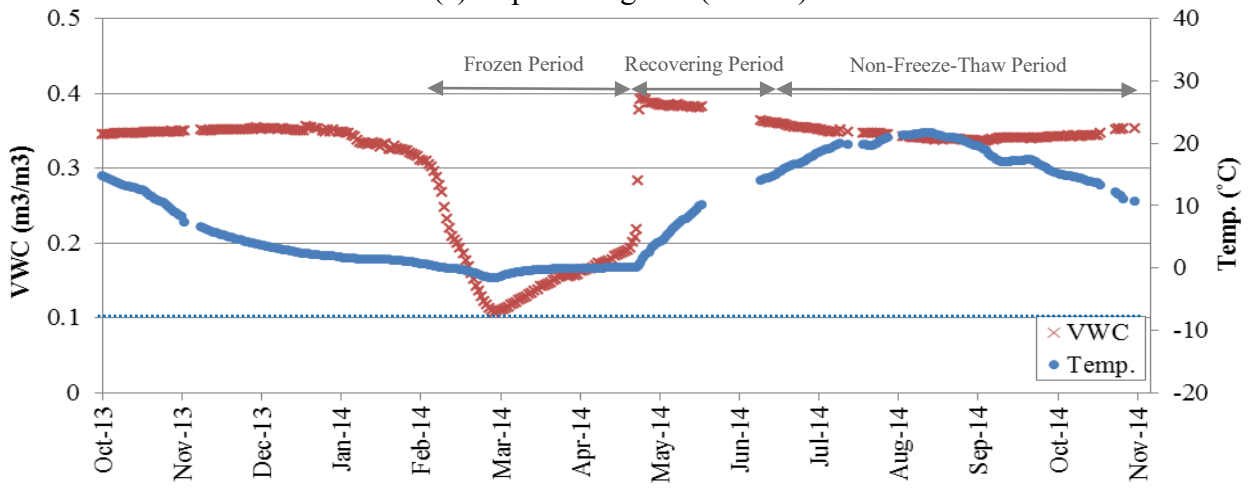

1.0 m in the subgrade (TDR 4)

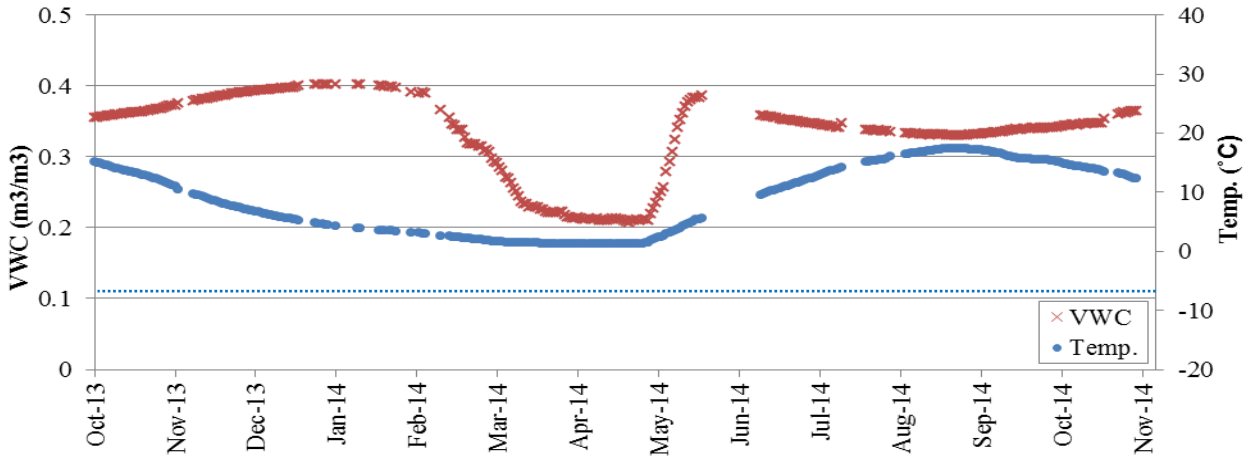

(c) 2.0 m in the subgrade (TDR 5)

Figure 4-6: Temperature and moisture distribution in three different depths of CS from Oct. 2013 till Oct. 2014

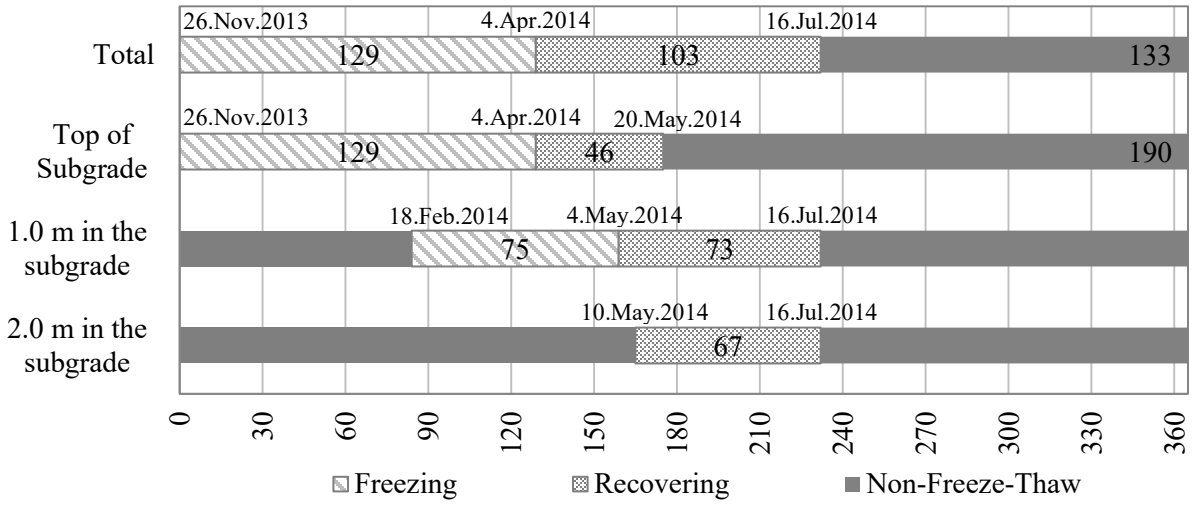

Figure 4-7: Condition of subgrade layer in depth and three zones of Freezing, Recovering and Non-Freeze-Thaw Season

4.4.2. Temperature Distribution in Depth during Non-Freeze-Thaw Period

As discussed in the previous section, the non-freeze-thaw season started in mid-July and lasted until November 2014. For investigating the condition of the insulated sections during this period, the daily average temperature distribution of each insulated section in 15-day intervals is plotted and presented in Figure 4-8. This figure indicates that during this month, the ground is not frozen in any of the sections. The temperature in the GBC layer varied between 7.0 and 27.9°C in the CS, 4.9 and 29.8°C in the B.ash, and 2.1 and 32.1°C in the Poly-10 section. However, the temperature directly underneath the insulation layer of the Poly-10 section varied between 9.5 and 12.4°C. If this small variation underneath the Poly-10 (2.9°C) compared to the temperature variation underneath the GBC layer of the B.ash and CS (20.9 and 24.9°C), it can be concluded that polystyrene with 10-cm thickness effectively blocked the temperature exchange with the above layers.

The temperature in the subgrade layer 1.7 m below the surface varied between 12.2 and 21.2°C in the CS, 12.0 and 15.9°C in the B.ash, and 8.7 and 10.5°C in the Poly-10. Similar to what was previously established by Tavafzadeh et al. (2014), this figure also indicates that the insulation layers changed the temperature distribution within the sections' depths.

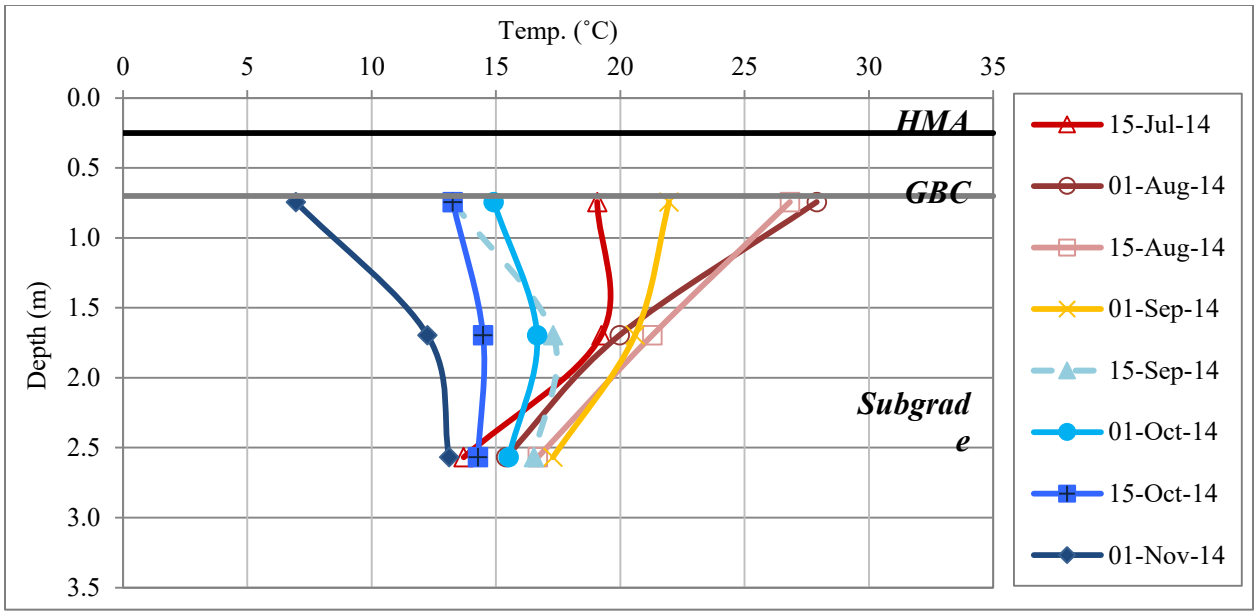

(a) Control Section

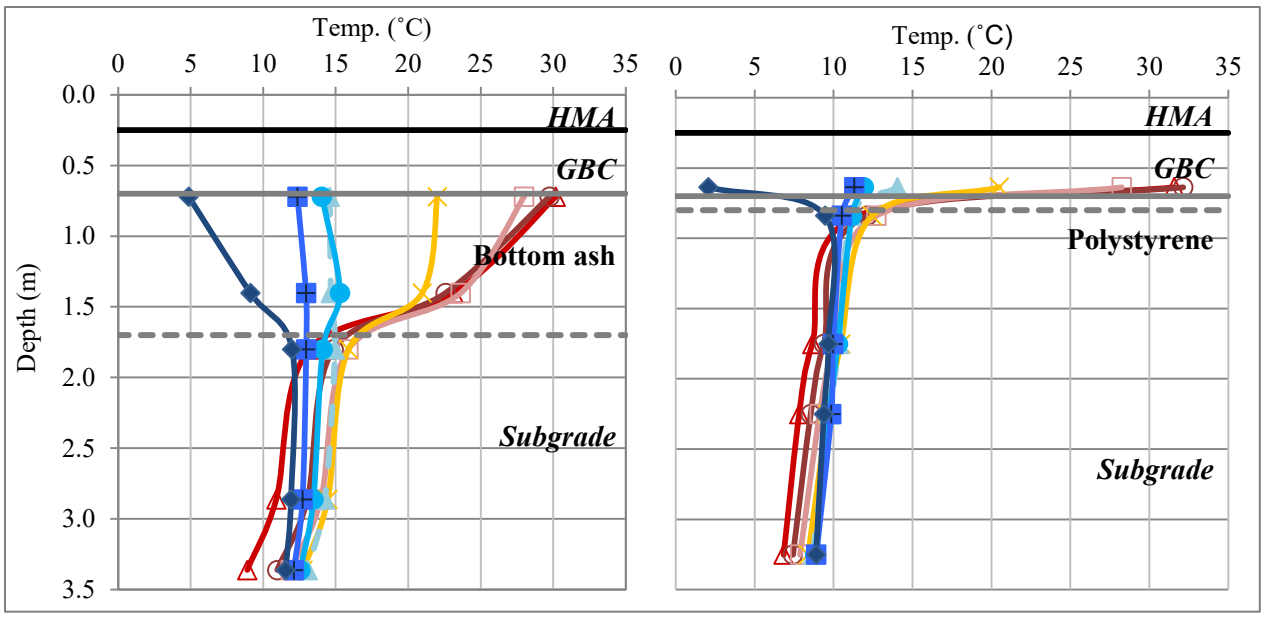

(b) Bottom ash (c) Polystyrene

Figure 4-8: Temperature distribution across the depth for (a) CS, (b) B.ash, and (c) Poly-10 during October 2014

4.4.3. Falling Weight Deflectometer (FWD) Testing

To evaluate the structural capacity of pavement in different sections of the IRRF's test road, FWD testing was conducted. The FWD is a non-destructive method of testing to evaluate the pavement response to a dynamic load applied on pavement surface. The aim of load application is to replicate passing a moving vehicle on the pavement. By applying the load, the pavement response is measured through measuring deflection of pavement surface at specific intervals from the point of load plate (Stubstad, 2002). A Dynatest 8000 with a nine-sensor configuration at 0, 200, 300, 450, 600, 900, 1200, 1500, and 1800 mm from the centre of the load plate was used. Figure 4-9 shows the FWD device used on the IRRF test road, also the location of the sensors are clear on the picture.

Figure 4-9: Overview of FWD equipment and the location of sensors

Based on the identified period in section 3.1., the results of FWD tests conducted on July 17, September 5 and October 17, 2014, were selected as representatives of the non-freeze-thaw season. The load was applied in 20-m intervals. The HMA layer's temperature at 20 mm from the surface was 22°C, 20°C and 7°C for the tests conducted in July, September and October 2014, respectively. Three stress levels of 26.7, 40.0, and 53.3 KN were applied at each station. However, in this study, only the results of deflections under a stress level of 40 KN were used to investigate the structural capacity of the different sections.

Before starting the analysis, the deflection data were normalized based on the exact FWD target load level by multiplying the deflections by the ratio of the applied load to the targeted load. The

applied load was selected based on the acceptable range defined by the *Long-Term Pavement Performance Program Manual for Falling Weight Deflectometer Measurements* (Schmalzer 2006). The resulting normalized deflections were then checked for possible irregularity in the deflection basin based on the method proposed by Xu et al. (2002). No irregularity was observed in the different section basins.

4.4.4. Structural Performance Analysis

Figure 4-9 (a) to (c) present the deflection basins of all sections during the tests performed in July, September and October 2014. It is noted that the CS and B.ash sections always exhibited less deflection than the polystyrene sections.

For ease of comparison, the maximum deflections of all sections underneath the loading plate from all three tests are shown in Figure 4-10. The maximum deflections followed the trend of HMA temperature, whereby they decreased from the test performed in July (22°C) to the test performed in October (7°C). As mentioned previously, the CS and B.ash sections outperformed the polystyrene sections by exhibiting smaller maximum deflections. When the average value of maximum deflections of each section observed during the non-freeze-thaw season compared to the average maximum deflections of the CS, the Poly-10 had a 22.3 percent higher maximum deflection than the CS, followed by the Poly-5 with 16.6 percent and B.ash with 4.2 percent.

4.4.5. Effective Modulus of Pavement

The E_p of each section was calculated using AASHTO (1993). According to this method, subgrade modulus could be calculated using Equation 4-2.

$$M_r = \frac{0.24 \times P}{D_r \times r} \qquad \text{Equation 4-2}$$

Where M_r is the resilient modulus of the subgrade, P is the target load, D_r is the normalized deflection under load P at distance r, and r is the distance of the selected geophone from the load plate. Based on the AASHTO method, to back-calculate the subgrade modulus, the selected deflection requires a sufficient distance from the centre of the load to ensure the back-calculated modulus is not affected by the structural capacity of other pavement layers. For complying with

this criterion, the selected deflection location is compared to $0.7 \times a_e$, which can be calculated for all the sections using Equation 4-3.

$$a_e = \sqrt{[a^2 + \left(D \sqrt[3]{\frac{E_p}{M_r}}\right)^2]} \qquad \text{Equation 4-3}$$

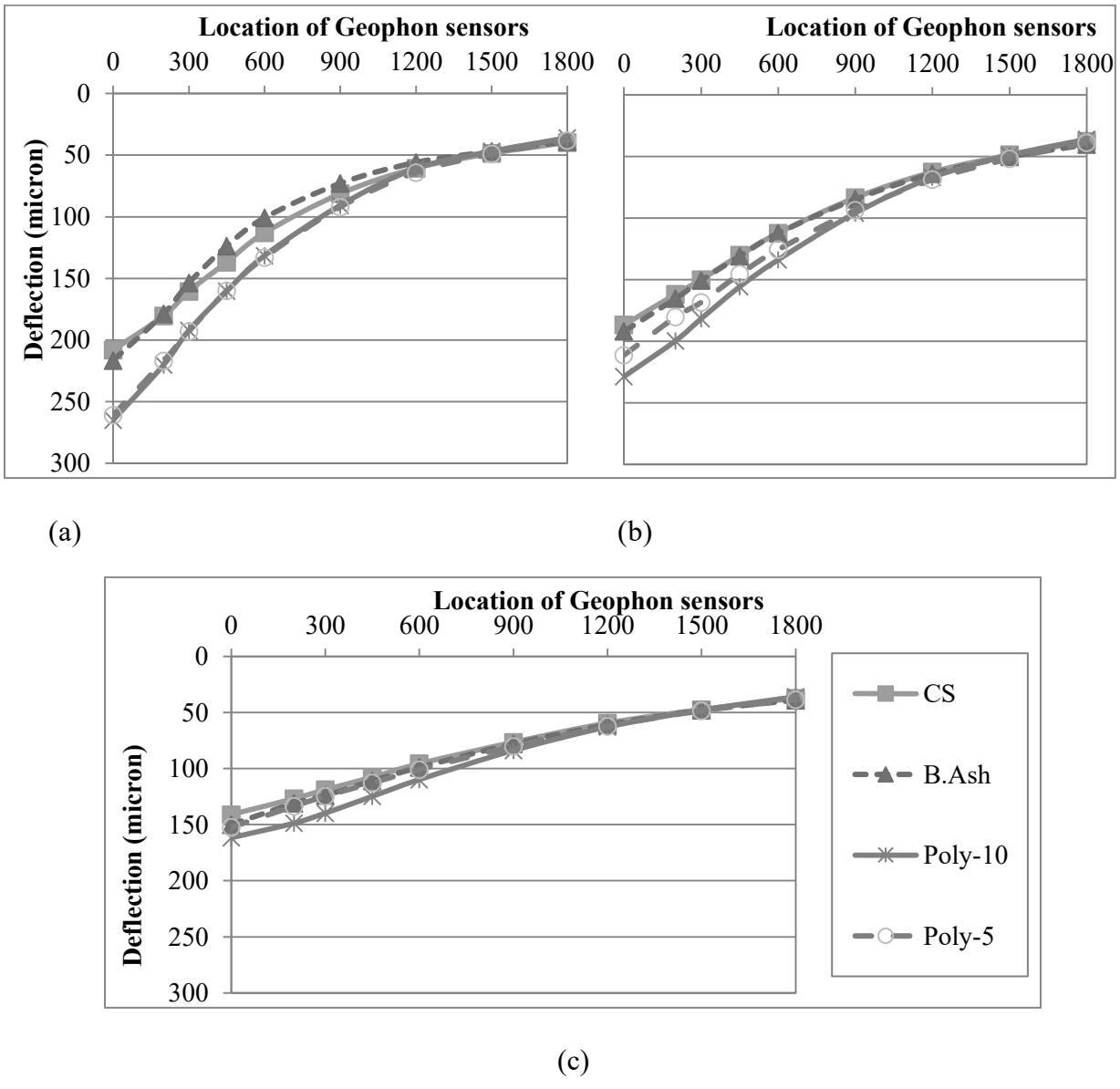

Figure 4-10: Deflection basin of FWD testing on top of the HMA layer on: (a) July 17, 2014 (b) September 5, 2014 and (c) October 17, 2014

Where a_e is the radius of stress bulb at the subgrade/pavement-interface, a is the load plate radius, and D is the total thickness of pavement layers above the subgrade, comprising the total thickness

of HMA and GBC. The deflection observed at the sensor located 1800 mm from the load point application (D9) meets the aforementioned requirement for all the tests and all the sections.

Table 4-3 presents the average D9 of each section. The values of D9 varied between 38.2 micron for the CS and 39.4 micron for the B.ash section. Considering all the sections, the average value of deflection of the sensor located at 1800 mm was 38.0 microns and the Coefficient of Variation (COV) was 3.9 percent. Since the deflection of different sections is similar, the calculated M_r values are also similar. The average back-calculated M_r value of each section is presented in Table 4-3. The average M_r value of all sections was 142.7 MPa with a COV value of 4.0 percent. Table 4-3 indicates that the difference in deflections of the furthest sensor creates a similar variation in the subgrade modulus of each section. The obtained M_r for each section was then applied in the AASHTO method (Equation 4-4) to calculate the E_p.

$$d_0 = 1.5\,Pa\left\{\frac{1}{M_r\sqrt{1+\left(\frac{D}{a}\sqrt[3]{\frac{E_p}{M_r}}\right)^2}}+\frac{\left[1-\frac{1}{\sqrt{1+\left(\frac{D}{a}\right)^2}}\right]}{E_p}\right\} \qquad \text{Equation 4-4}$$

Table 4-3 shows the average results of back-calculated E_p for all the sections. Since M_r was approximately the same for all sections (COV is equal to 4.0 percent), E_p is an indicator of how the insulation layer affects the structural capacity of the section. Similar to maximum deflection results, the CS outperformed other sections by showing a greater E_p. The B.ash, Poly-5 and Poly-10 sections exhibited 5.5, 18.5, and 27.4 percent lower E_p values, respectively, compared to the CS. The average value of E_p is equal to 1,207 MPa with COV equal to 14.3 percent.

Table 4-3: Deflection of the sensor located at1800 mm, M_r and Ep

Section	D_9 (micron)	M_r (MPa)	E_p (MPa)
CS	36.9	146.9	1,498
B.ash	40.9	132.6	1,458
Poly -10	35.9	150.8	1,225
Poly -5	38.1	142.1	1,340
Average	**37.9**	**143.1**	**1,380**
COV (%)	**5.5**	**5.5**	**8.9**

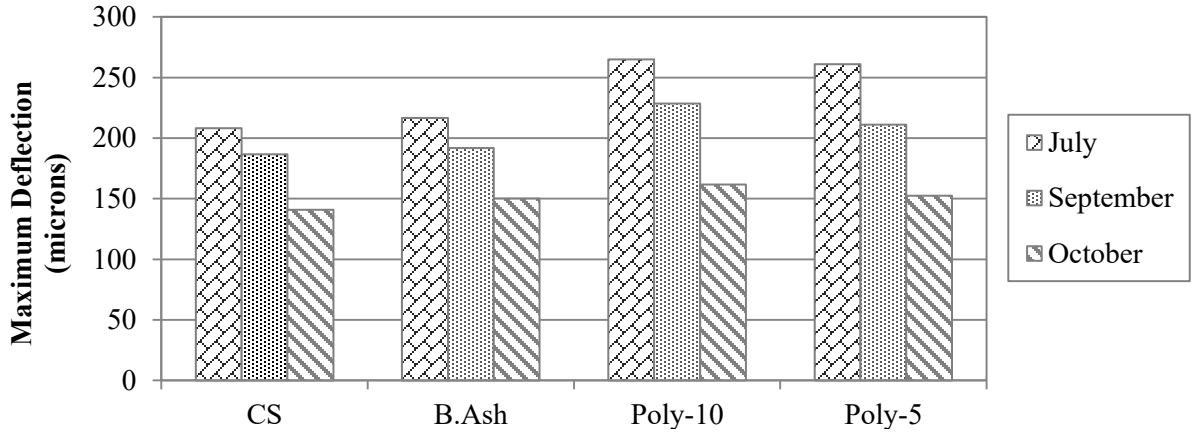

Figure 4-11: Maximum deflection (d0) projected during the test on October 17, 2014

4.4.6. Structural Number of Pavement

The total effect of different layers' moduli can be evaluated through comparing the SN of different sections. SN is an indicator of the total effective pavement thickness. It is possible to obtain the effective structural number of the pavement (SN_{eff}), based on back-calculated E_p, using Equation 4-5 suggested by AASHTO (1993).

$$SN_{eff} = 0.0045D\sqrt[3]{E_p} \qquad \text{Equation 4-5}$$

Figure 4-11 shows that the average SN of the CS, B.ash and Poly-5 varied between 6.5 and 7.2, which can be considered a wide range. Table 4-3 indicates that the M_r values of the sections are almost similar; therefore, SN could be an indicator that using a polystyrene layer may effectively reduce the total structural capacity of the pavement. Using polystyrene changed the SN of Poly-10 and Poly-5 by 10.5% and 6.9 percent, respectively. While, using bottom ash as an insulation layer changed the structural capacity in terms of SN by less than two percent. However, this research only investigated the non-freeze-thaw season, and further investigation into the effect of the insulation layer on overall pavement performance, especially during the recovering period, is within the future scope of this project.

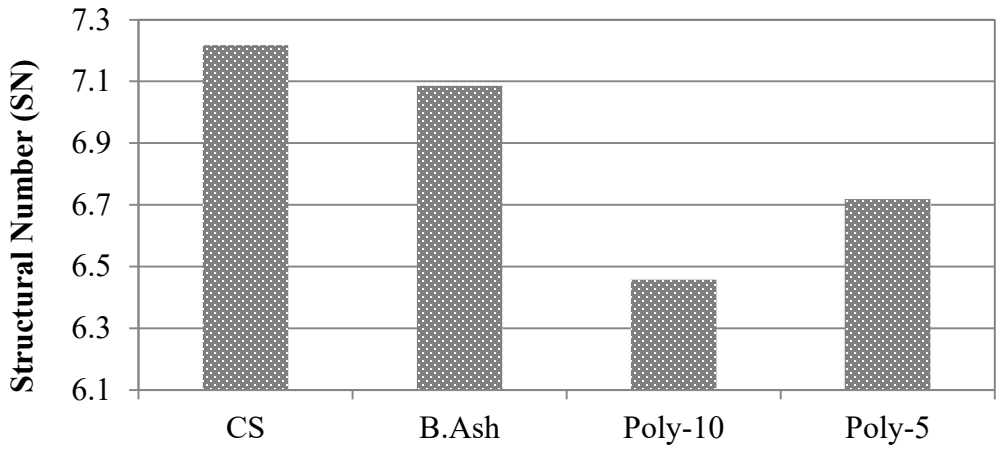

Figure 4-12: Structural Number (SN) of all sections.

4.5. SUMMARY AND CONCLUSIONS

With the exception of the Poly-5 section that was not instrumented, other sections of the IRRF's test road were instrumented using TDR and thermistors to capture temperature and moisture changes within different layers of the pavement through one year of monitoring from October 2013 until October 2014. Evaluating the temperature data from mid-July until November 2014 indicated that all the sections were free of the freeze and/or thaw effect in this duration. Therefore, three FWD test results conducted during July, September and October 2014 were applied to evaluate the structural capacity of insulated sections in comparison to a conventional section. Observations resulting from this study are summarized as follows:

1. Evaluating the temperature data of the CS indicated that the subgrade layer started freezing from November 26, 2013, until April 4, 2014 (129 days).
2. Based on the moisture data of the CS, the recovering period lasted from April 4, 2014, until July 16, 2014 (103 days).
3. The non-freeze-thaw season starts in mid-July, when the subgrade is completely recovered from thaw effect, and lasts until the beginning of next winter. Considering November as

the beginning of winter (based on the temperature data of winter 2013), the non-freeze-thaw period will last for about 133 days, which is about one third of a year.

4. The observed period of the non-freeze-thaw season is longer than 120 days, which is longer than the considered period in MEPDG.
5. Monitoring the temperature data during October 2014 indicated that the temperature distribution within the section depths is influenced by insulated layers. The variation of temperature directly underneath the insulation layer of the Poly-10 section was about 2.9°C, while this value underneath the GBC layer of the B.ash and CS was about 20.9 and 24.9°C.
6. Although previous study (Tavafzadeh et al. 2014) indicated that Poly-10 outperformed other sections as an insulation layer, the pavement section constructed with Poly-10 showed the weakest structural capacity of all the sections during the non-freeze-thaw season. The main reason is that polystyrene board is a soft layer, which decreased the load-bearing capacity of the pavement. This section had approximately 22 percent higher deflection and 27 percent smaller E_p than the CS.
7. The Poly-5 section exhibited approximately 16.6 percent higher deflection and 18.5 percent smaller E_p than the CS.
8. The B.ash section had the closest similarity in performance to the CS, as the maximum observed deflection was only 4.2 percent higher than the CS. The E_p of this section was approximately 5.5 percent lower than the CS.

Using insulation layers decreased the SN of B.ash, Poly-10 and Poly-5 by less than two percent, 10.5% and 6.9 percent, respectively.

Based on the above observations, it can be concluded that although the polystyrene layers effectively reduced frost depth and protected the subgrade soil, they also lowered structural capacity during non-freeze-thaw season, which is almost one third of a year. The section containing the bottom ash layer performed almost the same as the conventional section.

4.6. REFERENCE

Alberta Utilities Commission. http://www.auc.ab.ca/applications/decisions/Decisions/2012/2012-027.pdf, Accessed Jul. 1, 2014.

ARA, Inc., (2004). ERES Consultant Division. "*Guide for Mechanistic–Empirical Design of New and Rehabilitated Pavement Structures*". Final report, NCHRP Project 1-37A. Transportation Research Board of the National Academies, Washington, D.C. http://www.trb.org/mepdg/guide.htm.

Doré, G. and Zubeck H. K.. (2009). *Cold Regions Pavement Engineering.* New York: McGraw-Hill Education.

Environment Canada. *Canadian Weather*. http://weather.gc.ca/canada_e.html Accessed Jan. 1, 2014.

Esch, David C. (1972). *Control of Permafrost Degradation beneath a Roadway by Subgrade Insulation*. State of Alaska Department of Highways.

Havukainen, J. (1987). The Utilization of Coal ash in Earth Works. In *Advances in Mining Science and Technology, Vol. 2: Reclamation, Treatment and Utilization of Coal Mining Wastes*, Amsterdam: Elsevier, 245-252.

Nixon, D., Eng, P., & Lewycky, E. D. (2011). Edmonton Experience with Bottom ash and Other Insulating Materials for Mitigation of Frost Heave Induced Damage. In *Annual Conference of the Transportation Association of Canada , Edmonton, Alberta, September 11-14*. Edmonton, Alberta.

Penner, Edward. (1967). Experimental pavement structures insulated with a polyurethane and extruded polystyrene foam. *Physics of Snow and Ice: proceedings*. 1311-1322.

Stubstad, R.N. (2002) LTPP Data Analysis: Feasibility of Using FWD Deflection Data to Characterize Pavement Construction Quality. *National Cooperative Highway Research Program Web Document 52. National Cooperative Highway Research Program*, Washington, DC.

St-Laurent, D., and Roy, M. (1995). Évaluation structurale des chausses souples dansun contexte climatique nordique: une étude avec le FWD [Structural evaluation of flexible pavements in a northern context: A study using the FWD]. *Proceedings of the 30th Annual Conference of AQTR, Association Québécoise du Transport et des Routes*. Quebec, Canada.

Tavafzadeh, N., Nassiri, S., Shafiee, M., Bayat, A. (2014). Using Field Data to Evaluate Bottom Ash as Pavement Insulation Layer. *Transportation Research Record: Journal of the Transportation Research Board of the National Academies*. Washington, D.C.

The City of Edmonton Transportation. Roadway — Design Standard — Construction Specifications, 2012 Edition, http://www.edmonton.ca/city_government/documents/RoadsTraffic/Volume_2_-_Roadways_May_2012.pdf, Accessed March 1, 2015.

Transportation Officials. (1993). *AASHTO Guide for Design of Pavement Structures*. Vol. 1. AASHTO.

Schmalzer, Peter N. (2006). *Long-Term Pavement Performance Program Manual for Falling Weight Deflectometer Measurements*. Federal Highway Administration, Office of Research, Development and Technology, Turner-Fairbank Highway Research Center.

Xu, B., Ranjithan, R.S., Kim, R. Y. (2002). New Condition Assessment Procedure for Asphalt Pavement Layers, Using Falling Weight Deflectometer Deflections. *Transportation Research Record 1806*, Transportation Research Board, Washington, DC, 57-69.

5. THE EFFECT OF SEASONAL VARIATION ON LOAD BEARING CAPACITY OF PAVEMENTS COMPRISED OF INSULATION LAYERS

This section has been published as N.Tavafzadeh, L.Hashemian and A.Bayat, "The Effect of Seasonal Variation on Load Bearing Capacity of Pavements Comprised of Insulation Layers," Transportation Research Record,2016.

5.1. ABSTRACT

Seasonal variation in the subgrade resilient modulus is likely caused by external factors such as precipitation and freeze-thaw cycles. One of the strategies for minimizing this variation's impact on the subgrade modulus is using insulation layers to prevent frost penetration.

This study investigates the effects of using insulation layers on pavement performance in the fully instrumented Integrated Road Research Facility (IRRF) in Edmonton, Alberta, Canada. Three insulated sections of the test road were comprised of bottom ash (100 cm) and polystyrene boards of two different thicknesses (5 and 10 cm), while the adjacent conventional section was considered the control section (CS). The resilient modulus and the effective modulus of pavement were back-calculated using the data obtained from Falling Weight Deflectometer (FWD) testing conducted at the test road during a one year monitoring period from July 2014 to July 2015. Temperature and moisture probes, installed across the depth of sections, were used to determine the frozen, thawed or recovering condition of the pavement.

The study results revealed that polystyrene boards protected subgrade soil from freezing and thawing effects. The minimum ratio of the back-calculated subgrade modulus of each test to the resilient modulus of the test performed in September was 0.94 in the bottom ash (B.ash) section, while the ratio of the CS could decrease to 0.88 in the recovering period.

Comparison of the load bearing capacity of insulated sections and the control section indicated that, unlike bottom ash, polystyrene boards significantly decreased the load bearing capacity of the pavement.

Key words: Insulation Layer, Recovering Period, Resilient Modulus, Effective Modulus of Pavement, Bottom Ash, Polystyrene.

5.2. INTRODUCTION

External factors such as solar radiation, ambient temperature, precipitation and water table variations may directly or indirectly affect the modulus of pavement layers. This variation influences pavement performance by causing cracks and further deterioration. Pavement in cold regions often suffers from severe low temperatures in winter and multiple freeze-thaw cycles. During winter, when frost reaches the unbound layers, the asphalt modulus can increase to 13.8~20.7 GPa or more (MEPDG, 2004). At the same time, the water in unbound layers freezes, which leads to an increase in resilient modulus of about 20 to 120 times more than that of a normal or non-freeze-thaw condition. When the ambient temperature gradually increases in spring, the resilient modulus of asphalt layer may decrease to about 700 MPa. Meanwhile, the melted water in unbound layers creates pore water pressure that reduces the load bearing capacity (MEPDG, 2004). The ratio of subgrade resilient modulus during spring to the value of that of a normal condition may vary depending on the soil type. Alberta Transportation and Utilities' *Pavement Design Manual* suggests a ratio between 0.625 and 0.875 (Alberta Transportation and Utilities, 1997). However, the investigation conducted by Hein et al. in Ontario showed the ratio may drop to 0.20 for clay and silty-clay (Hein and Jung, 1994). A study conducted at the University of Waterloo's Centre for Pavement and Transportation Technology (CPATT) test track reported a ratio as low as 0.51 to 0.73 (Popik and Tighe, 2005), and the collected data and the back-calculated modulus of FWD road testing conducted during the spring thaw period in Sweden showed a 63% reduction in subgrade and a 48% reduction in granular base layer compared to the fully recovered conditions (Salour and Erlingsson, 2013).

Because of the combination of low HMA resilient modulus and low bearing capacity of unbound layers during spring, the pavement undergoes a considerably higher deflection than during the non-freeze-thaw condition. Because of the high moisture content in the subgrade, presence of a frost-susceptible subgrade soil underneath the pavement increases the risk of frost heave formation during winter and drastically reduces load bearing capacity in spring (Carlos and Zapata. ,2011), which also accelerates the rate of pavement deterioration. A survey conducted in Quebec throughout the 1990s revealed that 10 to 20 percent of the 30,000 kilometre provincial road network endured various damages induced by frost (Dore et. al. 1995). The estimated cost of repairing the pavement's frost-related damages, excluding indirect expenses such as spring load

ban, exceeded 100 million CAD (Dore et. al. 1995). Another study, conducted in Quebec in 1995, showed that the relative damage occurred during recovering-thawing season might be 1.5 to 3 times more than the average annual load-induced damage (St-Laurent and Roy, 1995).

One of the strategies for minimizing the seasonal effects on subgrade is using insulation layers to protect the frost-susceptible subgrade from being influenced by prolonged winter. An insulation layer controls the heat transfer between the ambient air and pavement layers underneath, which also delays thawing and/or freezing (Zhi et al. 2005). Polystyrene is one of the common insulation materials proved to be beneficial in decreasing the frost depth and minimizing the settlement. For instance, observations at the University of Alberta test road showed a minimum 40 percent decrease in frost depth in a 10 cm Extruded polystyrene section when compared to an uninsulated roadway (Tavafzadeh et al. 2014). Additionally, another roadway near Chitina, Alaska, constructed with a 10 cm polystyrene layer, exhibiteds settlement 11 times lower than the conventional section (Esch, 1972). Bottom ash, which is a waste material from the incineration of coal in power plants, is one of the materials recently introduced as an insulation layer. Mainly composed of silica, alumina, and iron, bottom ash is a by-product of coal combustion when burnt in the boiler furnace of an electric power plant. A project in Helsinki, Finland, showed a 40 to 60 percent decrease of frost depth in a roadway constructed with bottom ash insulated sections compared to traditional gravel sections during a three-year monitoring period (Havukanen, 1983). Furthermore, two different studies conducted in Edmonton, Alberta, Canada, (2001 and 2014) illustrated that bottom ash was able to keep frost from penetrating into the subgrade, and the frost depth was limited to the bottom ash layer (Tavafzadeh et al. 2014) and (Field et al. 2011).

Preventing frost from penetrating into frost-susceptible subgrade soil leads to a stable optimum modulus subgrade during the year, including spring season. However, incorporating a soft insulation layer into pavement structure may cause a loss of structural capacity, which must be considered in pavement design (Doré and Zubeck, 2009).

The main objective of the following study is to investigate and quantify (1) the effect of using insulation layers such as polystyrene board and bottom ash on subgrade modulus variation, and (2) pavement structural capacity in different seasons. For this reason, Falling Weight Deflectometer (FWD) tests were conducted in different months on the Integrated Road Research Facility (IRRF) test road. Using the FWD measurements, the resilient modulus of the subgrade

layer and the effective modulus of pavement were back-calculated and compared with the adjacent normal section. The temperature and moisture collected from embedded environmental probes were used to justify the result and establish the freeze-thaw conditions of pavement.

5.3. TEST ROAD DESIGN AND INSTRUMENTATION

The construction of the IRRF's test road facility, located in Edmonton, Alberta, Canada, started in May 2012 and was completed in August 2013. Based on the data collected from weigh-in-motion (WIM) systems during the spring of 2016, the road carries about 2,000 vehicles per lane each day to the Edmonton Waste Management Centre (EWMC). Road pavement consists of a 25 cm dense graded hot mix asphalt (HMA) on top of a 45 cm Granular Base Course (GBC). As illustrated in Figure 5-1, the insulated layers are located between the subgrade and the GBC layer. The 100 cm thick bottom ash layer (B.ash) and two polystyrene layers with 10 and 5 cm thicknesses (Poly-10 and Poly-5) were used as insulation layers. The adjacent conventional section served as a control section (CS).

In accordance with the City of Edmonton's specifications for Designation-1 asphalt concrete mix, this study used two types of dense-graded HMA mixes with a maximum nominal aggregate size of 12.5 and 25 mm based on Marshall Mix design (*Roadway Design Standard Construction Specifications,* 2012). The GBC layer, classified as Well-Graded Gravel (GW) based on the Unified Soil Classification System (USCS), was comprised of crushed aggregate with a maximum particle size of 19 mm (ASTM Standard C136-06, 2006). Sieve analysis of the subgrade soil classified it as Clayey Sand (SC) with a maximum particle size of 0.5 mm. Approximately 27 and 21 percent weight of the subgrade soil passed through sieves 0.075 mm and 0.02 mm, respectively. Subgrade soil has a liquid limit of 25 and a plastic index (PI) of 9 percent. Based on recommendations, the segregation potential of the subgrade soil is calculated to be more than $200 \times 10^{-5} \frac{\text{mm}^2}{\text{S.°C}}$ (Rieke and Mageau, 1983), which is considered moderate frost-susceptible subgrade according to Saarelainen's categorization (Saarelainen, Seppo. (1996).

Bottom ash was free of large lumps and impurities with a maximum particle size of about 5 mm. The amount of non-combusted coal particles was less than five percent of the material by weight. The optimum moisture content of bottom ash material is about 35 percent. The bottom ash layer was wrapped in geotextile to avoid mixing with natural soil. This project used closed-cell

Styrofoam Highload 100 extruded polystyrene boards, which have a compressive strength of 690 kPa and a minimum flexural strength of 585 kPa based on the manufacturer's data sheet.

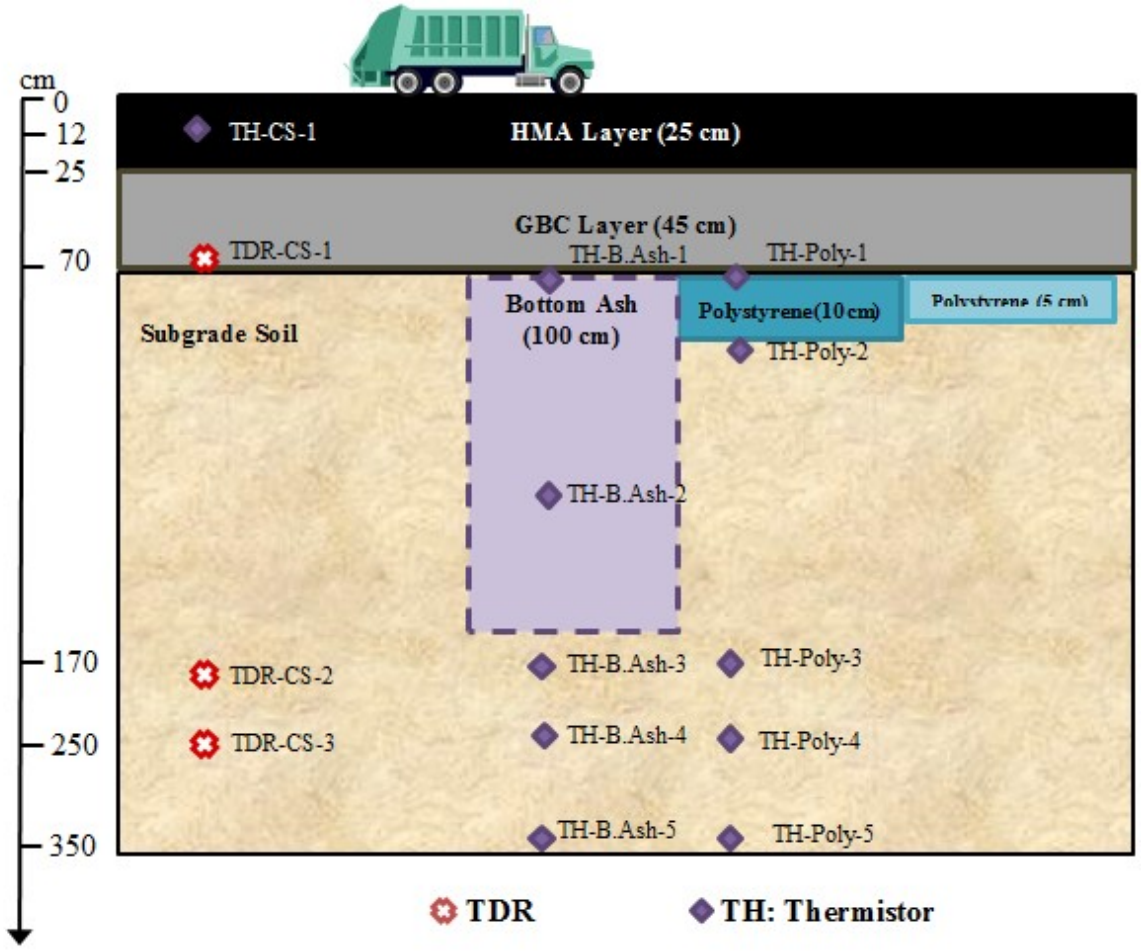

Figure 5-1: Cross-sections and depths of thermistors and moisture probes

To investigate freezing, thawing and recovery condition of the pavement, all of the sections, except for the Poly-5 section, were instrumented using 109AM-L thermistors and CS650 Time Domain Reflectometers (TDRs) from Campbell Scientific Canada at different depths of the pavement. The sensors in the CS are located as deep as the maximum anticipated frost depth. In insulated sections, the probes are installed deeper (3.5 m) to monitor the depth with approximate constant temperature. The TDR probes are able to collect both unfrozen volumetric water content (UVWC) and temperature data. The moisture data collected from the TDRs was corrected based on the formula obtained during the laboratory calibration. Figure 5-1 shows the location and type of

instrumentation at each section. The embedded thermistor elements provided by Omega at mid-depth of the CS HMA layer provided the HMA temperature during the tests.

A CR1000 Datalogger was programmed to collect data from the sensors in 15-minute intervals from all of the sections. The Datalogger was equipped with a spread spectrum Model RF401 radio with an antenna Model L14221 installed at an onsite trailer, where a computer transmitted the data regularly to the University of Alberta.

5.4. FALLING WEIGHT DEFLECTOMETER (FWD) TESTING

Falling Weight Deflectometer (FWD), which is a non-destructive testing, simulates the dynamic load resulting from a moving vehicle on the pavement. FWD testing has become a common method for evaluating the structural capacity of the pavement and back-calculating the modulus of different layers of the pavement. During the monitoring period, multiple FWD tests were conducted on all sections of the IRRF test road using a Dynatest 8000 with a nine-sensor configuration at 0, 200, 300, 450, 600, 900, 1200, 1500, and 1800 mm from the centre of the load plate. The load is applied at 20 m intervals on the outer wheel path and the middle of insulated sections to avoid any confusion from other sections. The FWD test was conducted at three stress levels: 26.7, 40.0, and 53.3 KN. It should be mentioned that during the monitoring period, the road was not open to traffic. However, in this study, the only results used for investigation purposes are of deflections under stress levels of 40 KN. Applying the precise target load on the pavement is a challenging task that may cause problems with the accuracy of the retrieved data. Based on the *Long-Term Pavement Performance Program Manual for FWD Measurements*, the acceptable applied load should not exceed the range of 36.0 to 44.0 KN for the target load of 40 KN (Schmalzer, 2006). Also, to have a common platform of comparison, all the deflections are normalized for the target load. Using the method suggested by Xu et al. (2002), the deflection basins are checked to uncover irregularities before commencing analysis. No irregularity was observed in the basins.

The exact dates of FWD tests are shown in Table 5-1. The one-year FWD testing on the test road started in the summer of 2014 on a monthly basis, bi-weekly during thaw season, and continued until the summer of 2015, excluding the time when the ground was completely frozen and ambient

temperature was less than -10°C. HMA temperature was measured 12 cm below the surface (approximately mid-depth of the pavement) using the installed thermistors.

Table 5-1: Temperature of the HMA layer during each test in different sections

Test ID	Summer	Fall		Winter	
	FWD 1	FWD 2	FWD 3	FWD 4	FWD 5
	17-Jul-14	5-Sep-14	17-Oct-14	18-Nov-14	14-Mar-15
Temp. (°C)	22.0	20.0	10.0	-1.0	9.0

Test ID	Recovering Period					Summer
	FWD 6	FWD 7	FWD 8	FWD 9	FWD 10	FWD 11
	8-Apr-15	21-Apr-15	5-May-15	25-May-15	5-Jun-15	4-Jul-15
Temp. (°C)	11.0	18.0	19.0	31.0	30.0	37.0

5.5. TEMPERATURE EVALUATION OF THE PAVEMENT SECTIONS

The ambient temperature decreases and remains below zero for a long period of time in the winter; frost penetrates into frost-susceptible subgrade, causing formation of ice lenses. In early spring, the gradual increase in the ambient temperature causes ice lenses to melt. Because of the high moisture content in the pavement for a short period of time without the possibility of it draining out of the system, the subgrade modulus declines dramatically in comparison to its normal condition. Furthermore, the modulus of the HMA layer decreases with rising ambient temperature. In early spring, when the ambient temperature increases, the combination of low HMA and subgrade modulus leads to higher pavement deflection, accumulation of fatigue, and evolution of cracks. During the recovering period, the subgrade loses its extra water and re-gains its strength (Doré and Zubeck, 2009). Considering the abovementioned constitutive procedure, recognizing the condition of the temperature and moisture temperature in the pavement is critically important for comprehending and evaluating the FWD test results. For this reason, Figure 5-2 illustrates the average daily temperature distribution across the depth of the IRRF sections on the day of conducting FWD tests.

Figure 5-2(a), which plots the temperature distribution in the CS, indicates that the subgrade layer was partially frozen during FWD 5 (Mar. 2015). Also, the GBC layer showed a below-zero

temperature during FWD 4 (Nov. 2014). These two tests were performed at the end and beginning of the winter season. Other than these two tests, none of the FWD testing was performed on the CS that would display any signs of freezing. By the beginning of April (FWD 6), the pavement was fully thawed and the recovering period started.

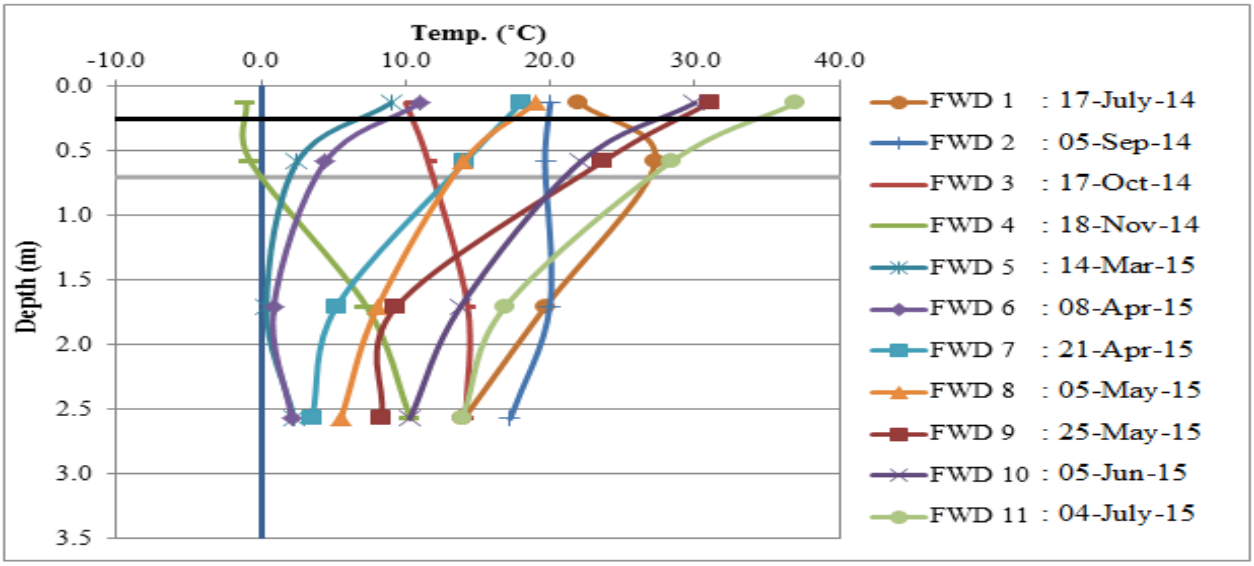

(a) Control Section

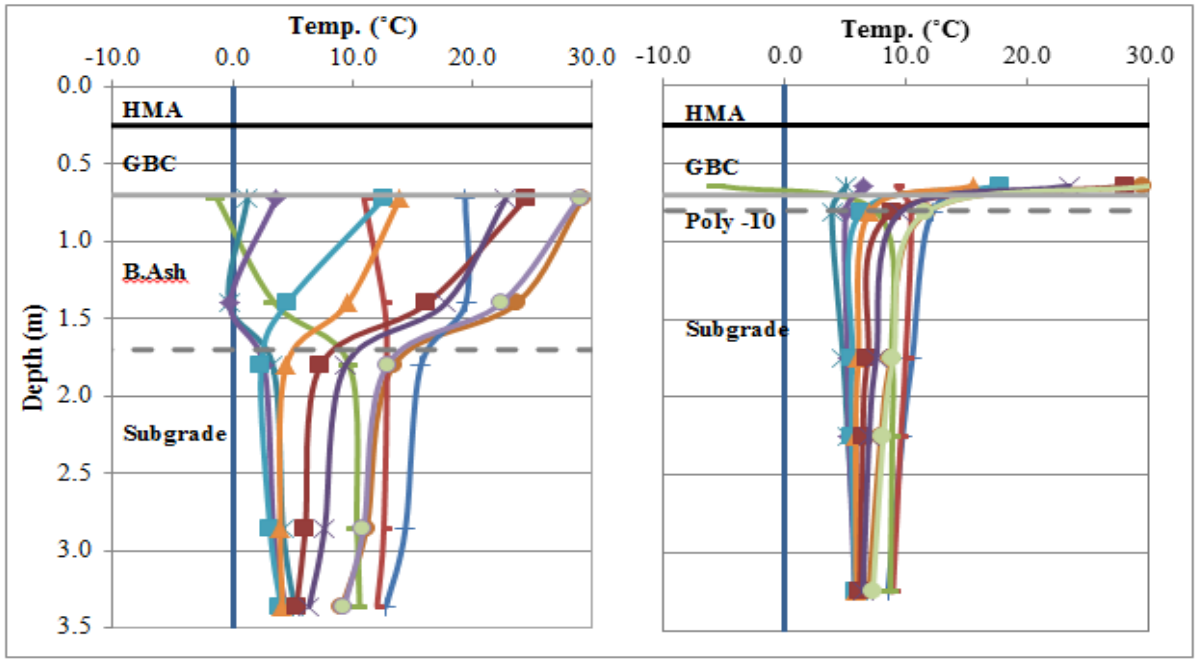

(b) B.ash Section (c) Poly-10 Section

Figure 5-2: The average daily temperature distribution across the depth of different sections on the day of FWD tests

Figure 5-2(b) illustrates the B.ash section was in a partially frozen condition from FWD 4 (Nov. 2014) to FWD 6 (Apr. 2015). The frost depth of the B.ash section was limited to 1.4 m below the surface and the subgrade is not affected by frost action.

Figure 5-2(c), which plots the temperature distribution in the Poly-10 section, shows that the 10 cm polystyrene layer protected the subgrade in a way that the subgrade was not under the effect of freezing at the time of the FWD testing. However, the GBC layer showed a considerably lower temperature range during FWD 4 (Nov. 2014) than other sections.

5.6. MOISTURE EVALUATION OF THE PAVEMENT SECTIONS

The unfrozen volumetric water content (UVWC), measured by TDR probes, is essential to understanding if the subgrade layer affected by frost has drained the extra water out of the system and obtained its normal condition. Figure 5-3 shows UVWC within the CS subgrade depth on the days of FWD testing. A sharp decline in UVWC is an indicator of frost occurrence, and small changes can be correlated to intake or discharge of water in the system.

The TDR located 1.7 m below the surface is assumed to be the point of interest for evaluating the condition of subgrade layer (freezing, thawing and fully-recovered), as the moisture at this level is barely affected by changes in moisture content of the GBC layer.

Moisture data indicates that the minimum moisture content was observed in September 2014, as low as 32.1 percent. After September, moisture content gradually increased until frost reached this depth in March 2015, when the moisture dropped to as low as 26 percent. Then, a sharp boost in moisture content occurred by the start of thawing in April 2015. During April 2015, the moisture gradually increased until it reached its maximum value, as high as 36.4 percent. After this point, a gradual decline in moisture content was observed from April to July 2015.

The increase in moisture content reveals influence of moisture intake from underneath and accumulation of water in the subgrade layer. The decreasing trend indicates that high moisture content begins to drain out of the system during the recovering period and the subgrade layer will reach its equilibrium in fall.

Based on the moisture data observation, FWD 2 (Sep. 2014) represents a fully recovered condition when the subgrade layer shows the highest modulus.

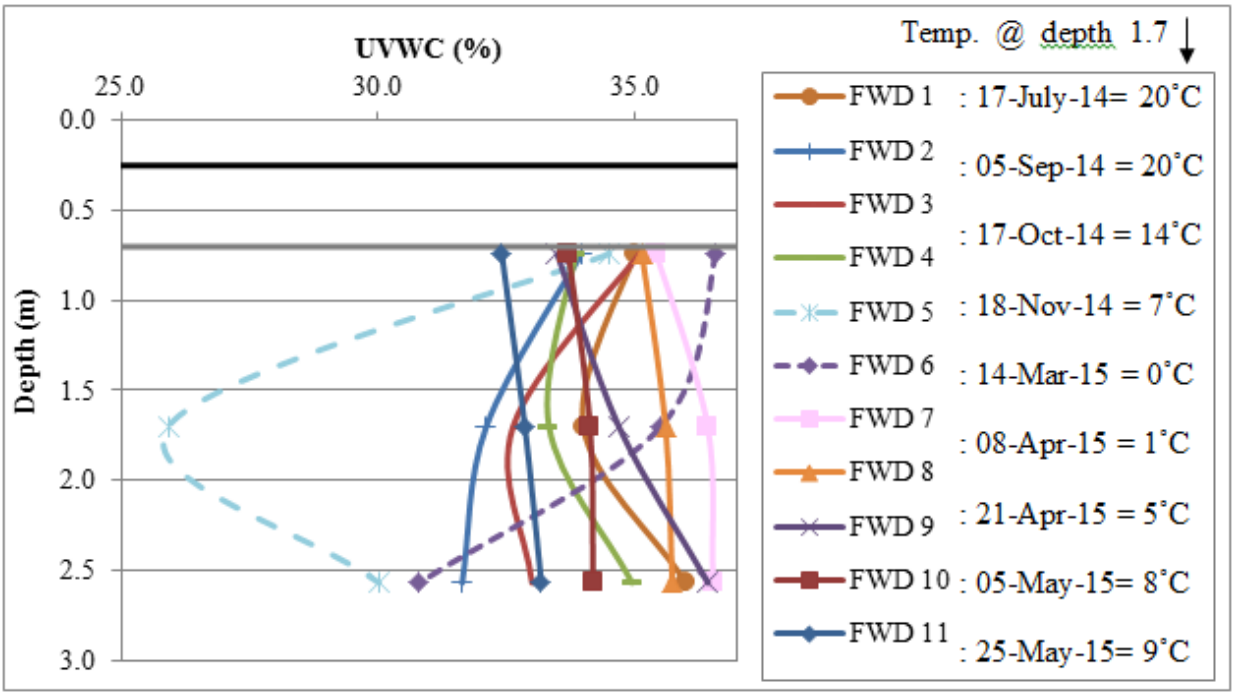

Figure 5-3: VWC distribution within depth of the CS on the day of conducting FWD tests

5.7. EVALUATION OF DEFLECTION DATA

5.7.1. The Maximum Deflection Analysis

Maximum deflections of pavement under the load plate (D0) are plotted in Figure 5-4. The figure also incorporates the measured HMA temperature during each FWD test. Comparing the values at the time of different FWD tests reveals that the observed fluctuation is compatible with the HMA temperature variation. In other words, a higher temperature resulted in a higher D0. The HMA layer had the highest temperature in July 2015 (FWD 11) and, consequently, the highest D0. This phenomenon indicates the temperature of the thick HMA layer (25 cm) significantly affects its stiffness and therefore the load bearing capacity of the whole pavement. Hence, the fluctuation in the HMA modulus arising from the temperature variations governs the maximum deflection of the pavement under load.

As expected, the sections constructed using polystyrene consistently exhibited a higher maximum deflection at D0 compared to the CS and B.ash sections because of a soft layer underneath the GBC layer. However, this difference is temperature-dependent. For instance, when the temperature

was low during FWD 6 (Apr. 2015), the maximum deflections of the Poly-10 and Poly-5 sections were about 27 and 4 percent higher than the CS, respectively. Whereas when the temperature reached its maximum at the time of FWD 11 (July 2015), this ratio increased up to about 59 and 53 percent for the Poly-10 and Poly-5 sections, respectively. The difference may be explained by the fact that the polystyrene sections have a higher top pavement layer temperature during summer and a lower temperature during winter when compared to conventional sections (Tavafzadeh et al., 2014). A higher temperature in summer months leads to a decrease in HMA modulus, resulting in a higher deflection of polystyrene sections in warm months. The same phenomenon caused a lower deflection of polystyrene sections during FWD 4 (Nov. 2014) when the frost penetrated into pavement. The polystyrene layers blocked the temperature exchange between the frozen top layer and the warm ground underneath; this traps the cold in the top layers and causes a higher HMA modulus compared to the CS during the cold seasons of the year.

The CS and B.ash sections always exhibited a comparable deflection during one year of data monitoring. The difference between these two sections' maximum deflection values at D0 never exceeded six percent.

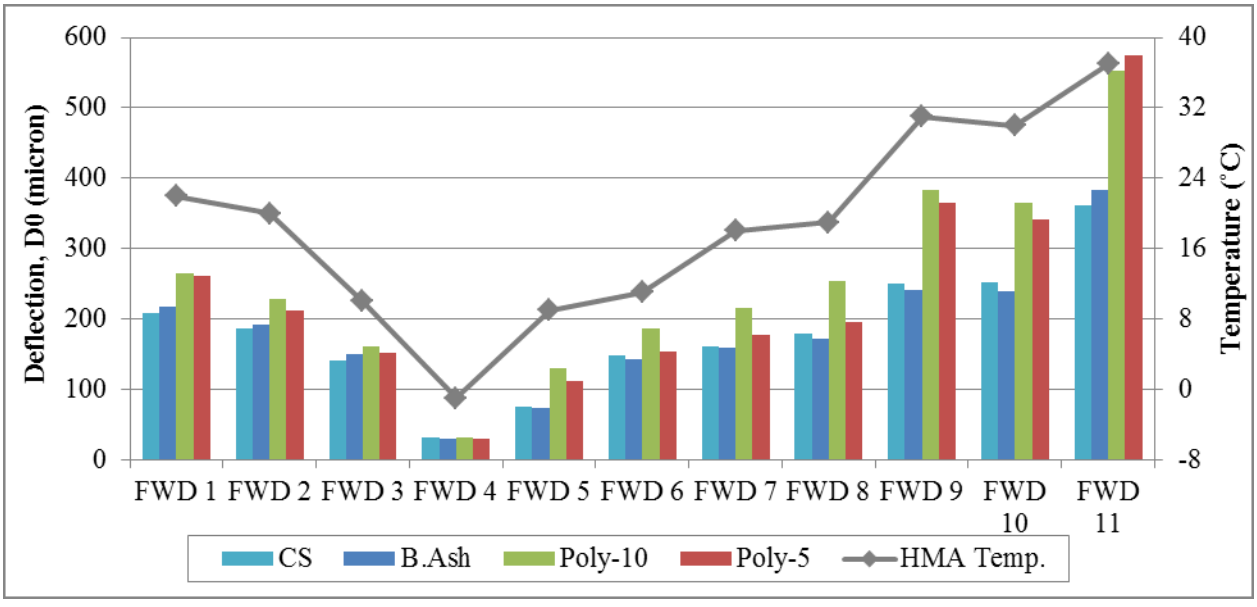

Figure 5-4: Maximum deflection (D0) measured during each FWD test on top of the HMA layer

5.7.2. Subgrade Modulus

The AASHTO method (1993) was used for back-calculating the subgrade modulus based on FWD data. It suggested calculating the modulus of subgrade using Equation 5-1:

$$M_r = \frac{0.24 \times P}{D_r \times r} \quad \text{Equation 5-1}$$

where P is the target load, M_r is the resilient modulus of the subgrade, and r is the distance of the selected geophone from the load plate. Based on the AASHTO method, accurate back-calculation of the subgrade modulus requires selecting a deflection of sufficient distance from the centre of the load to ensure the back-calculated modulus is not affected by the structural capacity of other pavement layers. For checking this criterion, the selected deflection location is compared with $0.7 \times a_e$, which can be calculated for all the sections using Equation 5-2:

$$a_e = \sqrt{[a^2 + \left(D \sqrt[3]{\frac{E_p}{M_r}}\right)^2]} \quad \text{Equation 5-2}$$

where a_e is the radius of stress bulb at the subgrade-pavement interface, a is the load plate radius, and D is the total thickness of pavement layers above the subgrade. In regards to pavement thickness, deflection observed using the sensor located 1,800 mm from the point of load application meets the aforementioned requirement for all sections.

Figure 5-5 shows the deflection data collected from the sensor located 1,800 mm from the load plate (D9) during each of the FWD tests. The deflection data revealed a sudden drop during FWD 4 (Nov. 2014) for all the sections and during FWD 5 (Mar. 2015) in the CS and B.ash sections. The temperature data (Figure 5-2) indicates that the subgrade layer of the Poly-10 sections never freezes. Hence, small deflections during FWD 4 can be explained by a low HMA temperature (-1.0°C), which causes a substantial increase in the HMA resilient modulus. This layer therefore attenuates most of the energy applied by dropping the load. During FWD 5, as explained before and indicated by the temperature 1.7 m below the surface, the ground was partially frozen in the CS and B.ash sections, which resulted in a lower deflection compared to other tests. Comparing the overall D9 trend of CS and B.ash sections reveals that since the thawing started in April 2015 until the extra water drained out of the system in July 2015 (FWD 6 to FWD 11), the observed D9

deflections were higher than those in fall and winter (from Sep. to Nov. 2014). The Poly-10 section exhibited the lowest values of deflections compared to the other sections in most of the FWD tests.

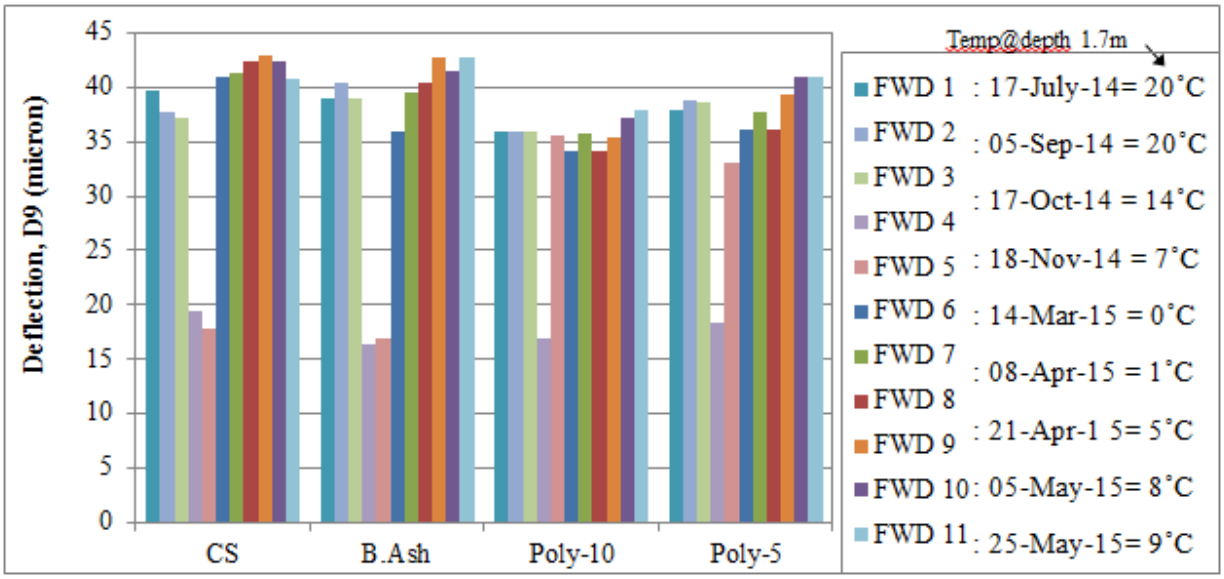

Figure 5-5: Deflection of the sensor located 1,800 mm from the centre of the load plate for all FWD tests

Using the deflection data presented in Figure 5-5, the resilient moduli of subgrade in different sections were calculated and presented in Table 5-2(a). The back-calculated moduli indicate that during the recovering period and in the summer, the subgrade resilient modulus of CS is considerably lower than that of the insulated sections. Since fall, when the extra water drained out of the system, the resilient modulus of CS gradually increases. As expected, the Mr value of the B.ash and CS sections almost doubled when the sections were partially frozen during FWD 4 and FWD 5.

Variations of resilient moduli can be considered as criteria for evaluating the efficiency of insulation layers. Thus, the coefficient of variation (COV) for the resilient moduli of all sections was calculated after excluding the result of FWD 4. Comparing the results indicated that the polystyrene sections had COV lower than seven percent, compared to the CS and B.ash sections that had COV as high as about 36 and 38 percent, respectively.

The COV for each of the FWD tests, which is an indicator of differences or similarities between various sections, was also calculated. The highest variation was observed in FWD 5 (Mar. 2015),

when the ground below the CS and B.ash sections was frozen, but the subgrade of the Poly-10 section was protected from frost penetration. The closest similarity between resilient moduli of different sections was observed during summer and fall, when the COV varied between three and five percent.

Table 5-2(b) presents the ratio of the back-calculated resilient modulus of each month to the resilient modulus of the test performed in September as representative of the fully-recovered season. The data demonstrates that the ratio of resilient modulus of the insulated sections reached the minimum values, as low as 0.94, during the warm months of the year, when the HMA modulus was highly affected by the warm weather and may have affected the state of stress on the subgrade, thus changing its resilient modulus.

When thawing started in the pavement, the CS had a resilient modulus ratio of 0.92. The ratio gradually decreased until reaching its minimum value in FWD 9 (May 2015), as low as 0.88. After this point, the resilient modulus steadily increased until it reached equilibrium in the fall season. The variation in resilient modulus is similar to the trend observed in the moisture distribution within the CS. In winter, when the ground starts to freeze, the ratio of resilient modulus in the CS and B.ash sections doubled compared to the value in September.

Table 5-2(c) shows the seasonal variation of resilient modulus for each section. If the efficiency of an insulation layer were evaluated by comparing the level of protection it provides frost-susceptible subgrade from freeze and/or thaw effects, then all the insulated sections outperformed the CS by exhibiting higher ratios of resilient modulus during the recovering period and fall season. During the thaw season, the CS had a ratio of 0.89, while the B.ash, Poly-10 and Poly-5 sections had ratios almost equal to 1.00. The comparison indicates that all insulation layers successfully protected the subgrade from freeze/thaw effects.

5.7.3. Effective Modulus of the Pavement

The obtained M_r for each section was applied in the AASHTO method (Equation 5-4) to calculate the Effective Modulus of the Pavement (E_p).

Table 5-2: (a) Back-calculated modulus of the subgrade for all FWD tests; (b) Ratio of back-calculated modulus of the subgrade for each FWD test to the recovered condition (FWD 2); (c) Average Seasonal Mr and the Mr Ratio

(a) Mr (MPa)

Test ID	FWD 1	FWD 2	FWD 3	FWD 4	FWD 5	FWD 6	FWD 7	FWD 8	FWD 9	FWD 10	FWD 11	COV
	17-Jul-14	5-Sep-14	17-Oct-14	18-Nov-14	14-Mar-15	8-Apr-15	21-Apr-15	5-May-15	25-May-15	5-Jun-15	4-Jul-15	
CS	136.6	143.5	145.3	279.7	305.1	132.3	130.9	127.6	126.3	127.7	133	36.2%
B.ash	139.1	134.2	138.9	329.6	319.6	150.7	136.7	134.2	126.7	130.3	127	38.2%
Poly-10	151.0	150.7	150.7	----	152.0	158.2	151.5	158.5	153.1	145.8	143	3.2%
Poly-5	142.5	139.4	140.4	------	164.1	149.9	143.5	150.2	137.8	132.2	132	6.7%
COV	4.4%	4.9%	3.7%	11.6%	38.0%	7.4%	6.3%	10.0%	9.3%	6.0%	5.0%	

(b) Mr Ratio Comparison to September

Test ID	FWD 1	FWD 2	FWD 3	FWD 4	FWD 5	FWD 6	FWD 7	FWD 8	FWD 9	FWD 10	FWD 11
	17-Jul-14	5-Sep-14	17-Oct-14	18-Nov-14	14-Mar-15	8-Apr-15	21-Apr-15	5-May-15	25-May-15	5-Jun-15	4-Jul-15
CS	0.95	1.00	1.01	1.95	2.13	0.92	0.91	0.89	0.88	0.89	0.93
B.ash	1.04	1.00	1.03	2.46	2.38	1.12	1.02	1.00	0.94	0.97	0.95
Poly-10	1.00	1.00	1.00	-----	1.01	1.05	1.01	1.05	1.02	0.97	0.95
Poly-5	1.02	1.00	1.01	-----	1.18	1.08	1.03	1.08	0.99	0.95	0.95

(c) Average Seasonal Mr and the Mr Ratio

	Average Mr (MPa)				Mr Ratio		
Season	**Summer**	**Fall**	**Winter**	**Recovering Period**	**Summer**	**Winter**	**Recovering Period**
CS	134.7	144.4	292.4	129.0	0.93	2.02	0.89
B.ash	133.0	136.5	324.6	135.7	0.97	2.38	0.99
Poly-10	146.9	150.7	152.0	153.4	0.97	1.01	1.02
Poly-5	137.3	139.9	164.1	142.7	0.98	1.17	1.02

$$d_0 = 1.5\,Pa\left\{\frac{1}{M_r\sqrt{1+\left(\frac{D}{a}\sqrt[3]{\frac{E_p}{M_r}}\right)^2}} + \frac{\left[1-\frac{1}{\sqrt{1+\left(\frac{D}{a}\right)^2}}\right]}{E_p}\right\} \qquad \text{Equation 5-4}$$

Table3(a) shows back-calculated E_p for all sections during the monitoring period. E_p values followed the same trend as D_0 (Figure 5-4). As expected, during FWD 4 (Nov. 2014), when the HMA temperature was low, E_p values exceeded the values of those in the summer. This value for CS during FWD was about eight times more than what was observed in the summer, and for the insulated sections, it even increased to ten times more than the summer. The calculated COV of E_p values during each FWD testing indicates that the sections were almost the same during the cold season (FWD 4) when the HMA modulus is dominant compared to other layers' moduli. With the increasing temperature, the E_p values of different sections were more distinguished from each other by showing a higher COV, which reached 42 percent during FWD 9 and FWD 11 (May and July 2015).

Table 5-3(b) compares the $E_p$of insulated sections with the CS for each season of a year. The comparison indicates that the B.ash section closely followed the CS and its difference with the CS never exceeded six percent within one year of data monitoring, while the Poly-10 and Poly-5 sections deducted at least 21 and 7 percent of the load bearing capacity during winter, respectively. In warmer summer months, the difference between the load bearing capacity of the polystyrene sections and CS reached 47 percent. On average, the Poly-10, Poly-5 and B.ash sections had 34, 23 and 2 percent lower E_p than CS, respectively.

Comparing the abovementioned results with Table 5-2(c) shows that, although the Mr values of Poly-10 and Poly-5 were greater than those of CS in both summer and the recovering period, the structural capacity of these sections was significantly lower because of the insulating material type. Hence, the interaction of subgrade protection and the pavement layer's stiffness reduction should be considered in the design of insulated pavements. It is worth mentioning that increasing the thickness of the polystyrene layer from 5 cm to 10 cm leads to decreasing the E_p value from 88 percent to 75 percent compared to the CS. In another words, doubling the thickness of polystyrene layers also doubles the E_p loss.

Table 5-3: (a) Back-calculated E_p for all FWD tests; (b) Ratio of back-calculated E_p of different sections to the CS value during similar FWD test.

(a) Ep (MPa) **(a)**

Test ID	FWD 1 17-Jul-14	FWD 2 5-Sep-14	FWD 3 17-Oct-14	FWD 4 18-Nov-14	FWD 5 14-Mar-15	FWD 6 8-Apr-15	FWD 7 21-Apr-15	FWD 8 5-May-15	FWD 9 25-May-15	FWD 10 5-Jun-15	FWD 11 4-Jul-15	Avr.
CS	1235	1325	1597	10388	2791	1659	1714	1449	1275	1230	980	**2,331**
B.ash	1171	1290	1468	10912	2822	1534	1711	1502	1383	1290	916	**2,364**
Poly-10	749	961	1307	9936	1753	1049	1011	716	588	625	447	**1,740**
Poly-5	841	1148	1398	11115	2196	1408	1353	1210	663	759	443	**2,048**
COV	24.0%	14.0%	8.5%	5.0%	21.5%	18.6%	23.3%	29.4%	41.9%	34.2%	41.9%	

(b) Comparing Ep with CS

Season	Summer	Fall	Winter	Recovering Period	Average
B.ash	6%	5%	-3%	-2%	**1.58%**
Poly-10	47%	23%	21%	46%	**34.19%**
Poly-5	43%	13%	7%	28%	**22.81%**

5.8. SUMMARY AND CONCLUSIONS

This chapter quantified the effects of using insulation layers on seasonal variation of subgrade modulus, as well as the structural capacity of the IRRF test road pavement during one year of data monitoring from July 2014 until July 2015. The freezing, thawing and recovering conditions of the pavement were evaluated using the temperature and moisture data. The observations resulting from this study are summarized as follows:

1- The temperature data underneath the Poly-10 section revealed that the subgrade of this section is fully protected from any freeze and/or thaw effects.

2- Investigating the moisture data indicated that the thawing in the CS started in mid-March and the section discharged extra moisture resulting from freeze-thaw by September.

3- Apart from the date of testing, the Poly-10 section always exhibited larger maximum deflection at D0, followed by the Poly-5 section. The maximum deflection at D0 of the CS and B.ash sections closely followed each other during one year of data monitoring, and their difference never exceeded six percent.

4- During one year of data monitoring, the polystyrene sections exhibited the smallest variations in resilient modulus within all sections, while monitoring the subgrade resilient modulus of the CS and B.ash sections showed to be more variable.

5- The Mr ratio (the calculated resilient modulus of each month to the resilient modulus of the test performed in September) was almost 1.00 for insulated sections in thaw season, while this ratio declined to 0.88 for the CS.

6- Poly-10 and Poly-5 sections deducted, on average, 34 and 23 percent of the structural capacity compared to the CS in summer and spring.

7- The bottom ash layer did not affect the overall performance of the pavement, as the E_p value of this section closely followed the CS, and their differences remained under six percent.

Based on the above observations, it is concluded that all the polystyrene sections outperformed the B.ash section by exhibiting the lowest variation in resilient modulus. However, the polystyrene layers may decrease the load bearing capacity of the section by half of that of the CS. Increasing the thickness of the polystyrene layer from 5 to 10 cm almost doubled the structural capacity lost, which should be considered when optimizing insulation layer thickness in design procedures. Although the B.ash section undergoes freeze-thaw effects, the ratio of resilient modulus of this

section never dropped below 0.94 during the recovering period, while this ratio in the CS dropped to 0.86. Overall, the bottom ash layer did not notably change the load bearing capacity of the section.

5.9. REFERENCE

Alberta Transportation and Utilities. (1997). *Pavement Design Manual*.

ARA, Inc., ERES Consultant Division. (2004). *Guide for Mechanistic-Empirical Design of New and Rehabilitated Pavement Structures*. Final report, NCHRP Project 1-37A.

ASTM Standard C136-06. (2006). *Standard Test Method for Sieve Analysis of Fine and Coarse Aggregates*. ASTM International, West Conshohocken, PA.

Cary Carlos E., and Claudia E. Zapata. (2011). "Resilient modulus for unsaturated unbound materials." *Road Materials and Pavement Design 12*, no. 3, 615-638.

Nixon, D., Eng, P., & Lewycky, E. D. (2011). Edmonton Experience with Bottom ash and Other Insulating Materials for Mitigation of Frost Heave Induced Damage. In *Annual Conference of the Transportation Association of Canada , Edmonton, Alberta, September 11-14*. Edmonton, Alberta.

The City of Edmonton Transportation. (2012). *Roadway Design Standard Construction Specifications* (2012 edition).

Denis St-Laurent and Marius Roy (1995). "Évaluation structurale des chausses souples dansun contexte climatique nordique: une étude avec le FWD" [Structural evaluation off flexible pavements in a northern context: A study using the FWD]. *Proceedings of the 30th Annual Conference of AQTR*, Association Québécoise du Transport et des Routes, Quebec, Canada.

Esch, D. C. (1972). Control of Permafrost Degradation beneath a Roadway by Subgrade Insulation. *Alaska Department of Transportation and Public Facilities*, Juneau, Alaska.

Salour, F., & Erlingsson, S. (2013). Investigation of a pavement structural behaviour during spring thaw using falling weight deflectometer. *Road Materials and Pavement Design 14*, no. 1, 141-158.Dore, G., Konrad, J. M., Roy, M., & Rioux, N. (1995). Use of alternative materials in pavement frost protection: Material characteristics and performance modeling. *Transportation Research Record 1481,* 63-74.Guy Doré and H. K. Zubeck, (2009). *Cold Regions Pavement Engineering* (1st edition). New York: McGraw-Hill Professional.

Havukanen, J. (1983). "The utilization of compacted coal ash in earth works." In *Proceedings of the 8th European conference on soil mechanics and foundation engineering*, vol. 2, 773-776.

Hein, D. K., and F. W. Jung. (1994). "Seasonal variations in pavement strength." In *4th International Conference, Bearing Capacity of Roads and Airfields*, vol. 1.

http://www.edmonton.ca/city_government/documents/RoadsTraffic/

Popik M.and Tighe . (2005). The Effect of Seasonal Variations on the Resilient Modulus of Unbound Materials. In *Proceedings of Annual Conference of Transportation Association of Canada*, Calgary, Alberta, 3-5.

Tavafzadeh N., Nassiri S., Shafiee M. and Bayat A. (2014). Using Field Data to Evaluate Bottom Ash as Pavement Insulation Layer. *Transportation Research Record: Journal of the Transportation Research Board 2433,* 39-47.

Rieke, R.D., Vinson T.S. and Mageau D.W. (1983). The Role of Specific Surface Area and Related Index Properties in the Frost Heave Susceptibility of Soils. *Proceedings of the Fourth International Conference on Permafrost*, National Academies Press, Washington, D.C., 1066–1071.

Saarelainen, S. (1996). Pavement Design Applying Allowable Frost Heave. *Proceedings of the Eighth International Conference on Cold Regions Engineering*, ASCE Press, Reston, VA.

Schmalzer, P.N. (2006). *Long-Term Pavement Performance Program Manual for Falling Weight Deflectometer Measurements*. Federal Highway Administration, Office of Research, Development and Technology, Turner-Fairbank Highway Research Center.

Transportation Officials. (1993). *AASHTO Guide for Design of Pavement Structures*. Vol. 1. AASHTO.

Volume_2_-_Roadways_May_2012.pdf, Accessed March 1, 2015.

Xu, B., Ranji Ranjithan, S., & Richard Kim, Y. (2002). New condition assessment procedure for asphalt pavement layers, using falling weight deflectometer deflections. *Transportation Research Record: Journal of the Transportation Research Board 1806,* 57-69.Zhi, Wen, et al. (2005). "Evaluation of EPS application to embankment of Qinghai–Tibetan railway." *Cold Regions Science and Technology 41.3,* 235-247.

6. LONG TERM PERFORMANCE EVLAUTION OF THE INSULATED PAVEMENTS

This section is accepted for publication as N.Tavafzadeh, L.Hashemian and A.Bayat., "Seasonal Response and Damage Evaluation of Pavements Comprised of Insulation Layers", International Journal of Pavement Research and Technology, 2018.

6.1. ABSTRACT

A well-known strategy for minimizing the negative effects of prolonged low temperatures on frost-susceptible subgrade is using insulation layers. Insulation layers help to mitigate the formation of ice lenses and frost heave in the subgrade.

This chapter evaluated the effect of using bottom ash (B.ash), as well as polystyrene boards, on the seasonal response of the pavement at the University of Alberta's Integrated Road Research Facility (IRRF) in Edmonton, Canada. Over the course of one year of data monitoring, from July 2014 until July 2015, different seasons (non-freeze-thaw, frozen, and recovering) were distinguished using the temperature and moisture data received from time domain reflectometers (TDRs) and thermistors installed across the pavement depth. Then, the time history data collected from falling-weight deflectometer (FWD) tests was used to identify the characteristic response of different sections.

Results revealed that the B.ash section performed similarly to the control section (CS) in terms of viscoelastic behavior, and the B.ash performed considerably better than the CS in terms of the risk of fatigue cracking. However, the polystyrene sections were more prone to damages during the summer when the hot mix asphalt (HMA) temperature was more than 25°C.

Key words: Insulation Layer, Seasonal, Bottom Ash, Polystyrene, Fatigue, Rutting

6.2. INTRODUCTION

Using insulation layers in pavement structures has become a common strategy for minimizing the effect of external factors, such as solar radiation, ambient temperature, precipitation, and water table variation, on pavement performance. As will be discussed in the following paragraphs, many reports have documented that roads comprised of insulation layers offer thermal protection and

alleviate settlement problems by minimizing freeze and/or thaw effects on the subgrade, leading to short-term performance success.

polystyrene boards have been commonly used as an insulation material in cold regions since 1967 (Penner). During the last 50 years, many roads in Alaska (Esch 1972), Quebec (Dore et al. 1995), Alberta (Nixon et al. 2011), Tibet (Zhi et al. 2005), and numerous other locations were constructed using polystyrene boards. However, more economical and environmentally friendly materials are being introduced as insulation layers in an attempt to move toward more sustainable road construction options. One of these materials is bottom ash, mainly composed of silica, alumina, and iron, which is the waste by-product of coal combustion in the boiler furnace of a power plant used for electricity generation. Performance of this material has also been investigated in different road tests in Alberta (Havukanen 1983) and Finland (David et al. 2011).

The idea of comparing the long-term performances of the aforementioned insulation layers resulted in using these materials to construct part of the Integrated Road Research Facility (IRRF) test road, which is located in Edmonton, Alberta, Canada. The thermal performance of these insulation layers (Tavafzadeh et al. 2014), their effect on seasonal subgrade modulus (Tavafzadeh 2016a), and pavement structural capacity in different seasons (Tavafzadeh 2016b), were previously investigated for the IRRF test road.

The main objective of the following study is to investigate the seasonal road damage in different insulated sections. For this reason, the pavement temperature and moisture were monitored and evaluated for one year (July 2014 to July 2015) using embedded probes at different locations in each section, and different seasons were distinguished and identified. Then, falling weight deflectometer (FWD) tests were conducted in different months on the IRRF test road, and the test results were used to quantify and compare pavement residual deformation and dissipated energy. Finally, to compare the long-term performance of different sections, the results were correlated with pavement fatigue life.

6.3. BACKGROUND

Construction for the IRRF test road started in September 2013 and opened to traffic in October 2015. Based on the data collected from weigh-in-motion (WIM) systems during the spring of 2016, the road carries about 2,000 vehicles per lane each day and approximately 38 percent of this traffic is composed of Class 5 trucks and higher according to the FHWA-13 vehicle classification

(Wyman et al. 1985). It should be mentioned that the WIM system is located on the test road, and at the time of this study, the road was not yet open to traffic.

The road pavement consists of 25 cm of dense-graded hot mix asphalt (HMA) on top of 45 cm of granular base course (GBC). In the insulated sections, a 100 cm thick bottom ash layer (B.ash) and two polystyrene layers with 10 and 5 cm thicknesses (Poly-10 and Poly-5 sections) were used as insulation layers, located between the subgrade and the GBC layer. The adjacent conventional section served as a control section (CS). The GBC layer, classified as well-graded gravel based on the Unified Soil Classification System, was comprised of crushed aggregate with a maximum particle size of 19 mm (ASTM Standard C136-06). Sieve analysis of the subgrade soil classified it as clayey sand (SC), with a maximum particle size of 0.5 mm and optimum moisture content of 16.5 based on the standard proctor test (ASTM Standard D698). The bottom ash (B.ash) was free of large lumps and impurities, with a maximum particle size of about 5 mm. The amount of non-combusted coal particles was less than 5 percent of the material by weight. The optimum moisture content of the bottom ash material was about 35 percent. The bottom ash layer was wrapped in geotextile to avoid it mixing with natural soil. This project used closed-cell Styrofoam Highload 100 extruded polystyrene boards, which have a compressive strength of 690 kPa and a minimum flexural strength of 585 kPa based on the manufacturer's data sheet.

To investigate freezing, thawing, and recovery condition of the pavement, the B.ash and Poly-10 sections were instrumented using 109AM-L thermistors. The CS was instrumented using CS650 time domain reflectometers (TDRs). The probes are installed at depths of 0.7 m (top of the subgrade), 1.7 m (about 1 meter in subgrade), and at 2.5 m from the pavement surface. Also, a thermometer was placed mid-depth in the HMA layer of the CS to capture the temperature of this layer. The TDR probes are able to collect both unfrozen volumetric water content (UVWC) and temperature data. The moisture data collected from the TDRs was corrected based on the formula obtained during the laboratory calibration. To measure strain, six asphalt strain gauges (ASGs), Model CEA-06-125UT-350, were installed at the bottom of the HMA layer of the CS in two rows. Figure 6-1 (c) shows the plan view of the location of the installed ASGs. Based on the data collected from all the gauges, the middle one, ASG-2, was selected as the representative of the strain at the bottom of the HMA layer because it showed the least noise.

A CR1000 datalogger was programmed to collect data from the moisture and temperature probes at 15 minute intervals from all of the sections. The datalogger was equipped with a spread spectrum Model RF401 radio with an antenna Model L14221 installed at an onsite trailer, where a computer transmitted the data regularly to the University of Alberta. Additionally, a high-speed CR9000X datalogger was used to collect the dynamic responses from the ASG of CS 500 Hz under current FWD tests. The datalogger is connected to the computer onsite, and the data is transmitted in the same format as the other datalogger. Figure 6-1 shows the cross-sections and thickness of layers, as well as the locations of probes, the weigh-in-motion, and the datalogger.

6.4. SEASONAL VARIATION IN PAVEMENT

Pavements in cold regions often suffer from severe low temperatures in winter. When frost reaches the unbound layers, the free water in pores starts freezing. Then, if the subgrade material is frost susceptible, it gradually sucks the water from the layers underneath, leading to the formation of ice lenses. When the ambient temperature gradually increases in spring, the melted water in the unbound layers creates high pore water pressure that reduces the load-bearing capacity of the pavement (Guide for Mechanistic–Empirical Design of New and Rehabilitated Pavement Structures 2004). The combination of low HMA resilient modulus (in high ambient temperature) and low bearing capacity of unbound layers during spring causes the pavement to undergo a considerably higher deflection than occurs during the non-freeze-thaw condition. Due to the high moisture content in the subgrade, the presence of a frost-susceptible subgrade soil underneath the pavement increases the risk of frost heave formation during winter and drastically reduces the pavement's load-bearing capacity in spring (Cary and Zapata, 2011), which also accelerates the rate of pavement deterioration. All these changes in load-bearing capacity and performance of the pavements have led to recognizing and distinguishing the seasons in pavement as vital of a process as pavement analysis.

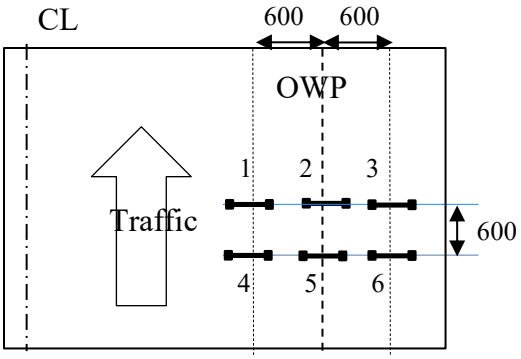
CL
600
600
OWP
Traffic
1
2
3
4
5
6
600

a)

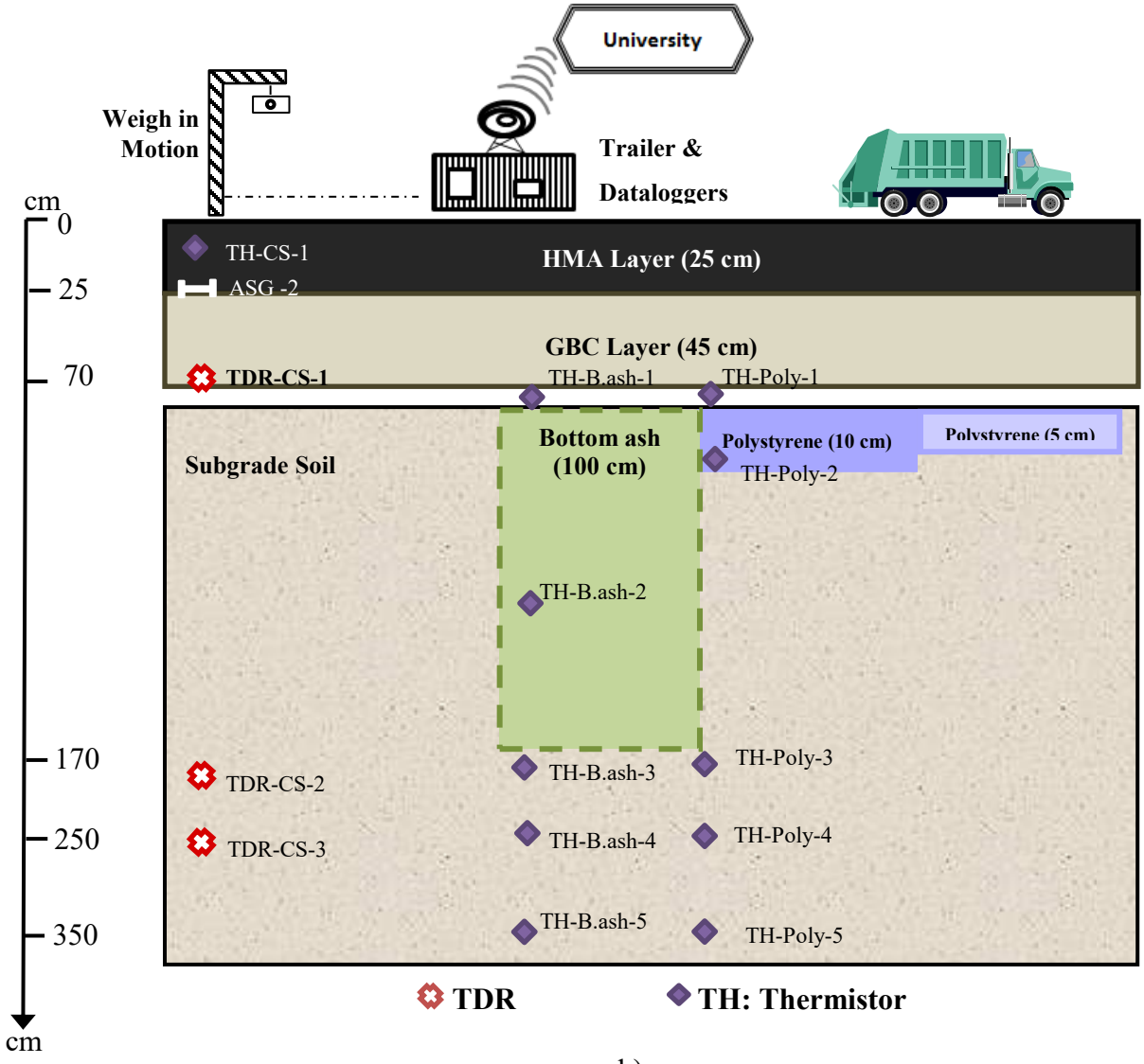
University
Weigh in Motion
Trailer & Dataloggers
cm
0
25
70
170
250
350
cm
TH-CS-1
ASG -2
HMA Layer (25 cm)
GBC Layer (45 cm)
TDR-CS-1
TH-B.ash-1
TH-Poly-1
Subgrade Soil
Bottom ash (100 cm)
Polystyrene (10 cm)
Polystyrene (5 cm)
TH-Poly-2
TH-B.ash-2
TDR-CS-2
TH-B.ash-3
TH-Poly-3
TDR-CS-3
TH-B.ash-4
TH-Poly-4
TH-B.ash-5
TH-Poly-5
TDR
TH: Thermistor

b)

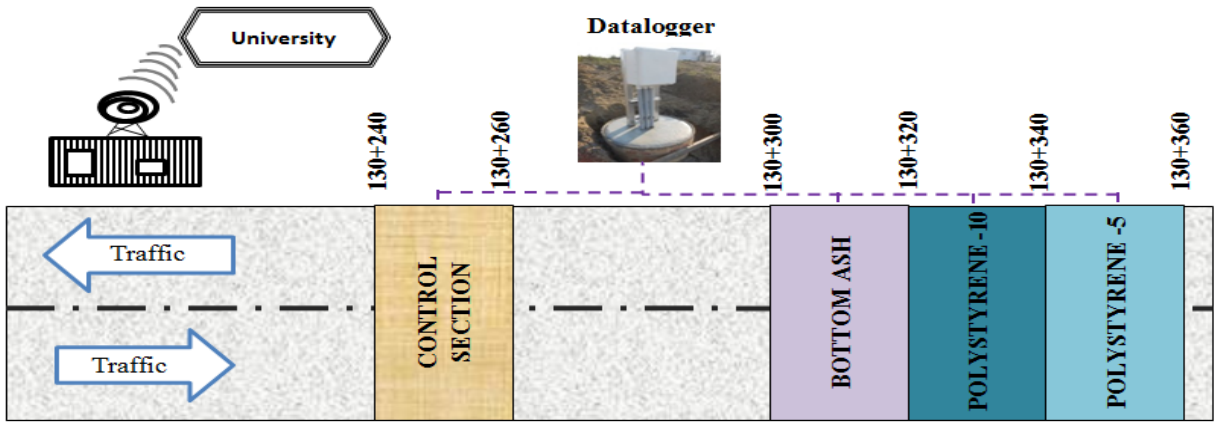

c)

Figure 6-1: a) Plan view of installed (ASGs) , b) Cross-section of the IRRF test road, c) Plan view of the test sections,

Figure 6-2 shows the temperature variation at different depth of sections along with UVWC of CS during one year of data monitoring. The discontinuity in the data from was due to technical issues with the data collection system. Evaluating the temperature data in Figure 6-2(c) indicates that frost never reached a depth of 2.6 m below the surface in any of the sections, whereas freezing at a depth of 0.7 m below the surface of the CS (Figure 6-2[a]) started on November 19, 2014, and lasted until March 11, 2015. At the same depth, freezing in the B.ash section started at the same time as the CS (November 2014) and lasted until March 18, 2015. At a depth of 1.7 m below the surface (Figure 6-2[b]), freezing of the CS ended on April 7, 2015, and the B.ash section never froze at this depth. Therefore, it can be concluded that the freezing period started in November 2014 and lasted until mid-March 2015.

The recovering period, which is the phase where the subgrade loses its extra water and re-gains its strength, started when thawing started in each section (Doré and Zubeck, 2009). This period started in the CS in mid-March 2015 (Figure 6-2[a]), as soon as the thaw reached the subgrade layer. The moisture at this depth had drained out of the subgrade by the beginning of May. At a lower depth (Figure 6-2[b]), moisture in the subgrade reached equilibrium in mid-June. It can be concluded that the recovering period in the subgrade started in mid-March 2015 and lasted until mid-June 2015.

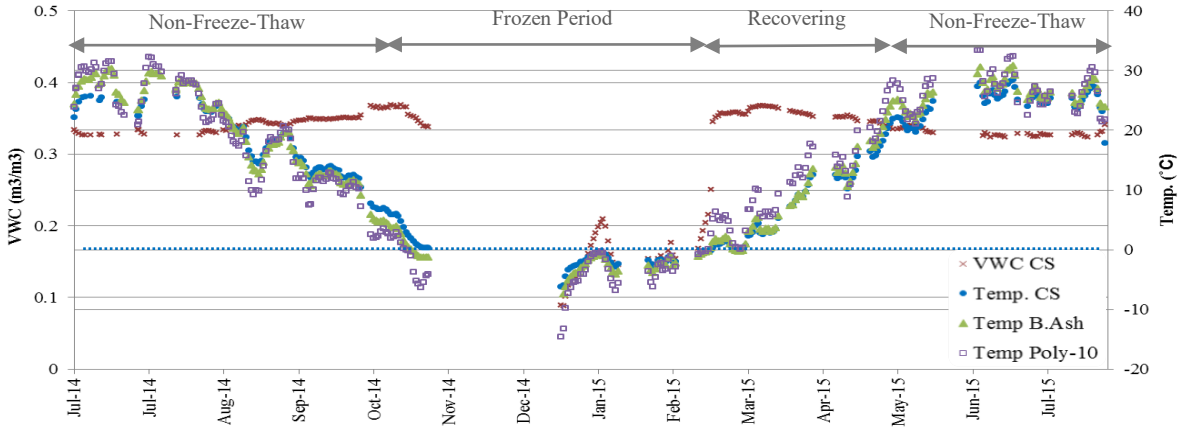

a. Top of subgrade

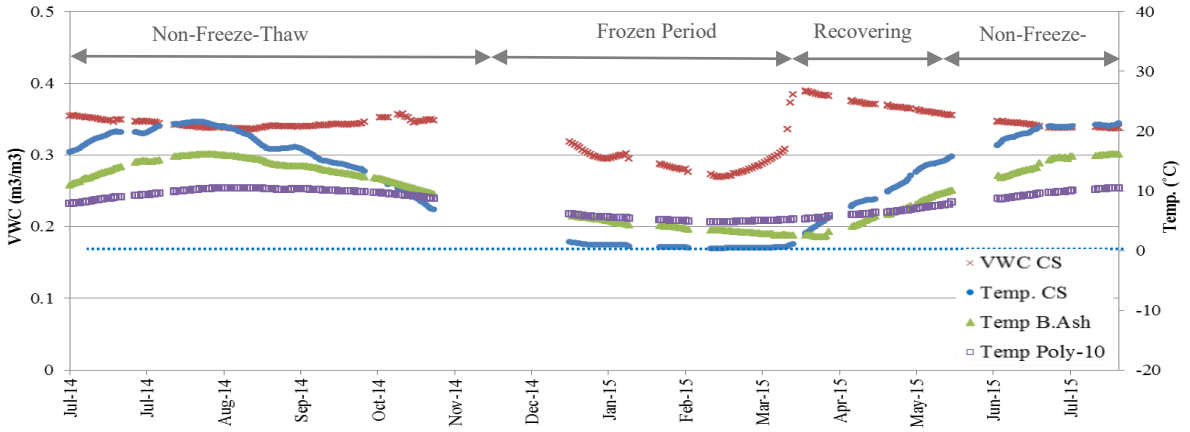

b. 1.0 m below the subgrade surface

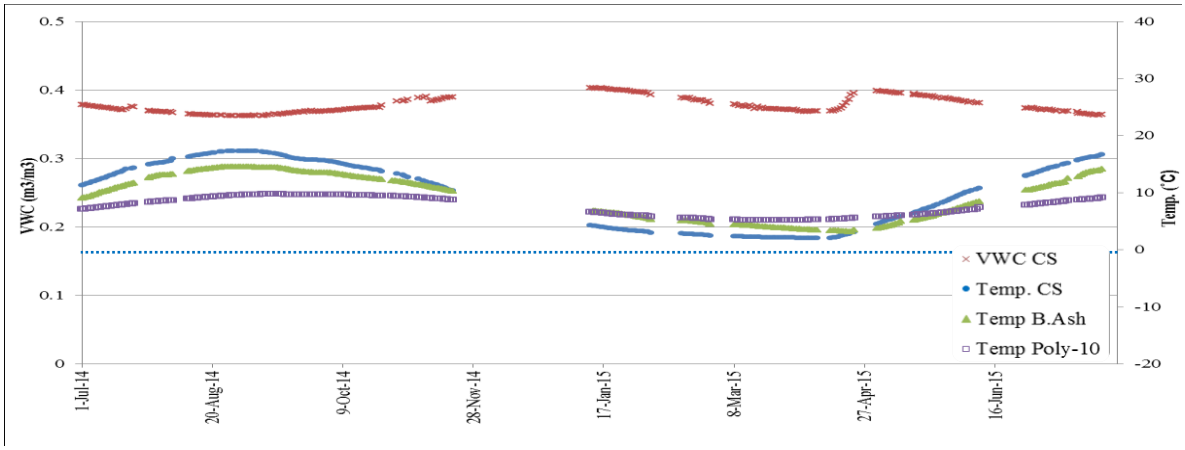

c. 1.9 m below the subgrade surface

Figure 6-2 Temperature and moisture distribution at three different depths from July 2014 until July 2015

Based on the collected temperatures at different depths of the pavement, the freezing/thawing depth of the CS and B.ash sections were calculated during the monitoring period, and results are

presented in Figure 6-3. In this figure, the duration when data was lost is illustrated using the dashed line. The data shows that, although the frost depth of the CS and B.ash sections in this period are approximately similar, freezing remained in the B.ash section for a longer period of time than the CS, and thawing in the B.ash section happened gradually due to penetration from the top. In the CS, however, thawing happened in a short period of time and occurred from both the bottom and top layers.

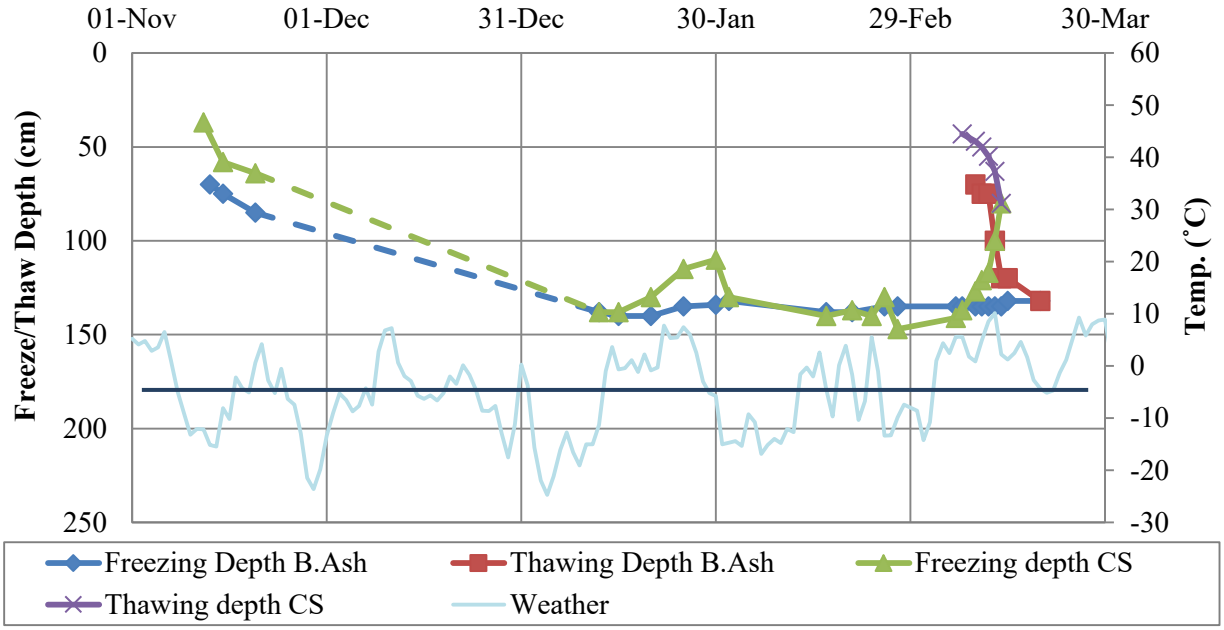

Figure 6-3 Freezing and thawing depth of the CS and B.ash sections during the monitoring period.

6.5. FALLING WEIGHT DEFLECTOMETER (FWD) TESTING

FWD, which is non-destructive, simulates the dynamic load that results from a vehicle moving on the pavement. FWD testing has become a common method for evaluating the structural capacity of pavement and back-calculating the modulus of different layers of pavement. To evaluate the risk of rutting (Widyatmoko et al. 1999) and fatigue cracking (Kim et al. 2000), a more advanced FWD application is used to investigate the long-term performance of the pavement through the time-history data collected while performing FWD.

During the monitoring period at the IRRF, multiple FWD tests were conducted on all sections of the test road using a Dynatest 8000 with a nine-sensor configuration at 0, 200, 300, 450, 600, 900, 1200, 1500, and 1800 mm from the center of the load plate. The load was applied at 20 m intervals

on the outer wheel path and the middle of the insulated sections to avoid any confusion from other sections. The FWD test was conducted at three stress levels: 26.7, 40.0, and 53.3 kN. However, in this study, the only results used for investigation purposes are of deflections under stress levels of 40.0 kN to represent the moderate traffic passing the road. Applying the precise target load on the pavement is a challenging task that may cause problems with the accuracy of the retrieved data. Based on the "Long-Term Pavement Performance Program Manual for FWD Measurements," the acceptable applied load should not exceed the range of 36.0 to 44.0 kN for the target load of 40.0 kN (Schmalzer 2006). To have a common platform of comparison, all the deflections are normalized for the target load. Using the method suggested by Xu et al. (Xu et a. 2002), the deflection basins are checked to uncover irregularities before commencing analysis. No irregularities were observed in the basins.

The one-year FWD testing on the test road started in the summer of 2014 on a monthly basis, bi-weekly during the thaw season, and continued until the summer of 2015, excluding the time when the ground was completely frozen and ambient temperature was less than -10°C. HMA temperature was measured 12 cm below the surface (approximately mid-depth of the pavement) using the installed thermistors. The exact dates of FWD tests, HMA temperature, and the distinguished seasons are shown in Table 6-1.

6.6. EVALUATION OF FWD DATA

6.6.1. Load-Deflection Response Data

For each FWD test, the applied load and the deflection history data was collected every 5 milliseconds (ms) for the duration of 60 ms. Figure 6-4 illustrates the load impulsion and deflection data from the sensor immediately underneath the load plate for different sections. For ease of comparison and optimizing the volume of presented data, only one test is selected as a representative for each season (non-freeze-thaw, frozen, recovering period).

It is clear that apart from the date of FWD testing, the generated load impulse had a duration of about 30 ms, which is compatible with other researchers' observations from other sites (Xu et al. 2002). Both loading time and load pulse shape can affect the maximum deflection observed during each test. The effect is more pronounced for materials with viscoelastic behavior (Deblois et al. 2010). As shown in Figure 6-4[a and c], two distinguished load peaks are observed during the

recovering period, while the peaks occur much closer together during the freezing period (Figure 6-4[b]). The phenomena occurred because all the sections display more viscoelastic behavior during the recovering period and warm weather as opposed to winter, which causes creep to occur during the load application. It is worth mentioning that two of the tests conducted in winter and in the recovering, Figure 6-4(b and c), had approximately similar HMA temperature (9 and 11°C); however, there is a clear difference between the response of these two tests that resulted mainly from the condition (frozen to thawed) of the underneath layers.

TABLE 6-1 Date and Temperature of the HMA Layer during Each Test in Different Seasons

Test ID	Period	Date	HMA Temp. (°C)
FWD 1	Non-Freeze-Thaw	17-Jul-14	22
FWD 2		5-Sep-14	20
FWD 3		17-Oct-14	10
FWD 4	Frozen	18-Nov-14	-1
FWD 5		14-Mar-15	9
FWD 6	Recovering	8-Apr-15	11
FWD 7		21-Apr-15	18
FWD 8		5-May-15	19
FWD 9		25-May-15	31
FWD 10		5-Jun-15	30
FWD 11	Non-Freeze-Thaw	4-Jul-15	37

Based on the load-deflection time history, Figure 6-5 presents the residual deflection 50 ms after the load application. The total data acquisition time is about 60 ms, and it is possible that the sections were still moving even after the collection of data; therefore, more time may be needed for the sections to recover fully from the loading pulse to show the final residual deflection (*21*). The residual deflection will follow the same trend as the temperature, and the polystyrene sections will always show a higher residual deflection as a result of having a soft layer. However, a clear exception is observed at the beginning of the recovering period (FWD 6 to FWD 8). During this period, the insulated sections exhibited less residual deflections compared to the CS, except for

the Poly-10 section in FWD 8 when the HMA temperature increased. The phenomenon is an indicator that during the critical recovering period, before the HMA temperature rises too high, the insulated sections are less prone to residual deflection and, consequently, rutting damages on the pavement.

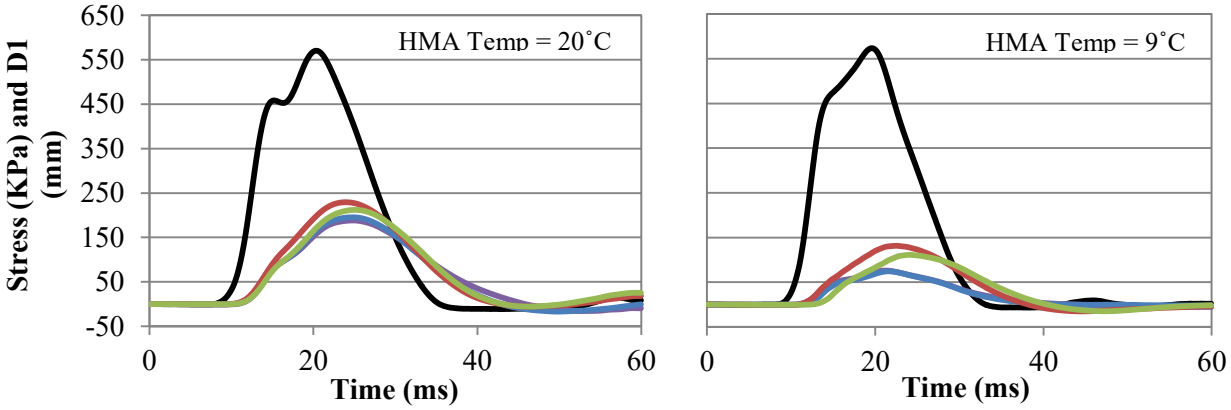

a) FWD 2 during non-freeze-thaw season

b) FWD 5 during frozen period

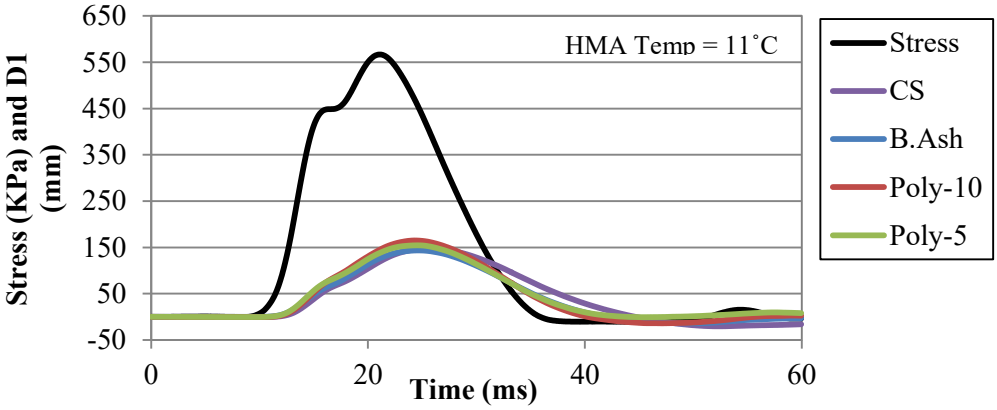

c) FWD 6 during recovering period

Figure 6-4 Load and deflection history over time for different test sections

During summer, when the HMA temperature reached 25°C or higher, the residual deflections of the polystyrene sections were considerably higher than that of the CS, which shows these sections' tendency toward more plastic deformation. This phenomenon may be correlated to a higher HMA temperature in the insulated section compared to the CS during the summer (*9*), which results in lower modulus of HMA in the insulated sections.

Apart from the date and temperature of FWD testing, the B.ash section closely followed the CS, which is an indicator of the similar pavement behavior of these two sections. Overall, the average

residual deflection of the B.ash sections is 12 percent less than the residual deflection of the CS, whereas the average of the polystyrene sections showed their residual deflection value as twice the value of the CS.

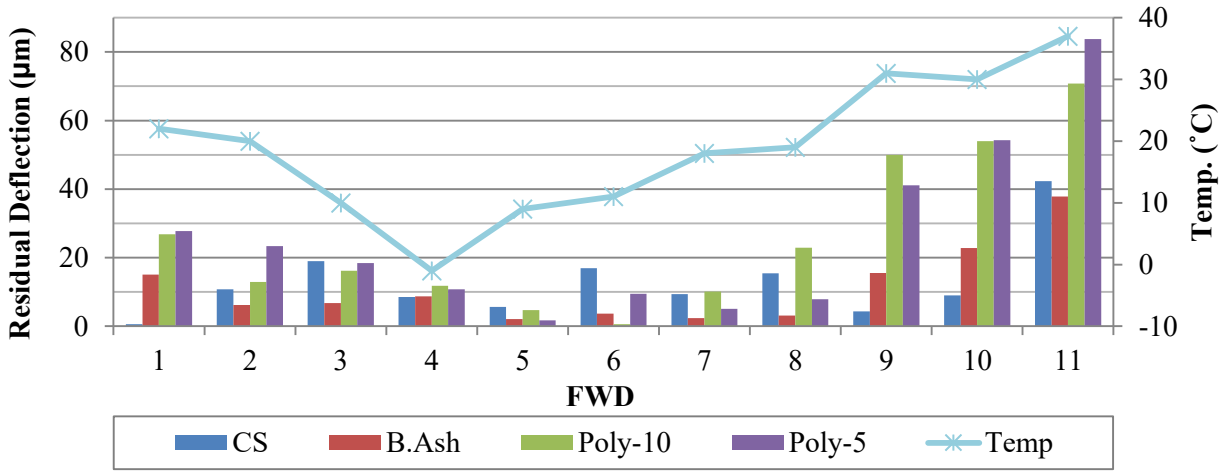

Figure 6-5 Residual deflection of different sections at time 50 ms after load application.

6.6.2. Dissipated Energy

Dissipated energy is defined as the surface area limited to the boundary of the hysteresis loop formed in a FWD load-deflection graph (Quintus and Killingsworth, 1998). The hysteresis consists of two loops: 1) loading, when the deflection is increasing and 2) unloading, when the pavement tends to return to its initial position (St-Laurent 1995). The shape of a hysteresis graph is affected by the HMA thickness and the type of pavement. It is also an indicator of the elastic and viscoelastic behavior of the material. If the unloading and loading overlap, the material is purely elastic and the higher area underneath the graph is a reflection of more viscoelastic behavior (Ghuzlan and Carpenter, 2006).

Figure 6-6 shows the hysteresis graphs for three FWD tests representing different seasons, and a noticeable difference exists between the hysteresis loops of different seasons. Particularly in winter, the FWD (Figure 6-6[b]) showed the tendency of the polystyrene sections to display more elastic behavior than the CS and B.ash sections. This is because the lower HMA temperature forced this layer to exhibit less viscose behavior. Additionally, apart from the date of testing, the polystyrene sections always exhibited higher deflection and higher dissipated energy compared to other sections.

The amount of dissipated energy for each section during different FWD tests is calculated and presented in Figure 6-7. The figure shows that the dissipated energy followed the same trend as the HMA temperature. The pavement tended to behave more elastically during winter by dissipating less energy, and it tended to act more viscoelastic during the summer and recovering period. The viscoelastic behavior of the polystyrene sections was more pronounced during summer (FWD 9 to FWD 11) when the HMA temperature was higher than 25°C.

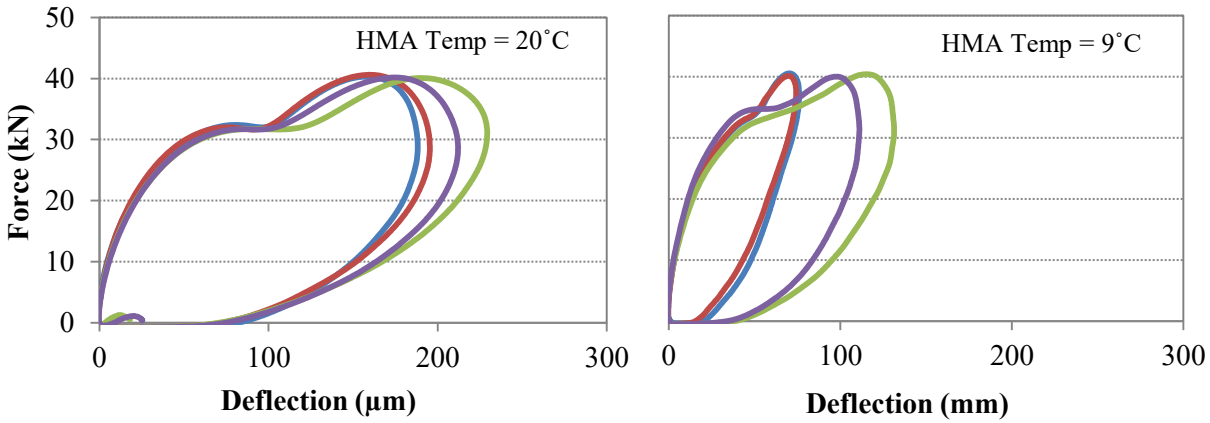

a) FWD 2 during non-freeze-thaw season

b) FWD 5 during frozen period

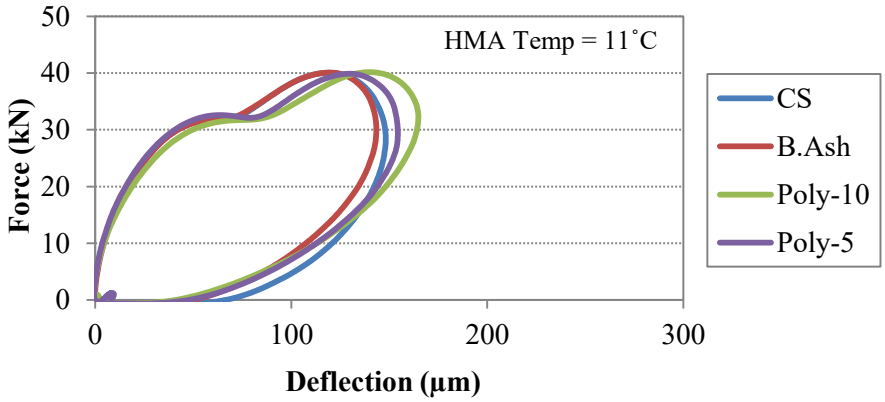

b) FWD 6 during recovering period

Figure 6-6 Dissipated energy over time for different test sections

Considering the fact that higher dissipated energy is an indicator of the lower resistance to permanent deformation or rutting (Widyatmoko et al, 1999), all the sections performed approximately the same during the monitoring period, except for the polystyrene sections when the HMA temperature reached over 25°C. During the last three tests, the average dissipated energy of the polystyrene sections was approximately 45 percent higher than the value of that for the CS,

whereas the B.ash section maintained a maximum difference of 10 percent during the monitoring period.

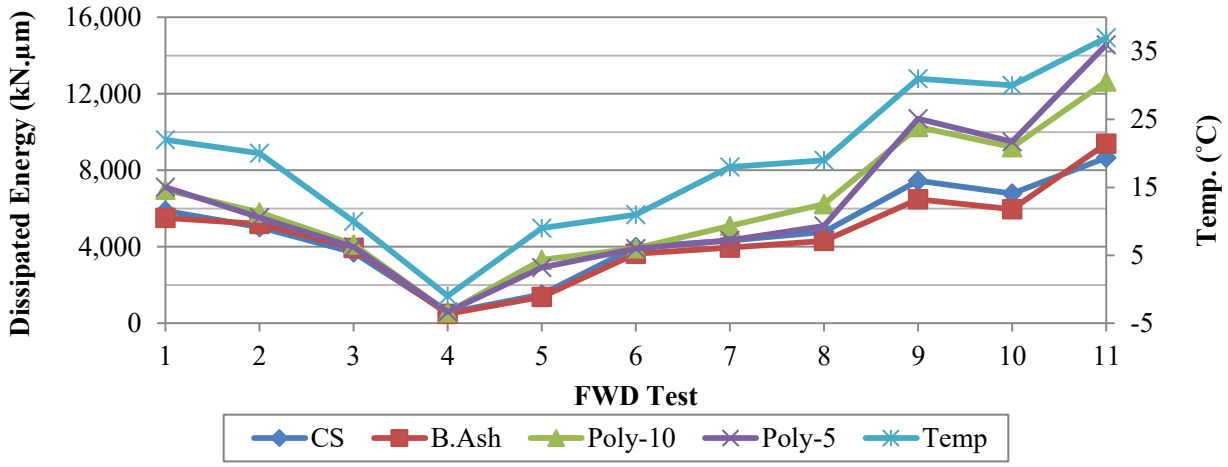

Figure 6-7 The dissipated energy evolution during monitoring period for different sections.

6.6.3. Pavement Fatigue Performance

Previously, researchers utilized the concept of dissipated energy to describe the fatigue behavior of viscoelastic materials such as asphalt mixtures (Dijk 1976) (Dijk and Visser, 1977) (Chomton and Valayer, 1972). There is an assumption behind this description that all dissipated energy produces damages in the material (Shen and Carpenter, 2007). However, this assumption cannot explain the reality of what happens to the pavement during the loading condition when some of the energy will be dissipated in the form of heat, plasticity, and other forms, and does not contribute to damage (Redles et al. 2016). Despite the abovementioned deficiency, the researchers agree that the dissipated energy can be correlated to the number of load repetitions until fatigue cracking occurs (N_f) (St-Laurent and Roy, 1995). This connection may lead to a correlation between the dissipated energy and the fatigue life of the test sections. It is possible to calculate the repeated number of loads (N_f) using the Asphalt Institute (AI) model (Asphalt Institute, 1982) based on the tensile strain at the bottom of the HMA layer. Equation 6-1 shows the fatigue life prediction model used in the AI model:

$$N_f = 0.00432 \times C \left(\frac{1}{\varepsilon_t}\right)^{3.291} \left(\frac{1}{E_{HMA}}\right)^{0.854} \quad \text{Equation 6-1}$$

where, N_f = number of load repetitions before fatigue cracking, C = laboratory to field adjustment factor, ε_t is the tensile strain at the bottom of the HMA, and E_{HMA} is the elastic modulus of HMA

(psi). The ε_t is measured at the bottom of the HMA layer using the ASG-2 installed in the CS (Figure 6-1[b]). The elastic modulus of HMA can be obtained from the developed master curve in the laboratory based on AASHTO TP79 (2009) (Figure 6-8 [a]).

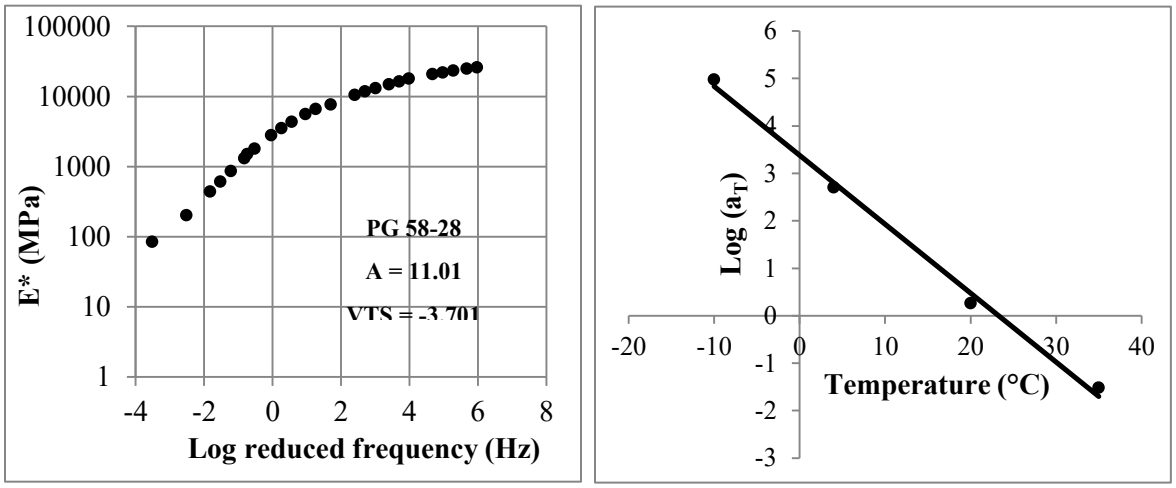

(a) **(b)**

Figure 6-8 (a) Master curve and (b) shift factor for the HMA *(*Shafiee et al. 2015*)*

As mentioned before, the FWD pulse duration for all tests is about 30 ms, which is associated with 33 Hz loading frequency. For converting the Mr* to the elastic modulus of HMA during each FWD test, a temperature shift factor is used which is presented in Figure 6-8[b]. The shift factor converts the frequency using the following equation:

$$f_r = f.a_T \qquad \text{Equation 6-2}$$

where, f_r is the frequency of loading at desired temperature, T is temperature of interest, and a_T is the shift factor as a function of temperature. Table 6-2 presents the shift factors and dynamic modulus of CS during each FWD test. Using Equation 6-1, the number of load repetitions until fatigue occurs is calculated and its correlation with dissipated energy (DE) is extracted. The correlation is illustrated in Figure 6-9.

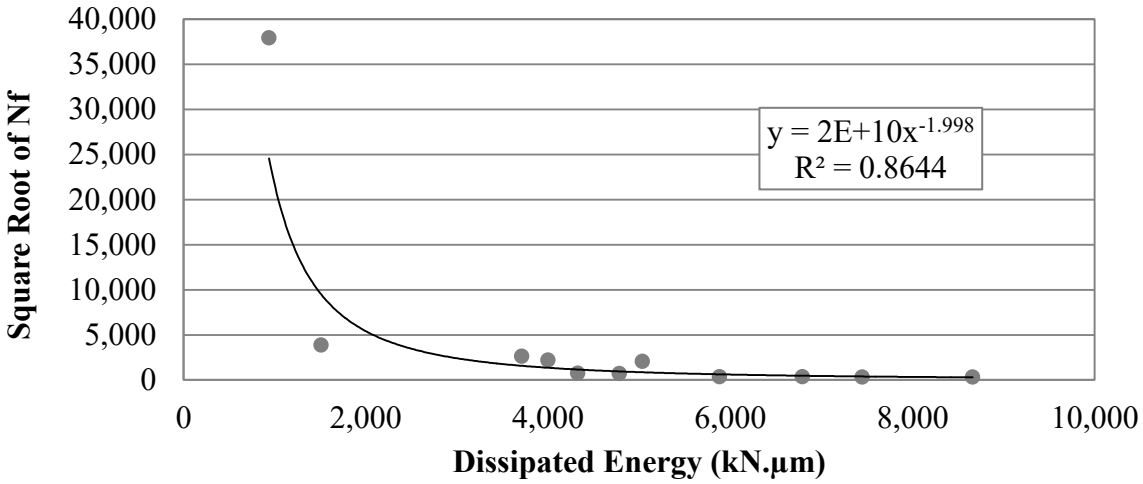

Figure 6-9 Correlation between the dissipated energy and N_f.

Since the same HMA, granular base materials, and thicknesses were used on the entirety of the IRRF test road, it is assumed the same correlation exists between the dissipated energy (DE) and N_f of the different sections as exists in the CS. Based on this assumption, and using the formula developed in Figure 6-9, the number of load applications until fatigue occurs in sections other than the CS was calculated using the dissipated energy of each section for each FWD test. The values of the CS are also recalculated based on the developed formula to provide a platform for different section comparisons. Then, the average seasonal values were calculated. The results are shown in Table 6-3. As expected, the freezing period shows the highest N_f for all sections, which resulted from low HMA temperatures and frozen ground. In the CS, the recovering period and non-freeze-thaw season have approximately the same N_f values. The phenomenon may occur as a result of low subgrade resilient modulus during the recovering period and low HMA modulus in summer due to high temperatures. In contrast, for the insulated sections, the combination of a stable subgrade and low ambient temperature during the recovering period resulted in higher N_f values than the non-freeze-thaw season, which included hot summers. Having the least coefficient of variation during non-freeze-thaw season is an indicator of similarity in performance of all sections during the non-freeze-thaw season.

TABLE 6-2 Shift factor, Frequency and dynamic modulus of pavement for each FWD

Test ID	Summer	Fall		Winter		Recovering Period					Summer
	FWD 1	FWD 2	FWD 3	FWD 4	FWD 5	FWD 6	FWD 7	FWD 8	FWD 9	FWD 10	FWD 11
	17-Jul-14	5-Sep-14	17-Oct-14	18-Nov-14	14-Mar-15	8-Apr-15	21-Apr-15	5-May-15	25-May-15	5-Jun-15	4-Jul-15
Temp. (˚C)	22.0	20.0	10.0	-1.0	9.0	11.0	18.0	19.0	31.0	30.0	37.0
a_T	1.0	2.0	66.7	3133.3	94.6	47.0	4.1	2.9	0.0	0.1	0.0
f_r (ms)	33.0	66.5	2200.5	103,398.4	3,122.6	1,550.7	133.8	94.3	1.4	2.0	0.2
Mr* **(Mpa)**	7,150	8,150	14,500	22,000	15,500	14,000	9,300	8,800	3,000	3,600	1,500

TABLE 6-3 Re-calculated N_f using the developed formula for different seasons

Season	Non-Freeze-Thaw Period	Freezing Period	Recovering Period
CS	648,897	2,264,929,791	784,000
B.ash	695,807	3,329,049,136	1,158,117
Poly-10	495,569	1,954,268,623	545,276
Poly-5	558,039	1,638,600,272	726,143
COV	15.0%	32.0%	32.0%

TABLE 6-4 Comparison of re-calculated N_f of different sections with the value of that of CS

Season	Non-Freeze-Thaw Period	Freezing Period	Recovering Period	Average
B.ash	107%	147%	148%	**134%**
Poly-10	76%	86%	70%	**77%**
Poly-5	86%	72%	93%	**84%**

Table 6-4 provides a seasonal comparison of N_f values of insulated sections with the values of that of CS. Apart from the seasons, the B.ash section showed a higher N_f value compared to the CS. The highest similarity was observed in the non-freeze-thaw season, and during the freezing and recovering period, the B.ash section outperformed the CS. On average, the Poly-10 and Poly-5 sections had N_f values of 77 and 84 percent of the value of that of the CS.

6.7. SUMMARY AND CONCLUSIONS

This chapter investigated the effects that insulation layers had on seasonal response variations during one year of data monitoring at the IRRF test road in Edmonton, Alberta, Canada. Different seasons were identified and distinguished using thermistors and moisture probes installed throughout the pavement depth. FWD testing time history data was applied to evaluate and characterize the behavior of the different sections throughout the year. Study observations are summarized as follows:

1- Analyzing the temperature data indicated that freezing began in the sections in mid-November and lasted until mid-March when thawing occurred in the pavement. Using the moisture data, the recovering period is identified as mid-March until mid-June.
2- Load-deflection response data revealed more viscoelastic behavior during summer and the recovering period compared to the winter season for all the sections.
3- The average residual deflection of the B.ash sections is 12 percent less than the value of that of the CS, whereas this average for the polystyrene sections was twice the value of the CS.
4- For all the sections, the dissipated energy followed the same trend as the HMA temperature.
5- The viscoelastic behavior of the polystyrene sections was more pronounced during summer. In this period, the average dissipated energy of the polystyrene sections was approximately 45 percent higher than the CS during the last three tests.
6- The B.ash section, in terms of dissipated energy, performed better than the CS during the monitoring period, with a maximum difference of 10 percent.
7- The B.ash section could carry approximately twice the number of load applications until it reached fatigue cracking compared to the CS during freezing and the critical recovering season.
8- The Poly-10 and Poly-5 sections could carry 77 and 84 percent, respectively, of the number of load applications until they reach the fatigue cracking compared to the CS.

Based on the above observations, one can conclude that the B.ash section performed similarly to the CS in terms of viscoelastic behavior, and performed considerably better than the CS in terms of fatigue cracking risk. However, the polystyrene sections were more prone to damages, especially during the summer when the HMA temperature was more than 25°C.

6.8. ACKNOWLEDGMENTS

The authors greatly appreciate Alberta Transportation, the City of Edmonton, and Alberta Recycling for their financial and in-kind support of this project. The authors also acknowledge Alberta Transportation for conducting the FWD tests for this study and ISL Engineering, Land Services, and DeFord Contracting for coordinating the construction and instrumentation activities of the IRRF's test road. The authors would also like to thank Ms. Sheena Moore for lending her editorial assistance in the review of this chapter.

6.9. REFERENCE

AASHTO. (2009). Determining the Dynamic Modulus and Flow Number for Hot Mix Asphalt (HMA) Using the Asphalt Mixture Performance Tester (AMPT), *AASHTO TP79-09*, American Association of State Highway and Transportation Official.

ARA, Inc., ERES Consultant Division. (2004) *Guide for Mechanistic–Empirical Design of New and Rehabilitated Pavement Structures*. Final report, NCHRP Project 1-37A.

Asphalt Institute. (1982) Research and Development of the Asphalt Institute's Thickness Design Manual (MS-1), 9th edition. Research Report 82–2.

ASTM Standard C136-06. (1984) *Standard Test Method for Sieve Analysis of Fine and Coarse Aggregates*. ASTM International, West Conshohocken, PA.

ASTM Standard D698. (2012) *Standard Test Methods for Laboratory Compaction Characteristics of Soil Using Standard Effort*. ASTM International, West Conshohocken, PA.

Cary, C. E., & Zapata, C. E. (2011). *Resilient modulus for unsaturated unbound materials*. Road Materials and Pavement Design, 12(3), 615-638.

Nixon, D., Eng, P., & Lewycky, E. D. (2011). Edmonton Experience with Bottom ash and Other Insulating Materials for Mitigation of Frost Heave Induced Damage. In *Annual Conference of the Transportation Association of Canada , Edmonton, Alberta, September 11-14*. Edmonton, Alberta.Deblois, K., Bilodeau J., and Dore G. (2010) Use of Falling Weight Deflectometer Time History Data for the Analysis of Seasonal Variation in Pavement Response. *Canadian Journal of Civil Engineering* 37.9, pp 1224-1231.DOI:10.1139/L10-069.

St-Laurent D. and Marius R. (1995) Évaluation structurale des chausses souples dansun contexte climatique nordique: une étude avec le FWD [Structural evaluation off flexible pavements in a northern context: A study using the FWD]. *Proceedings of the 30th Annual Conference of AQTR*, Association Québécoise du Transport et des Routes, Quebec, Canada.

Doré, G. and Zubeck H.K. (2009) *Cold Regions Pavement Engineering.* McGraw-Hill Education, New York.

Dore, G., Konrad J.M., Roy M., and Rioux N.(1995) Use of Alternative Materials in Pavement Frost Protection: Material Characteristics and Performance Modeling. In *Transportation Research Record: Journal of the Transportation Research Board, No. 1481*, Transportation Research Board of the National Academies, Washington, D.C., pp. 63–74.

Esch, D. C. (1972) *Control of Permafrost Degradation beneath a Roadway by Subgrade Insulation*. State of Alaska Department of Highways.

Chomton G.and Valayer P.J. (1972) Applied Rheology of Asphalt Mixes Practical Application. In Proceedings of Third International Conference on the Structural Design of Asphalt Pavements, London

Ghuzlan, K.A. and Carpenter S.H. (2006) Fatigue Damage Analysis in Asphalt Concrete Mixtures Using the Dissipated Energy Approach. *Canadian Journal of Civil Engineering*, Vol. 33, No. 7, pp. 890–901.

Havukanen, J. (1983) The utilization of compacted coal ash in earth works. In *Proceedings of the 8th European conference on soil mechanics and foundation engineering*, vol. 2, pp. 773-776.

Kim, Y. R., B. Xu, and Kim Y. (2000) A New Backcalculation Procedure Based on Dispersion Analysis of FWD Time-History Deflections and Surface Wave Measurements Using Artificial Neural Networks. In *Nondestructive Testing of Pavements and Backcalculation of Moduli*: *Third Volume*. ASTM International.

Nixon, D., Eng, P., & Lewycky, E. D. (2011). Edmonton Experience with Bottom ash and Other Insulating Materials for Mitigation of Frost Heave Induced Damage. In *Annual Conference of the Transportation Association of Canada , Edmonton, Alberta, September 11-14*. Edmonton, Alberta.

Penner, E. (1976) Experimental Pavement Structures Insulated with a Polyurethane and Extruded Polystyrene Foam. *Physics of Snow and Ice: Proceedings*, pp. 1311–1322.

Redles, T. A., Ali, A. W., Mehta, Y. A., & Cleary, D. (2016) Estimating Fatigue Endurance Limits of Flexible Airfield Pavements. International Journal of Pavement Engineering, pp. 1–9. DOI: 10.1080/10298436.2016.1176168Shafiee, M.H., Hashemian L., and Bayat A. (2015) Seasonal Analysis of Flexible Pavement Response to Falling Weight Deflectometer." *International Journal of Pavement Research and Technology* 8, no. 5: 346-352.

Schmalzer, P.(2006) *Long-Term Pavement Performance Program Manual for Falling Weight Deflectometer Measurements*. Federal Highway Administration, Office of Research, Development and Technology, Turner-Fairbank Highway Research Center.

Shen, S., & Carpenter, S. H. (2007) Dissipated Energy Concepts for HMA Performance: Fatigue and Healing. Technical Report of Research Supported by the Cooperative Agreement DOT 05-C-AT-UIUC-COE.St-Laurent, D. (1995) *Évaluation Structurale de Chaussées Souples dans un Contexte Climatique Nordique*. Universite Laval.

Tavafzadeh, N., Nassiri S., Shafiee M.H., and Bayat A. (2014) Using Field Data to Evaluate Bottom Ash as Pavement Insulation Layer. In *Transportation Research Record: Journal of the*

Transportation Research Board, No. 2433, Transportation Research Board of the National Academies, Washington, D.C., pp. 39–47.

Tavafzadeh, N., Hashemian L, and Bayat A. (2016 a)The Effect of Insulation Layers on Pavement Strength During Non-Freeze-Thaw Season. *International Journal of Pavement Engineering*, in press.

Tavafzadeh, N., Hashemian L, and Bayat A. (2016 b)The Effect of Seasonal Variation on Load Bearing Capacity of Pavements Comprised of Insulation Layers. In *Transportation Research Record: Journal of the Transportation Research Board of the National Academies*, Washington, D.C., DOI: 10.3141/2579-10.

Van Dijk W/, (1975) Practical Fatigue Characterization of Bituminous Mixes. *Proceedings of the Association of Asphalt Paving Technologists (AAPT)*, vol. 44, p. 388.

Van Dijk W. and Visser W. (1977) The Energy Approach to Fatigue for Pavement Design. *Proceedings of the Association of Asphalt Paving Technologists (AAPT)*. vol. 46, pp. 1-40.

Von Quintus, H., and Killingsworth B. (1998) *Analyses Relating to Pavement Material Characterizations and Their Effects on Pavement Performance*. No. FHWA-RD-97-085.

Widyatmoko, I., C. Ellis, and J.M. Read. (1999) The Application of the Dissipated Energy Method for Assessing the Performance of Polymer-Modified Bituminous Mixtures. *Materials and Structures*, Vol. 32, No. 4, pp. 304–310.

Wyman, J. H., Braley, G. A., & Stevens, R. I. (1985) *Field Evaluation of FHWA Vehicle Classification Categories*. *Executive Summary (No. 8405) Maine Department of Transportation, Bureau of Highways, Materials and Research* Division.Xu, B., Ranji Ranjithan, S., & Richard Kim, Y.(2002) New Condition Assessment Procedure for Asphalt Pavement Layers, Using Falling Weight Deflectometer Deflections. In *Transportation Research Record: Journal of the Transportation Research Board, No. 1806*, Transportation Research Board of the National Academies, Washington, DC, pp. 57–69.

Zhi, W., S. Yu, M. Wei, and Jilin Q. (2005) Evaluation of EPS Application to Embankment of Qinghai–Tibetan Railway. *Cold Regions Science and Technology*, Vol. 41, No. 3, pp. 235–247.

7. THICKNESS OPTIMIZATION OF INSULATION LAYER

This section is accepted for publication as, N.Tavafzadeh, M. Ahmadian N. M., L.Hashemian and A.Bayat. Capital Cost Comparison of Pavements Comprised of Insulation Layers- A Case Study in Edmonton, Canada, ASCE's Journal of Construction Engineering and Management, 2018.

7.1. ABSTRACT

Using insulation layers is the go-to strategy for alleviating winter frost heave and subgrade weakening during spring thaw, but the cost-effectiveness of using insulation layers compared to conventional methods needs to be evaluated.

This study quantifies (in Canadian dollars) the capital cost for construction of roads comprised of insulation layers, along with substituting the subgrade material with high quality granular base course (GBC) material based on a test road in Edmonton, Alberta, Canada.

The insulated sections of the test road consist of bottom ash and polystyrene boards. Using the thermal performance analysis, the minimum required thickness for substituting the insulation layers with GBC material was calculated. This calculation was followed by a comparison of the structural capacity of the three different sections.

Comparing the capital cost of construction of different sections indicates that, at locations where the frost depth is less than 1.6 m, using bottom ash and GBC material will be more cost effective than polystyrene boards; however, this implication depends on the availability of each material and the distance of the material compared to the project location. For frost depths between 1.6 m and 3.5 m, using a bottom ash layer as insulation will be the most cost effective way to insulate the subgrade.

Keywords: Insulation Layer, Recovering Period, Resilient Modulus, Effective Modulus of Pavement, Bottom Ash, Polystyrene, Construction Cost.

7.2. INTRODUCTION

Seasonal variation in solar radiation, ambient temperature, precipitation, and a shallow water table causes pavement performance variation throughout a year (MEPDG Guide 2004). The performance alteration is more pronounced for pavements that undergo severe freeze-thaw cycles during winter and spring, especially in cold regions. Frost penetration in susceptible subgrade soils

leads to heave during winter, which negatively influences the riding quality of roads. In early spring, the ice lenses formed during winter start melting and the available water in subgrade soil decreases the subgrade strength and weakens the pavement support (Doré and Zubeck 2009). This weakening leads to pavement damages, including cracks and fatigue (Doré and Zubeck 2009). In a study conducted in Quebec by St-Laurent and Roy (1995), it was revealed that the relative damage that occurred during the recovering/thawing season might be 1.5 to 3 times more than the average annual load-induced damages (St-Laurent and Roy 1995). The construction costs of pavement to withstand such a high range of temperature fluctuation, and the resultant damages, is more than the construction cost of conventional pavements, and the cost is proportional to the temperature fluctuation (Sakulich 2011). All expenses are presented in Canadian dollars.

Using insulation layers to protect the frost susceptible subgrade from frost penetration and subsequent thaw weakening is one of the strategies for diminishing the aforementioned problems. The insulation layer provides a heat barrier between the ambient and underneath layer, which controls the heat transfer and delays thawing or freezing (Zhi et al. 2005). Polystyrene is one of the insulation materials with a long history of application in cold climates. In a project constructed at the University of Alberta's test road, the use of 10 cm of Extruded polystyrene decreased the frost depth by at least 40 percent compared to a conventional roadway (Tavafzadeh et al. 2014). In another roadway near Chitina, Alaska, 11 times lower settlement was observed in a section constructed with a 10 cm polystyrene layer compared to the normal section (Esch 1972). However, using polystyrene is not a cost effective solution. For instance, a runway rehabilitation performed in Churchill Falls Airport in Labrador under harsh conditions revealed that using polystyrene is the most costly solution (Uzarowski et al. 2013). The cost of rehabilitation using polystyrene injection in Wyoming is reported to be $\$210/m^2$, which is an expensive solution when comparing reconstruction using polystyrene panels of $\$206/m^2$; however, both timesaving and safety in this method are the advantages of using polystyrene injection (Edgar 2015).

In recent years, researchers have moved towards using more sustainable materials as insulation, including waste materials. Using disposable and recycled materials in pavement construction has a low environmental impact and is becoming a more accepted practice. Bottom ash, which is a waste material from the incineration of coal in power plants, is being introduced and used as an insulation layer in pavement construction. Alberta produces a large quantity of its electricity through coal power stations and, consequently, bottom ash is easily available.

Bottom ash is mainly composed of silica, alumina, and iron. A study conducted in Helsinki, Finland revealed that frost depth in bottom ash sections was 40 to 60 percent of that in conventional sections (Field et al. 2011). Furthermore, two different studies conducted in Edmonton, Alberta (2001 and 2014) illustrated that bottom ash was able to keep frost from penetrating into the subgrade, and frost depth was contained to the bottom ash layer (Havukanen 1983), (Edgar et all 2015). Application of this material was also economically investigated at Delhi Technological University, where researchers introduced pond ash as a new type of industrial waste subbase material, which can replace conventional subbase material in pavement construction. The saving in the total cost of construction was 11.5 to 12.4 percent when the subbase layer was made of pond ash with no additions. It has been revealed that using pond ash mixed with fibre and lime would save 5.2 to 13.0 percent of construction costs (Sarkar and Dawson 2015).

Preventing frost from penetrating frost-susceptible subgrade soil leads to limiting the seasonal variation in pavement (MEPDG Guide 2004). However, waste and recycled material applications need to meet specific property requirements for the intended usage. Accordingly, this would be a process of recycling and improving relevant specifications and performance. Using waste materials in road construction would be cost effective for transporting and processing the material (Huang et al. 2007). Hence, conducting a cost-benefit analysis to compare the initial and long-term cost of incorporating an insulation layer in pavement must be investigated.

The main objective of the following study is to provide a capital cost comparison for the construction of roads, which are comprised of different insulation materials, along with replacing the frost susceptible subgrade with high quality base material. Granular base course (GBC) material is an ideal substitution for frost susceptible subgrade as the material is strong and is minimally affected by freeze-thaw cycles. For the purposes of this study, it is assumed that GBC material is used instead of an insulation layer alternative. Using GBC material increases the life expectancy of the pavement, but it is important to know the minimum required thickness and how much the insulation extends the predicted lifetime of the road.

For this reason, the Integrated Road Research Facility (IRRF)'s test road, which is a unique road located in Edmonton, Alberta, is investigated. The road was equipped to measure temperature and moisture at different pavement depths using thermistors and time domain reflectometer (TDR)s, while falling weight deflectometer (FWD) tests were regularly conducted along the road and

weather data was collected from an on-site weather station. During construction, the data was collected for cost calculation.

The comparison was initially started by calculating the minimum required thickness of the substitute material. Two criteria were used for estimating the minimum required thickness: complete prevention of frost from reaching the frost susceptible subgrade; and ability to decrease the heave occurrence to zero, despite frost occurring in the subgrade. Using the calculated and available thicknesses for different materials in the test road, the effective modulus of pavement of different sections was calculated and compared to provide a platform of the structural performance of different sections. Next, the number of loads each section can carry during the pavements' lifetime was calculated and compared. To estimate the initial cost of each section, the data collected during the construction of the IRRF's test road was utilized. It is worth mentioning that comparing the life cycle cost will be another important indicative for selecting the insulation material used for road construction; however, that goal is out of the scope of this study.

7.3. TEST ROAD DESIGN AND INSTRUMENTATION

The construction of the the IRRF test road facility started in May 2012 and was completed in August 2013. Based on the data collected from WIM systems at the Edmonton Waste Management Centre during the spring of 2016, the road carries about 2,000 vehicles per lane each day. Approximately 38 percent of this traffic is composed of Class 5 trucks and higher according to the FHWA-13 vehicle classification.

Road pavement consists of 25 cm dense graded hot mix asphalt (HMA) on top of 45 cm GBC. In this test road, bottom ash and polystyrene were used as insulation layers and were located between the subgrade and the GBC layer. The adjacent conventional section served as a control section (CS). Figure 7-1 shows the location and thickness of different layers.

In accordance with the City of Edmonton's specifications for Designation-1 asphalt concrete mix, this study used two types of dense-graded HMA mixes with a maximum nominal aggregate size of 12.5 and 25 mm, based on Marshall Mix design (2015). The GBC layer was classified as well-graded gravel according to the Unified Soil Classification System (ASTM C136-06 2006). Sieve analysis of the subgrade soil resulted in a classification of clayey sand. Subgrade soil has a liquid limit of 25 and a plastic index (PI) of 9 percent.

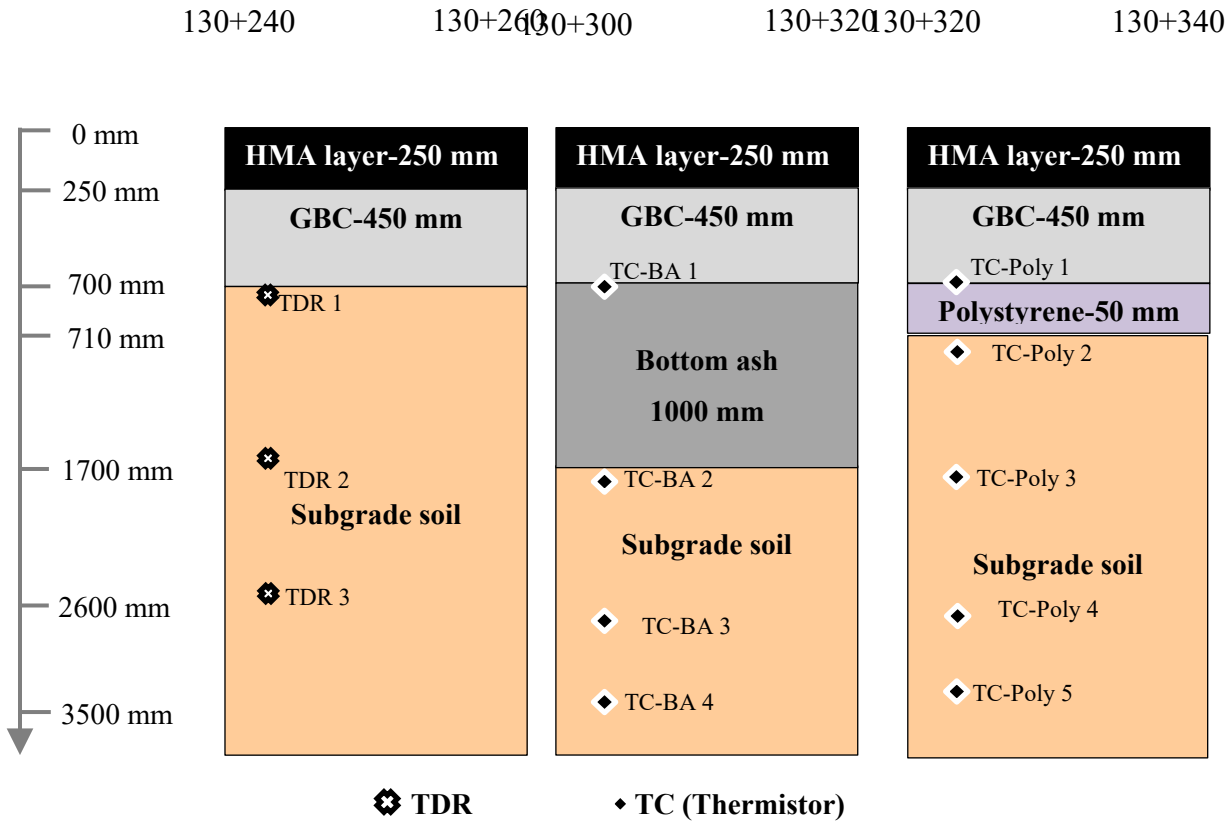

Figure 7-1: The cross section of the IRRF test sections

The bottom ash was free of large lumps and impurities. The amount of non-combusted coal particles was less than 5 percent of the material by weight, and the optimum moisture content of bottom ash is about 35 percent. The bottom ash layer was wrapped in geotextile to avoid mixing with natural soil. Table 7-1 shows the volumetric water content and dry density, as well as the thermal conductivity of the material.

This project used closed-cell Styrofoam Highload 100 extruded polystyrene boards, which have a compressive strength of 690 kPa and a minimum flexural strength of 585 kPa based on the manufacturer's data.

All the sections are instrumented using CS650 time-domain reflectometers (TDR) and thermistors from Campbell Scientific Canada at a depth of 0.7 m below the GBC layer, and depths of 1.7 m and 2.5 m in the subgrade layer (Figure 7-1). The TDR probes are able to collect both unfrozen volumetric water content and temperature data.

TABLE 7-1: Material property used at IRRF test road

Material	K (kJ/day/m/°C)	Density (ton/m^3)	VWC (m^3/m^3)	Reference
HMA	205	2.35	0.001	Measured in Lab
GBC	300	2.10	0.16	Côté & Konrad (2005)
Subgrade	189	1.85	0.32	Measured in Lab
B.ash	50	0.950	0.34	Measured in Lab
Polystyrene	0.6	-	-	Dow Solutions. (2016)

A CR1000 Datalogger was programmed to collect data from the sensors at 15-minute intervals from all of the sections. The Datalogger was equipped with a spread spectrum Model RF401 radio with an antenna Model L14221 installed at an onsite trailer, where a computer transmitted the data regularly to the University of Alberta.

7.4. PERFORMANCE EVALUATION

7.4.1. Thermal Performance

The main objective of applying insulation layers in pavement is to protect the frost susceptible subgrade from freeze and thaw damages. When a thick layer of material, such as bottom ash, is used as an insulation layer, the intention is both to protect the underneath subgrade and to substitute the top portion of frost susceptible subgrade with a non-vulnerable material. Subgrade soil has a liquid limit of 25 and a PI of 9 percent. Based on recommendations by Rieke et al. (1983), the segregation potential of the subgrade soil is calculated to be more than $200 \times 10^{-5} \frac{\text{mm}^2}{\text{S.℃}}$, which is considered moderate frost-susceptible subgrade according to Saarelainen's categorization (Saarelainen 1996) where mm^2, S, and ℃ are the units for surface area, time, and temperature.

It has been previously proven, at the IRRF test road, that 1 m of bottom ash could effectively prevent frost from penetrating into the subgrade layer (Zhi et al. 2005). The minimum required thickness of the polystyrene layer can also be computed using the equivalent thermal resistivity R-value concept (Doré and Zubeck 2009), where it is calculated using the following equation:

$$R - value = D/k \qquad \text{Equation 7-1}$$

D is the layer thickness and k is the thermal conductivity; therefore, the required thickness of polystyrene material is equal$\mathrm{D_{Poly}} = {D_{B.Ash}}/{\mathrm{k_{B.ash}}} \times \mathrm{k_{Poly}}$. The thermal conductivity of bottom ash and polystyrene material is shown in Table 7-1. Assuming 1 m of thickness of bottom ash, the minimum required thickness of the polystyrene is 1.2 cm. However, the polystyrene boards are typically produced in a minimum thickness of 5 cm, which was used in the IRRF road (Figure 7-1)."

7.4.2. Minimum Required Thickness of GBC

One of the solutions considered in order to rectify the frost-heave occurrence in pavement is to substitute the subgrade material with quality GBC. In this study apart from using the GBC as the structural component of the pavement, it is assumed to apply GBC material as substitution for frost susceptible subgrade. The first criterion for obtaining the minimum required thickness of GBC is determining its thermal performance. The thickness can be calculated based on the same concept explained in the previous section for the polystyrene layer. According to Côté and Konrad's investigation (Côté and Konrad 2005), the thermal conductivity of the GBC layer, with an optimum moisture content of 7.5 percent and more than 60 percent quartz (based on the x-ray chemical composition conducted at the University of Alberta), is assumed to be as high as 300 KJ/day/m/˚C (Table 7-1). Hence, the required thickness of the GBC layer to prevent frost penetration to the subgrade soil was calculated to be equal to 6 m.

The second criterion for estimating the GBC thickness is evaluating the risk of heaving. Based on the modified method proposed by Rajaei and Baladi (2015), the heave rate is calculated using the following formula:

$$V_H = \frac{v_i^2}{g.v_w} K_{ff}[\frac{-T_l.L}{v_m.T_a} - P_{OB} + P_{wf}] \qquad \text{Equation 7-2}$$

where V_H =the frost-heave rate (m/s), v_i =specific volumes of ice (0.00109 m^3/kg), K_{ff} =hydraulic conductivity of frozen fringe (m/s), T_l =temperature at the base of the active ice lens (˚C), L =latent heat of fusion of water (J/kg), v_m =specific volumes of water (0.001 m^3/kg), T_a =bulk freezing temperature, P_{OB} =overburden pressure (Pa), and P_{wf} = water pressure at the edge of the frozen fringe (Pa). P_{wf} can be calculated using Equation 7-3 (Rajaei and Baladi 2015).

$$P_{wf} = -g\frac{z}{v_w}\left(1 + \frac{v_w\left(V_H + \rho_{si}\Delta v\frac{dz}{dt}\right)}{v_i.K_{uf}}\right)$$ Equation 7-3

where z =distance between bottom of soil column and position of ice penetration (m); ρ_{si} =mass of ice per unit volume of soil (kg/m^3); Δv =specific volume difference of ice; water= $v_i -$; v_w = 0.00009 m^3/kg; $\frac{dz}{dt}$ =frost depth propagation rate, which is equal to 3.24^{x}10^{-6} m/s based on the temperature data collected at depth 1.7 m below the surface of the CS; k_{uf} =thermal conductivity of the unfrozen zone (W/˚C.m); and other parameters are previously defined. Z is assumed 6 m below the surface, as soil temperature becomes constant through the year at this depth (Rieger 1983). For calculating the mass of ice per unit volume of soil, it is assumed that all water in the subgrade soil is frozen. Hence:

$$\rho_{si} = \frac{m_{ice}}{V_s} = VWC \times 1.09 \times \rho_{ice} = 0.32 \times 1.09 \times 916.7 = 320\ Kg/m^3$$

where VWC was measured and shown in Table 7-1. It is assumed that the GBC layer is thick enough that no heaving occurs in the pavement, and the heave rate should be zero and no ice lenses should form in the system. Thus:

If $V_H = 0 \rightarrow P_{wf} - P_{OB} = \frac{T_l.L}{v_m.T_a}$ Equation 7-4

T_l, temperature at the base of the active ice lens, is calculated using the following formula (Rajaei and Baladi 2015):

$$\mathrm{T_l} = \mathrm{T_{ff}} - \frac{\mathrm{a}}{\mathrm{K_p}} \times \left(\rho_{\mathrm{si}}\mathrm{L}\frac{\mathrm{dz}}{\mathrm{dt}} + \frac{\mathrm{k_{uf}(T_{Bot} - T_{ff})}}{\mathrm{z}}\right)$$ Equation 7-5

where T_{ff} =temperature at the base of the frozen fringe (˚C) (Gilpin 1980), a = thickness of the frozen fringe (m), K_p =thermal conductivity of the partially frozen zone (W/˚C.m), T_{Bot} =temperatures at the bottom of the soil column (˚C), and other parameters are previously defined. Since no ice lenses will be formed in the system, below equations will be used to calculate:

$$\mathrm{a} = 0 \rightarrow \mathrm{T_l} = \mathrm{T_{ff}}$$ Equation 7-6

$$\mathrm{T_{ff}} = -\frac{8\sigma_{\mathrm{iw}}\mathrm{v_w}\mathrm{T_a}}{\mathrm{D_{10}.L}}$$ Equation 7-7

where σ_{iw} =the surface tension between ice and water which was assumed to be 0.4 (N/m); D_{10} = the soil diameter at 10 percent passing, which is equal to 0.001 m (based on the laboratory test)

and other parameters are previously defined. Using the above Equations P_{OB} is calculated as high as 55,660 Pa. The extra GBC required to impose the same overburden pressure on the subgrade layer is equal to 1.85 m.

By comparing the thicknesses obtained from the two criteria, the extra GBC layer thickness was selected to be 1.85 m to avoid frost-heave damages. Even if the frost reaches the subgrade layer of this section, heave will not occur in the system due to the high overburden pressure on the subgrade layer, making the smaller GBC value an acceptable choice.

7.4.3. Structural Performance

In the previous section, the thicknesses of different materials are re-calculated in a way to provide same or almost equivalent thermal performance up until the subgrade layer. Although all the sections of road satisfied the minimum thickness criteria, it is also important to compare their structural performances. The structural performance of the CS, bottom ash (B.ash), and polystyrene (poly-5) sections was previously investigated, and the data summarized in Table 7-2 (Tavafzadeh et al. 2016). In this table, the year is divided into three main periods: non-freeze-thaw season (when the subgrade is not affected by frost action and has recovered from extra water of thaw occurrence); freezing (when the subgrade is frozen); and the recovering period (when the thaw started in the system until the water content has reached its stable value). Following those periods, the annual average values were calculated accordingly. For the section of the road constructed using the extra GBC material, the subgrade strength (Mr value) is estimated based on the subgrade modulus of CS during the non-freeze-thaw season, which is equal to 139.6 MPa.

The SN numbers of the sections are calculated using the following formula (AASHTO 1993) and presented in Table 7-3:

$$\mathrm{SN} = 0.0045\mathrm{D}\sqrt[3]{\mathrm{E_p}} \qquad \text{Equation 7-8}$$

where *D* is the total thickness of pavement layers above the subgrade (in) and Ep is the Effective Modulus of the Pavement (psi).

The SN number of the Extra-GBC section is calculated using AASHTO formula (AASHTO 1993):

$$SN = a_1 D_1 + m_2 a_2 D_2 \qquad \text{Equation 7-9}$$

where a_1 and a_2 are the layer coefficient, D_1 and D_2 are the layer thicknesses, and m_2 is the coefficient for considering drainage for unbound layer (GBC). Based on the developed master curve, the 450,000 psi (3,100 MPa) elastic modulus of HMA layer results in $a_1 = 0.45$, and its thickness is 0.25 m. The GBC layer, by having the modulus as high as 30,000 psi (210 MPa) based on the laboratory data, expressed $a_2 = 0.14$, $m_2 = 1.05$ and its thickness is 1.85 m of extra GBC. Taking into account the usual 0.45 m GBC layer, which creates 2.3 m total thickness of GBC; hence, the SN of the extra GBC section will be as high as 17.74.

For comparing the structural capacity of the sections, the accumulated expected 18-kip equivalent single axle load is estimated for different sections using the following AASHTO formula (1993):

$$log\, W_{18} = Z_R \times S_0 + 9.36\, log(SN+1) - 0.20 + \frac{log\left[\frac{\Delta PSI}{4.2-1.5}\right]}{0.40+\frac{1094}{(SN+1)^{5.19}}} + 2.32\, log\, M_R - 8.07 \quad \text{Equation 7-10}$$

where, considering the reliability of 90 percent, Z_R= -1.28, $S_0 = 0.45$ is the standard deviation, $\Delta PSI =$ present serviceability loss that is assumed to be 1.9, and the other parameters are previously defined.

TABLE 7-2: a) Effective modulus of pavement (Ep); b) Resilient Modulus (Mr), of different sections of IRRF (modified based on the data presented in (Tavafzadeh et al. 2016)

a) Ep

Season	Average Ep (MPa)			Ep (MPa)
	Non-Freeze-Thaw Period	Freezing Period	Recovering Period	Average
CS	1,284	6,589	1,466	3113
B.ash	1,211	6,867	1,484	3187
Poly-5	957	6,655	1,079	2503

b) Mr

Season	Average Mr (MPa)			Average Mr (MPa)
	Non-Freeze-Thaw Period	Freezing Period	Recovering Period	
CS	140	305	129	191
B.ash	135	320	136	197
Poly-5	139	164	143	148

Based on the AASHTO method, the Mr values obtained from back calculating FWD tests have to be adjusted to the values representative of AASHO Road Test subgrade in the development of the

flexible design equation. The correction factor for flexible pavement is C=0.33 (Alberta Transportation and Utilities 1997). Hence, the Mr values back-calculated in Table 7-2 (b) are multiplied by 0.33 and can be used in the design procedure. Using Equation 7-9, the future traffic is estimated and presented in Table 7-3. The calculated future traffic indicates that the sections constructed using bottom ash can carry 14 percent more traffic compared to the CS during the life expectancy period. The extra GBC section can carry more than 10 thousand traffic units, and the polystyrene sections can carry less than half the traffic that the CS can carry during the lifetime of the pavement.

In another approach for comparing the performance of the different sections, the pavement life (PL) is calculated by assuming the traffic of 9 million equivalent single axle load (ESAL) for the first year and a growth rate of 4 percent. The PL of different sections are calculated and presented in Table 7-3. This table shows that B.ash and CS have approximately same life expectancy, while Poly-5 section life is almost half of the value of that of CS and B.ash sections. As expected, the PL of extra-GBC section is almost 6 times of the value of that of CS, which is resulted from substituting the subgrade material with the higher quality GBC material.

TABLE 7-3: Predicted traffic for each sections

Sections	SN	Mr (MPa)	w_{18} (×10^6)	Traffic Comparison	Pavement Life (Years)
CS	9.5	63	3,405	-	20
B.ash	9.6	65	3,886	14%	22
Poly-5	9.3	50	1,548	-55%	11
Extra GBC	17.7	49	362,570	10,547%	124

7.5. COST ESTIMATION

Pavement selection is one of the most challenging engineering decisions facing roadway administrators. Many municipalities are seeking ways to manage their budgets more efficiently while improving roadway performance (Hendrickson and Au 1989). It is important for professional designers and construction managers to have an estimation of the construction costs. From the owner's perspective, it is equally important to estimate the corresponding construction cost of each alternative for a proposed facility (Hendrickson and Au 1989). The unit costs of various construction tasks are required to estimate total costs. These unit costs are then multiplied by the expected quantities required by different projects.

Using the reports gathered during the IRRF construction and recent RS Means online (2017) construction cost database, which is valid in North America for both hourly and daily cost estimations of labor and machinery, unit initial costs of different structural and insulation material were estimated. The cost estimate for GBC, bottom ash, and polystyrene layers above subgrade are shown in Tables 7-4, 7-5, and 7-6. The subgrade is assumed finished and ready for construction of the upper layers. The cost analysis consists of the layers above the subgrade. As the section length in the IRRF project was about 20 m, the details of construction is first estimated for 20 m of the road and then the cubic meter of cost is estimated based on the applied volume. The cost estimation for each material consists of four main parts: (a) labour component, (b) machinery, (c) material, and (d) contractor's profit and overhead charges. For all road sections, the construction volume was calculated considering a width of 14.1 m and a length of 20 m. All the sections of the road (Figure 7-1) were excavated up to the desired depth with a slope of 2:1, and then filled with proper material.

The cost analysis per cubic meter of GBC layer construction is shown in Table 7-4. The GBC material was provided by a local supplier at an approximate distance of 25 km from the IRRF construction site. The material was transported to the site using 12 CY trucks. A Caterpillar dozer D7R XR series II was used for spreading the material and a tandem roller and grader were used for fine grading and compaction of the GBC layer. Lifts of 150 mm were used to spread the GBC.

The cost analysis per cubic meter of constructing the bottom ash layer is shown in Table 7-5. During construction, when the excavation was complete, a woven geotextile with an apparent open size of 0.212 mm was used to wrap the bottom ash material. A minimum overlap of 0.6 m was maintained at every seam. The geotextile was in rolls 3.66 m × 91 m. There are different sources of bottom ash material in Alberta, including Transalta Sundance Generating Station, located in Parkland County; Keephills Generating Station at Range Road 40 Kapasiwin; and Genesee Generating Station near Warburg. All the stations are located at an approximate distance of 95 km from the IRRF construction site. As bottom ash is a waste material in these generating stations, there is no cost considered for material procurement. The bottom ash was transported to the site by 20 CY trucks and a Caterpillar dozer D7R XR series II dozer spread it over the subgrade. A water tanker and vibratory roller were used for mixing water with bottom ash and compacting the layer. A combination of 500 mm, 300 mm, and 200 mm layers were used to spread bottom ash

in this section. A 500 mm layer was used whenever the bottom ash was placed on top of geotechnical instrumentation to avoid damaging the sensors with the construction equipment.

TABLE 7-4: Cost analysis of layer constructed by Granular Base Course (GBC)

Construction volume: 144 m^3					
(a)	**Labour component**	Unit	Quantity	Rate(CAD)	Amount (CAD)
	Labour	Day	1.25	303.2	379
	Equipment Operator	Day	1.87	408.8	764.46
	Truck Driver	Day	1.75	345.6	604.8
	Water Tanker Driver	Day	0.25	292.8	73.2
				Total :	1821.46
				Total per m^3 :	**12.64**
(b)	**Machinery**	Unit	Quantity	Rate(CAD)	Amount (CAD)
	Dozer	Hr	5	174.62	873.1
	Truck 12CY	Hr	14	86.35	1208.9
	Grader, 30000 lb	Hr	5	89.3	446.5
	Tandem Roller 10 ton	Hr	5	29.92	149.6
	Water Tanker	Hr	2	510	1020
				Total :	3698.1
				Total per m^3 :	**25.68**
(c)	**Material**	Unit	Quantity	Rate(CAD)	Amount (CAD)
	GBC	Ton	302.4	22	6652.8
				Total :	6652.8
				Total per m^3 :	**46.2**
				Grand Total per m^3 = [1+ CP&OC(12.5%) × (a+b+c) :	**95.08**

The cost analysis per square meter of section covered by one 5 cm board of polystyrene is shown in Table 7-6. The polystyrene boards were provided by a local supplier at 0.6 m×2.4 m, and a thickness of 5 cm. The calculation is based on the surface coverage.

It can be concluded from Tables 7-4, 7-5, and 7-6 that the cost of construction per cubic meter of the GBC and the bottom ash layers is $95.00 and $49.00, respectively. The construction cost for each square meter of road using polystyrene boards as an insulation layer on top of the subgrade was estimated to be as high as $79.00. As expected, the cost per cubic meter of bottom ash material

is lower than the GBC as there is no surcharge for procuring the waste material. The price of cubic meter of bottom ash is approximately half the value of GBC.

TABLE 7-5: Cost analysis of layer constructed by bottom ash

Construction volume: 298 m^3					
(a)	**Labour component**	Unit	Quantity	Rate(CAD)	Amount(CAD)
	Labour	Day	2	303.2	606.4
	Equipment Operator	Day	2	817.6	1635.2
	Truck Driver	Day	4.5	345.6	1555.2
	Water Tanker Driver	Day	0.5	292.8	146.4
				Total :	3943.2
				Total per m^3 :	**13.23**
(b)	**Machinery**	Unit	Quantity	Rate(CAD)	Amount(CAD)
	Dozer	Hr	8	174.62	1396.96
	Vibratory Roller	Hr	8	70.75	566
	Truck 20CY	Hr	36	92.5	3330
	Water Tanker	Hr	4	510	2040
	Total :				7332.96
	Total per m^3 :				**24.6**
(c)	**Material**	Unit	Quantity	Rate(CAD)	Amount(CAD)
	Bottom Ash (30% extra)	m^3	387.4	0	0
	Geotextile	m^2	654.88	2.65	1735.43
				Total :	1735.43
				Total per m^3 :	**5.82**
Grand Total per m^3 = [1+ CP&OC(12.5%) × (a+b+c) :					**49.1**

In the following section, the authors aim to calculate the construction cost for 1 m of the road of different sections. It is assumed that the subgrade surface is ready for executing different layers of material (Figure 7-2). The necessary thickness is calculated in the previous section based on the possibility of heave accumulation and thermal performance of materials. Hence, the construction cost of one meter of road using bottom ash, poly-5, and extra-GBC sections is calculated to be as high as $977.00, $1,334.00, and $3,946.00, respectively. By comparing the capital cost of construction of these sections, it can be concluded that the cost of construction of one meter of the

road using GBC is about four times that of the bottom ash section, and about three times the poly-5 section.

TABLE 7-6: Cost analysis of layer insulated by polystyrene

Construction surface: 338 m^2					
(a)	**Labour component**	Unit	Quantity	Rate(CAD)	Amount(CAD)
	Labour	Day	0.5	303.2	151.6
	Truck Driver	Day	0.12	345.6	41.47
				Total :	193.07
				Total per m^2 :	**0.68**
(b)	**Machinery**	Unit	Quantity	Rate(CAD)	Amount(CAD)
	Truck 12CY	Hr	1	86.35	86.35
				Total :	86.35
				Total per m^2 :	**0.31**
(c)	**Material**	Unit	Quantity	Rate(CAD)	Amount(CAD)
	Polystyrene	m^2	338	69.17	23379.46
				Total :	23379.46
				Total per m^2 :	**69.17**
Grand Total per m^3 = [1+ CP&OC(12.5%) × (a+b+c) :					**78.93**

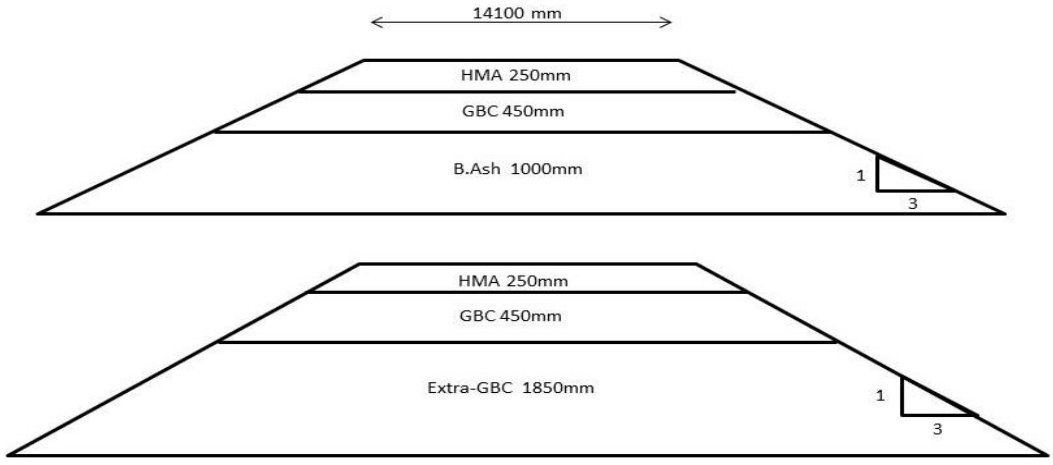

Figure 7-2: Pavement structure with different insulation layers

In the case of an approximately equal shipping distance for different sites, it is possible to estimate the construction cost when affected by different frost depths. Table 7-7 presents the estimated required thickness of different material when using GBC, bottom ash, and polystyrene layers. The

frost depth is calculated based on the approximate total frost that penetrates into the subgrade layer. The minimum required thickness of each section followed the same method of calculation explained in the previous section for the GBC. It can be seen that in all cases, 5 cm of polystyrene boards (the minimum applicable thickness) satisfied the thermal condition, while for the GBC layer the second criterion (minimizing the heave occurrence in subgrade) is the governing factor.

Using the information provided in Table 7-7, the construction costs for different insulation material is compared based on the required thickness of each material for frost depths of 1.3, 2, 2.6, 3.3, 3.9, and 4.6 m, as represented in Figure 7-3. Considering the construction site location and the availability of material, the proper method of insulation can be selected. For instance, for a frost depth of 1.3 m, the construction cost of one meter of roadway, if considering equivalent depth for different material, is $688.00 for GBC, $452.00 for bottom ash, and $1,334.00 for polystyrene.

Figure 7-3 also indicates that for sites where the availability of each material and the distance of the source to the project location are the same as the IRRF test road, and the frost depth is less than 1.6 m, using bottom ash and GBC will be more cost effective than polystyrene boards. For frost depths between 1.6 m and 3.5 m, using bottom ash as insulation will be the most cost effective way to insulate the subgrade. When the frost depth is higher than 3.5 m, polystyrene boards can outperform the other two materials to prevent frost ingress through deeper layers. In addition, it can be concluded that the construction cost of bottom ash has less sensitivity to change in thickness than the GBC material. This stems from the inexpensive availability of bottom ash as opposed to the costly GBC material. This cost comparison is based on the IRRF's site construction costs and would be valid for construction sites with similar access to material sources.

TABLE 7-7: Required thickness of insulation layers for different frost depths

Total Frost Depth(m)	**Material**		
	Extra GBC	**Bottom ash**	**Polystyrene**
1.3	0.4	0.5	0.006
2	1.15	0.75	0.009
2.6	1.85	1	0.012
3.3	2.6	1.25	0.015
3.9	3.3	1.5	0.018

As shown in Table 7-3, the life expectancy of pavements constructed using the polystyrene with 5 cm thickness is almost half the life expectancy of conventional section. In addition, the

bottom ash will not affect the life expectancy of the pavement. The considerable high cost of construction of roads using GBC material in high freezing zones (for instance frost depth of 3.3 m) can be justified by their higher PL as the life expectancy will considerably will increase by using GBC (Almost 170 years compare to the 20 years or less for CS).

Figure 7-4 depicted the required R-Value (day.˚C/kJ) in case of using any material other than the material used at this research for different frost depth prediction.

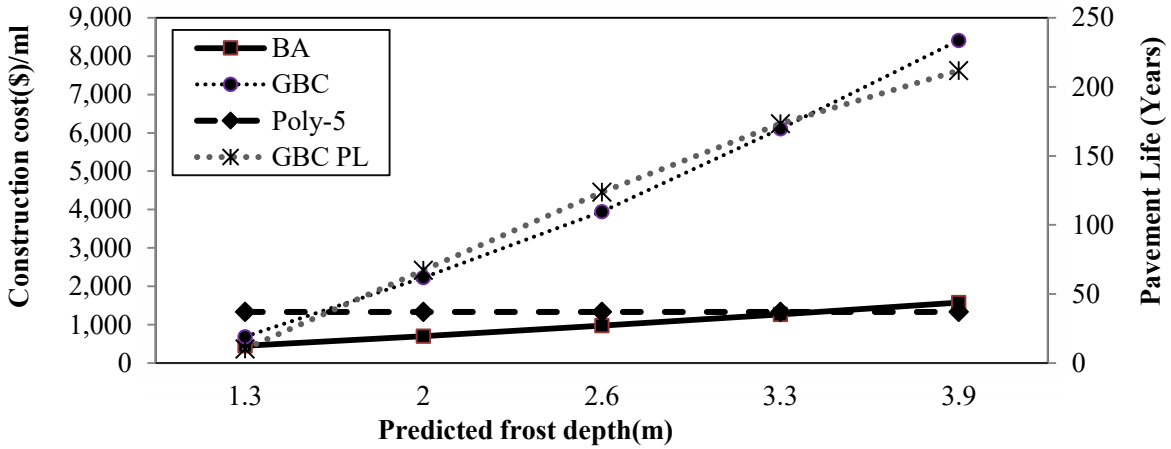

Figure 7-3: Comparison of construction cost of different insulation layers

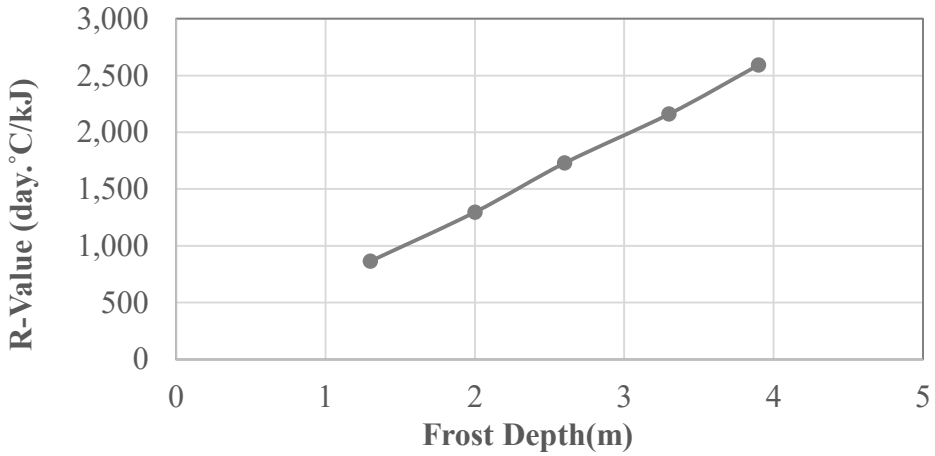

Figure 7-4: Required R-Value versus frost depth

7.6. SUMMARY AND CONCLUSIONS

This study provides a performance and cost comparison of the utilization of different insulation materials in pavement constructions, along with substituting the high quality base material with frost susceptible subgrade. The study focused on cost estimations of GBC, bottom ash, and polystyrene layers. The estimated unit cost values were considered reasonable at the time of this

study, but may vary significantly from project to project depending on conditions, specific project requirements, equipment availability, and location of the project. Observations resulting from this study are summarized as follows:

1. The main criterion that contributed to the selection of GBC thickness was overburden pressure, while for bottom ash and polystyrene boards, the criterion was thermal performance of the layer to prevent the frost from penetrating into the subgrade.
2. The selected thicknesses of bottom ash, polystyrene, and GBC material to conduct the comparison are 1.00 m, 0.05, and 1.85 m, respectively.
3. The total traffic that the B.ash section could carry was estimated to be 14 percent of the value of that of CS. While the poly-5 section can carry half of the traffic of the CS section, the extra-GBC section can tolerate more than 10,000 times the traffic of the CS.
4. The construction cost per cubic meter of the GBC and the bottom ash layers was $95.00 and $49.00, respectively. In addition, the insulation cost for each square meter of road with polystyrene boards was $79.00.
5. The total cost of construction of insulation layers for 1 m of bottom ash was $977.00, for 5 cm of polystyrene the cost was $1,334.00, and for 1.85 m extra GBC the cost was $3,964.00.
6. At locations with similar material availability and source distance from the site, and with a frost depth less than 1.6 m, bottom ash and GBC material will be more cost effective than polystyrene boards; however, this implication depends on the availability of each material and the distance of the source to the project location.
7. For frost depths between 1.6 m and 3.5 m, using a bottom ash layer as insulation will be the most cost effective way to insulate the subgrade. At locations where the frost depth is higher than 3.5 m, polystyrene boards can outperform the other two materials to prevent frost ingress through deeper layers.
8. The high capital construction cost of pavement using granular base material can be justified by high life expectancy of these pavements.

7.7. ACKNOWLEDGMENTS

The authors greatly appreciate Alberta Transportation, the City of Edmonton, and Alberta Recycling for their financial and in-kind support of this project. The authors also acknowledge Alberta Transportation for conducting the FWD tests for this study and ISL Engineering, Land

Services, and DeFord Contracting for coordinating the construction and instrumentation activities of the IRRF's test road.

7.8. REFERENCES

Alberta Transportation and Utilities. (1997). Pavement Design Manual.

ARA, Inc (2004). ERES Consultant Division. Guide for Mechanistic-Empirical Design of New and Rehabilitated Pavement Structures. Final report, NCHRP Project 1-37A.

ASTM Standard C136-06. (2006). "Standard Test Method for Sieve Analysis of Fine and Coarse Aggregates." ASTM International, 04.02.

Doré, G., and Zubeck, H. K. (2009). *Cold Regions Pavement Engineering*, McGraw-Hill Professional, New York.

Côté, J., and Konrad, J. M. (2005). Thermal conductivity of base-course materials. *Canadian Geotechnical Journal*, (42)1, 61–78.

Dow Building Solutions. (2016). <http://dow-styrofoam.custhelp.com/app/answers/detail/a_id/11273/kw/styrofoam%20r-value> (Mar. 1, 2016)

Edgar, T., R. Mathis, and Potter, C. (2015). Injection of Structural Polymer Foam to Control Highway Frost Heave. Airfield and Highway Pavements . 873–884.

Esch, D. C. (1972). Control of Permafrost Degradation beneath a Roadway by Subgrade Insulation. Alaska Department of Transportation and Public Facilities, Juneau, Alaska.

Nixon, D., Eng, P., & Lewycky, E. D. (2011). Edmonton Experience with Bottom ash and Other Insulating Materials for Mitigation of Frost Heave Induced Damage. In *Annual Conference of the Transportation Association of Canada , Edmonton, Alberta, September 11-14*. Edmonton, Alberta.

Gilpin, R. R. (1980). A Model for the Prediction of Ice Lensing and Frost Heave in Soils. *Water Resources Research*, (16)5, 918–930.

Havukanen, J. (1983). The utilization of compacted coal ash in earth works. *Proceedings of the 8th European conference on soil mechanics and foundation engineering.* Vol. 2, 773–776.

Hendrickson, C., and Au, T. (1989). *Project Management for Construction: Fundamental Concepts for Owners, Engineers, Architects and Builders.* Prentice Hall.

Holt, A., Sullivan, S., and Hein, D. K. (2011). Life Cycle Cost Analysis of Municipal Pavements in Southern and Eastern Ontario. *Presented at the 2011 Annual Conference and Exhibition of the Transportation Association of Canada*, Edmonton, AB.

Huang, Y., Bird, R. N., and Heidrich, O. (2015). A review of the use of recycled solid waste materials in asphalt pavements. *Resources, Conservation and Recycling*, (52)1), 58–73.

Sarkar, R., and Dawson, A. R. (2015). Economic assessment of use of pond ash in pavements. *International Journal of Pavement Engineering*, 1–17.

Rieke, R.D., Vinson, T.S., and Mageau, D.W. (1983). The Role of Specific Surface Area and Related Index Properties in the Frost Heave Susceptibility of Soils. *Proceedings of the Fourth*

International Conference on Permafrost, National Academies Press, Washington, D.C., 1066–1071.

Rajaei, P., and Baladi, G. (2015).Frost Heave: A Semi-Empirical Model Based on Field Data. *16th International Conference on Cold Regions Engineering*, 382–393.

Rieger, S. (1983). *The Genesis and Classification of Cold Soils.* Academic Press, New York.

RS Means. (2017). <https://www.rsmeans.com/products/online.aspx> (Mar. 1, 2015)

Saarelainen, S. (1996). Pavement Design Applying Allowable Frost Heave. *Proceedings of the Eighth International Conference on Cold Regions Engineering*, ASCE Press, Reston, VA.

Sakulich A. R., (2011) Reinforced geopolymer composites for enhanced material greenness and durability. *Sustainable Cities and Society*, (1)4, 195–210.

St-Laurent, D., and Roy, M. (1995) Évaluation structurale des chausses souples dansun contexte climatique nordique : une étude avec le FWD [Structural evaluation of flexible pavements in a northern context: A study using the FWD].” *Proceedings of the 30th Annual Conference of AQTR, Association Québécoise du Transport et des Routes*, Quebec, Canada.

The City of Edmonton Transportation. (2012) Roadway Design Standard Construction Specifications. <http://www.edmonton.ca/city_government/documents/RoadsTraffic/Volume_2_-_Roadways_May_2012.pdf.> (Mar. 1, 2015).

Tavafzadeh, N. T., Hashemian, L., and Bayat, A. (2016). The Effect of Seasonal Variation on Load Bearing Capacity of Pavements Comprised of Insulation Layers. *Transportation Research Record: Journal of the Transportation Research Board of the National Academies*, 2579, 2016b, 87–95.

Tavafzadeh, N., Nassiri, S., Shafiee, M., and Bayat, A. (2014). Using Field Data to Evaluate Bottom Ash as Pavement Insulation Layer. *Transportation Research Record: Journal of the Transportation Research Board*, 2433, 39–47.

Transportation Officials. (1993). AASHTO Guide for Design of Pavement Structures. Vol.1

Uzarowski, L., Rizvi, R., Krzewinski, T. G., Ulring, J. D., and Maher, M. L.J. (2013). Runway Pavement Rehabilitation Design and Construction in Remote Areas in the North-Case Study.*ISCORD 2013: Planning for Sustainable Cold Regions*, 585–596.

Zhi, W., Yu, S., Wei, M., and Jilin, Q. (2005). Evaluation of EPS application to embankment of Qinghai–Tibetan railway. *Cold Regions Science and Technology*, (41)3, 235–247.

8. THERMAL MODELING OF AN INSULATED PAVEMENT

8.1. ABSTRACT

Using insulation layers in cold region is going to become a common strategy for decreasing the risk of frost penetration into the frost susceptible subgrade. As the method becomes more acceptable, assessing the influence of insulation layers on pavement performance and fluctuation of different layers moduli will be more essential.

This study investigates the accuracy of the modeling system in investigating the thermal regime in pavements comprised of the insulation layers. Using Geo-Studio, the Temp/W module, the different sections of insulated pavement constructed in Edmonton, Alberta is modeled. The predicted values are compared against the observation at site. An acceptable compatibility between the result and the field temperature variation was observed.

Then the predicted temperatures were used to re-calculate the dynamic modulus (Mr*) of the hot mix asphalt (HMA) of different sections. The result indicates that on a yearly average basis, Mr* values of the insulated sections may drop by up to 11 percent compared to conventional sections.

Key words: Insulation Layer, Thermal Modeling, Geo-Studio, Temp/W, Bottom Ash, Polystyrene

8.2. INTRODUCTION

Using insulation layers has become one of the strategies for alleviating and/or preventing the frost-heave problem during winter and thaw-weakening during spring. Surface heave alters the road profile and can negatively affect the road's ride quality, especially if the heave is differential and uneven (Doré, & Zubeck, 2009). Thaw weakening during spring may force the transportation agencies to impose the spring load restriction (SLR) on low volume roads. The weak subgrade support during thaw season results in higher deflections that cause accumulation of fatigue in the pavement and leads to different types of cracks and deterioration (Doré, & Zubeck, 2009). If the insulation layer provides an adequate load bearing capacity for the pavement and does not create an unfavorable moisture regime in the system, using it will result in reducing the depth of frost penetration into the pavement structure. This can enable design engineers to moderate the base/subbase layers' thicknesses, thus, limit the depletion of natural aggregate resources, and move towards more economical and sustainable design strategies (Doré, & Zubeck, 2009).

It is important to incorporate an adequate amount of insulation material in pavement construction to avoid probable risks such as differential icing and soft pavement structure. The minimum required thickness of insulation material depends on the thermal properties of the different pavement layers and the climate (Dore and Zubeck, 2009). As a result, changing the thermal regime in the pavement structure caused by insulation materials should be investigated using proper modeling software to provide an accurate and reliable estimation of required thickness of insulation material to avoid the above-mentioned problems.

In the early 1990's, the thermal modeling of insulated and uninsulated road was performed by the Alaska Department of Transportation (AK DOT) using an MS-DOS computer program, MUT1D (Multilayer User-Friendly Thermal Model in 1 Dimension). The software applied one dimensional implicit finite difference techniques for estimating the thermal regime of a multilayered model (Braley and Zarling, 1990). Although the MUT1D model yields results with acceptable accuracy, it is limited to producing the depth of phase change along a single line of analysis. The limitation of previous software leads the designer to use TEMP/W (which is one of modules in software Geostudio 2012, GeoSlope International, Calgary, Alberta). This two-dimensional (2-D) finite element program provides heat flow analysis for an entire cross-section and, because it uses 2-D boundary effects, it is more reliable than a 1-D model.

The main objectives of this chapter are to enhance understanding of insulation layers performance and their influence on the thermal regime of the pavement. The the values extracted from the model will be used to evaluate the changes dynamic modulus of the HMA layer in aim for performance evaluation of the pavements comprised of insulation layers. For this reason, an instrumented test road in Edmonton, Alberta, Canada is simulated using Temp/W software; then the temperature data was evaluated and compared against the site observation.

8.3. TEST ROAD DESIGN AND INSTRUMENTATION

The construction of the (Integrated Road Research facility) IRRF's test road facility, located in Edmonton, Alberta, Canada, started in May 2012 and was completed in August 2013. The 500-m two-lane test road serves about 2,000 vehicles per lane each day to access the Edmonton Waste Management Center (EWMC), based on the data collected from weigh-in-motion (WIM) systems during the spring of 2016. Road pavement consists of two types of dense graded hot mixed asphalt (HMA) with a total thickness of 25-cm located on top of 45 cm Granular Base Course (GBC). The

insulated layers are located between the subgrade and the GBC layer. 100-cm thick bottom ash layer (B.Ash) and two Polystyrene layers with 10 and 5 cm thicknesses (Poly-10 and Poly-5) were used as insulation layers. The adjacent conventional section served as a control section (CS).

The HMA layers were designed based on the Marshall Mix design in accordance with the City of Edmonton's specifications for Designation-1 asphalt concrete mix (*Roadway Design Standard Construction Specifications,* 2012). The Granular Base Course (GBC) and subgrade layers were classified as Well-Graded Gravel (GW) and Clayey Sand (SC), respectively, based on the Unified Soil Classification System (USCS) (ASTM Standard C136-06, 2006). The Gradation of different layers was plotted in Bottom ash, which is a waste material from the incineration of coal in power plants, and free of large lumps and impurities. The amount of non-combusted coal particles was less than five percent of the material by weight. Closed-cell Extruded polystyrene Highload 100 extruded Polystyrene boards were used in this project. The boards have a compressive strength of 690 kPa and a minimum flexural strength of 585 kPa based on the manufacturer's data sheet.

To measure the temperature distribution, freezing, thawing and recovery condition of the pavement, all of the sections, except for Poly-5 section, were instrumented using 109AM-L thermistors and CS650 Time Domain Reflectometres (TDRs) from Campbell Scientific Canada at different depths of the pavement at distances of 0.6 or 1.2 m from the centerline. The TDR probes are able to collect both unfrozen volumetric water content (UVWC) and temperature data. In this investigation only the temperature data collected from TDRs are used in analysis.

Figure 8-2 shows the location and type of instrumentation at each section. The location of the instrumentation used in this study is in the middle of the lane at a distance of 1.2 m from the centerline. The embedded thermistor elements provided by Omega at mid-depth of HMA layer of CS provided the HMA temperature during the tests. A CR1000 Datalogger was programmed to collect data from the sensors in 15-minutes intervals from all of the sections. The Datalogger was equipped with a spread spectrum Model RF401 radio with an antenna Model L14221 installed at an on-site trailer, where a computer transmitted the data regularly to the University of Alberta.

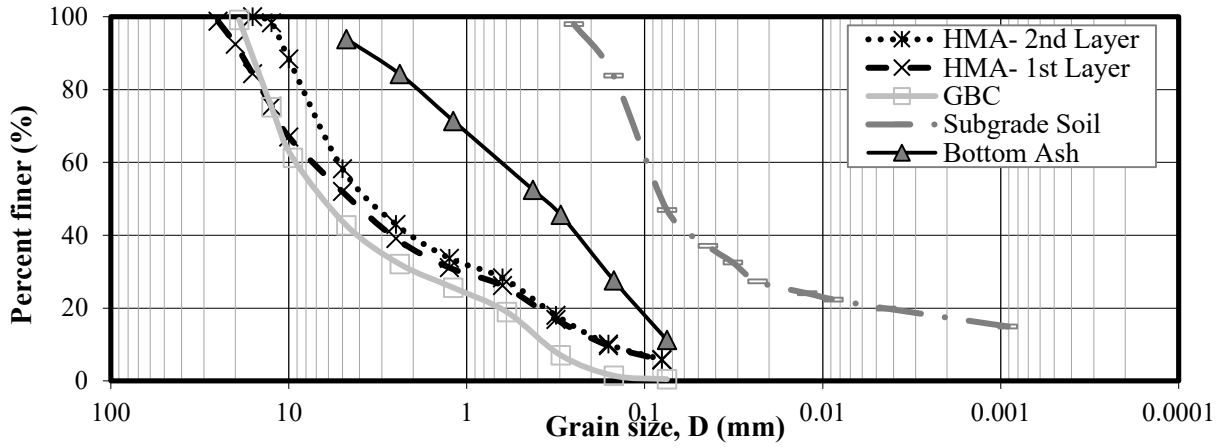

Figure 8-1: Particle size distribution of different layers of road

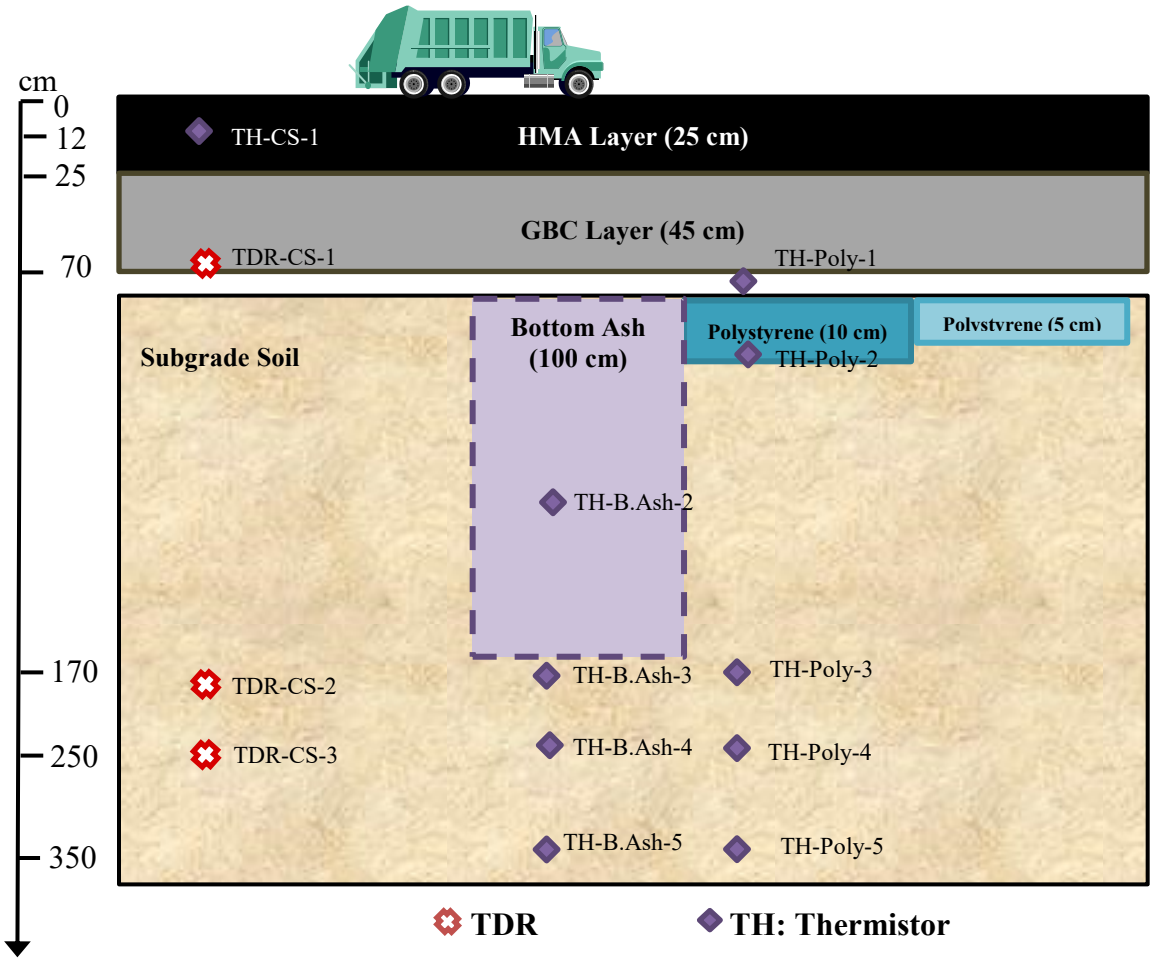

Figure 8-2: Cross sections and as-built depth of thermistors and moisture probes

8.4. THERMAL MODELING

The main goal of thermal modeling is to simulate the condition of different sections of IRRF test roads, enhance understanding of performance of insulation layers, and to make predictions about pavements future behaviour. A model in reasonable agreement with observed behaviour can lead to improved design and maintenance practices for road embankments in the case of using insulation material. In this research, the finite element modeling is conducted using TEMP/W software (GeoStudio, 2012) to simulate the thermal regime in the pavement. It is worth mentioning that there are some deficiency and limitation in using TEMP/W software for modeling the pavement thermal regime. The main limitation is the assumption of no mass (water) transport in the pavement. Based on this limitation, heave occurrence or changes in heat transfer and heat capacity of pros media (soil) is not predictable in the model (GeoStudio, 2012).

Following differential equation governs the calculations in the TEMP/W program during each step and for the boundary of each element:

$$\frac{\partial}{\partial x}\left(K_x \frac{\partial T}{\partial x}\right) + \frac{\partial}{\partial y}\left(K_y \frac{\partial T}{\partial y}\right) + Q = \left(C + L.UVWC.\frac{\partial VWC}{\partial T}\right)\frac{\partial T}{\partial t} \qquad \text{Equation 8-1}$$

where T is temperature, K_x and K_y are thermal conductivities in the x- and y-directions, respectively, Q is the applied boundary flux, C is the volumetric heat capacity, L is the latent heat of water, VWC is the volumetric water content, UVWC is the unfrozen water content, and t is time (Krahn, 2004). The right side component of the equation shows the capacity of the system in keeping or releasing energy during water phase change; and the left hand side is an indication of the heat transfer in each element of the system.

8.4.1. Basic assumption for modeling

Creating a model in TEMP/W (or any other finite element base numerical modeling) has three steps: discretization, defining material properties, and defining the boundary conditions. To increase the efficiency, it is assumed that the sections are symmetric, so the geometric model is defined as a half cross-section. The symmetric assumption of the pavement system on the centerline leads to assuming a zero heat transfer at the centerline (GeoStudio, 2012).

The discretization of the model is performed by dividing the cross section of the model into smaller pieces called finite elements. The finite element mesh is comprised of rectangular or triangular elements (GeoStudio, 2012). The mesh size is assumed to be 0.6 m.

The materials properties defined in the previous section are used in the modeling. Also, the measured volumetric water contents obtained from TDR probes installed at site are applied to define the institute VWC.

8.4.2. Material

The required material properties in the simplified thermal model are the unfrozen and frozen thermal conductivity (K_u , K_f), unfrozen and frozen volumetric heat capacity (C_u , C_f), and the institute volumetric water content (VWC). The K and C in unfrozen and frozen conditions are measured in the laboratory for Bottom ash, Subgrade soil, and HMA layer using Hot Disk TPS 500 S. Figure 8-3 shows the probe and sample prepared for measurement.

Figure 8-3: Thermal properties measurement a) HOT DISK TPS 500 S. b) prepared sample. C) Sample in the equipment for measurement

Thermal conductivity in frozen and unfrozen conditions are assumed to be constant but different from one another. For the GBC layer, the value collected available from the literature is used in this study. The VWC is based on the reported and tested values during road construction. The measured and assumed values are presented in Table 8-1.

8.1.1. Boundary condition

Boundary conditions must be applied on all borders of the model. But before that, the model is divided into two different analysis procedures. The first portion of analysis is a “steady state” analysis where the initial condition for the starting point is defined. The second portion of the analysis is a “transient analysis” where dynamically the boundary condition are applied to the

performance analysis. The transient analyses are in a constant state of change and require a start time to establish the initial conditions. For the steady state, the author selected October 1, 2013 as the model start date for data collection from the field instrumentation. The initial conditions are defined as table 8.2.

Table 8-1: Material Properties

Material	K (KJ/day/m/˚C)		C (KJ/m3/˚C)		VWC (m3/m3)	Reference
	Ku	Kf	Cu	Cf		
HMA	177	177	1,728	1,728	0.001	Measured in Lab
GBC	216	346	2,400	2,300	0.16	(Batenipour, 2012)
Subgrade	163	225	2,461	790	0.32	Measured in Lab
B.Ash	74	128	1,870	602	0.25	Measured in Lab
Polystyrne	0.52	0.52	2,313	2,313	0	Dow Construction webpage (2016)
Snow Cover	-	21.6	-	-	-	(Riche, & Schneebeli, 2013)

The asphalt surface temperature was collected at site and measure by thermistors. Although the thermistors were only located at the CS, the same initial temperature was used for all the sections for the steady state. The temperature of soil in depth was measured at site and was plotted based on the location and values of the deepest sensor. As the sections are symmetric, it was assumed that along the center line there is a zero flux. This assumption is important to increase the computing accuracy. Assuming an isotherm on the right hand side of the model, the boundary condition will be zero heat flux.

Table 8-2: Boundary Condition of Steady state

Location	Condition Type	Value	Unit	Reference
Asphalt Surface	Thermal	11	˚C	Measured at site
Soil Surface Temperature	Thermal	6	˚C	Measured at site
Soil temperature at depth	Thermal	-	˚C	Measured at site
Along the center line	Flux	0	kJ/days/m²	Symmetry Rule
Far boundary on right hand side	Flux	0	kJ/days/m²	Isotherm
Far boundary at the bottom	Thermal	5	˚C	Toogood, J. (1976)

Based on the data collected in Edmonton, the temperature at minimum depth 15 m below the surface changes between 5±0.5˚C. Also measurement at various depths of Siberia, northwestern Canada, and the Rocky Mountains of Montana through the year demonstrated that at depth more than 14 m below the surface (Rieger, 2013), the temperature is approximately constant and it is not affected by changes in ambient temperature (Toogood, 1976). The depth is called mean zero annual temperature amplitude (DMZAA). As a result, at depth 15 m below the surface, the temperature was assumed to be constant and equal to 5˚C. There are other studies which consider the depth at 30 m to remove the interference between top and bottom boundary conditions (Darrow, 2010).

After analyzing the steady state, the transient analysis was started. The boundary condition of this portion was different from the steady state. On the top surface of the model, a thin layer of finite elements called a surface layer must be constructed to apply a climate boundary condition in a TEMP/W model. TEMP/W uses daily climate data (maximum and minimum temperature, maximum and minimum relative humidity, wind speed, amount of precipitation, and starting and ending times of the precipitation events) and latitude of the site, as the surface boundary condition. The predicted climate data was downloaded from Environment Canada's monitoring station at the closest location to Edmonton. (climate.weatheroffice.ec.gc.ca). A cover of snow was applied on the soil surface of the model as soon as the precipitation occurred while the data remained under zero for five days. Similarly, the cover snow was assumed to be removed as soon as five continuous days of average daily temperature of above zero occurred at site. Another difference between the steady and transient boundary conditions is a constant unit heat flux of 3 kJ/m^2.day was used based on the unfrozen thermal conductivity of clay sand and a geothermal gradient of 3˚C per 100 m (Flynn, 2015).

During the modeling it was observed that numerical convergence may not be reached at some time steps. Also, the predicted temperature was not acceptably accurate enough when compared to the site observation values. So, to address these problems, several thermal models were developed and the improvement of the result was investigated through several modifications. For instance, the boundary conditions were modified by changing DMZAA temperature and its depth based on different available literature. Also, the material properties, geometry and mesh size were modified to become a better representative of site situation.

8.2. THE RESULT AND DISCUSSION

8.2.1. Thermal Regime

Figures 8-4 to 8-6 present the measured and predicated temperature at different depth of CS. As is shown in Figure 8-4 to 8-6, there is an acceptable agreement between the measured and the predicated temperature at all depths of CS.

Although the measured and predicted lines followed the same trend at all depths, the maximum and minimum temperatures occurred on different days. For instance, the maximum variation from the measured values at depth 0.7 m below the surface was observed on days 1,200 and 1,350. On these days, although the measured temperature reached the minimum value of -3.5˚C, the predicted value dropped almost -15˚C. It can be an indicator that the predicted values may be more affected by the ambient temperature change.

At depth 1.7 m below the surface (Figure 8-5), the predicted and measured values match the maximum temperature occurrence. However, the minimum temperature predicted at this depth, dropped 5 to 10˚C below the value of that observed. In contrast, there is a more acceptable agreement between the peak predicted and measured values at depth 2.5 m below the surface (Figure 8-6). A lag between the measured and predicted temperatures at this depth is observable during the monitoring period. The lag is more pronounced between days 1,100 and 1,200 and also days between 1,500 and 1,600.

The overall conclusion by comparing the measured and predicted temperatures at different depth of CS (Figures 8-4 to 8-6) is that, the deeper the location is the better prediction possible with Temp/W modeling software. This phenomenon may happened as the most important contributor to temperature variation is ambient temperature (as boundary condition), and its fluctuation can highly affect the top layers temperature prediction rather than the deeper locations.

Figure 8-7 and 8-8 depict the temperature variation at depth 1.0 m and 2.5 m below the surface of the B.Ash section. Figure 8-7 shows that the predicted and measured temperature variation followed the same trends of temperature change. However, the magnitude of minimum values are different. The maximum difference between the predicted and measured peak values reached 7.1˚C during the first winter.

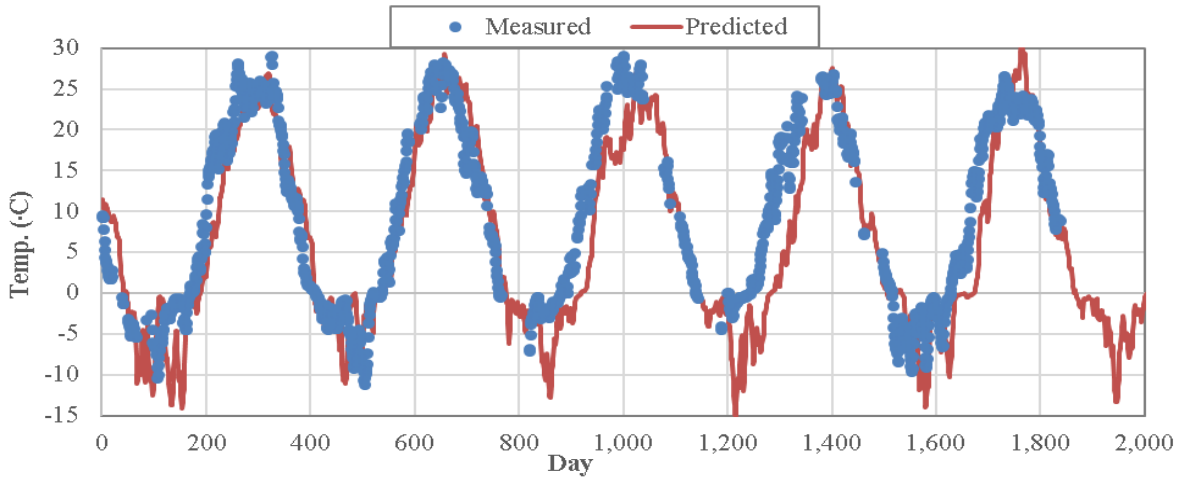

Figure 8-4: The measured and predicted temperatures – CS at depth 0.7 m below the surface

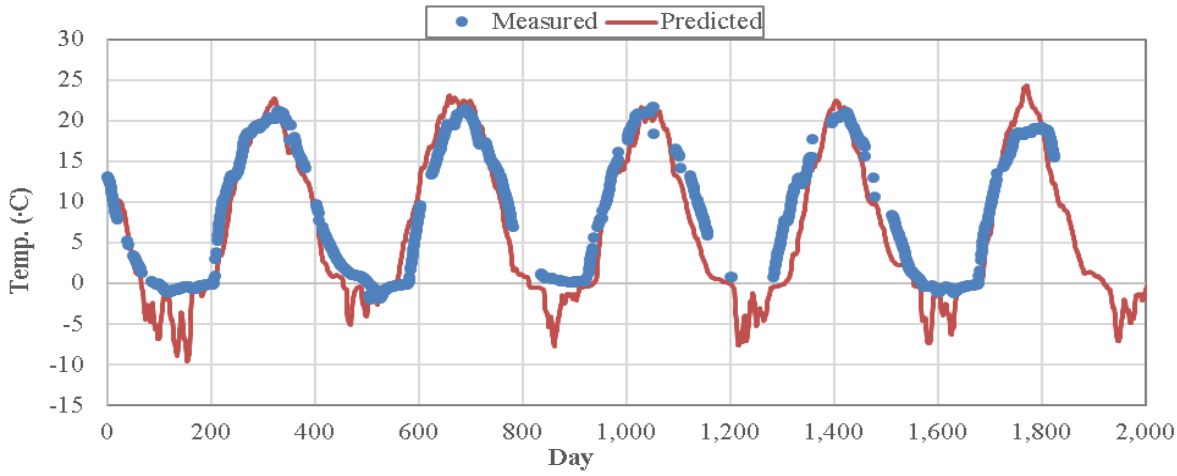

Figure 8-5: The measured and predicted temperatures – CS at depth 1.7 m below the surface

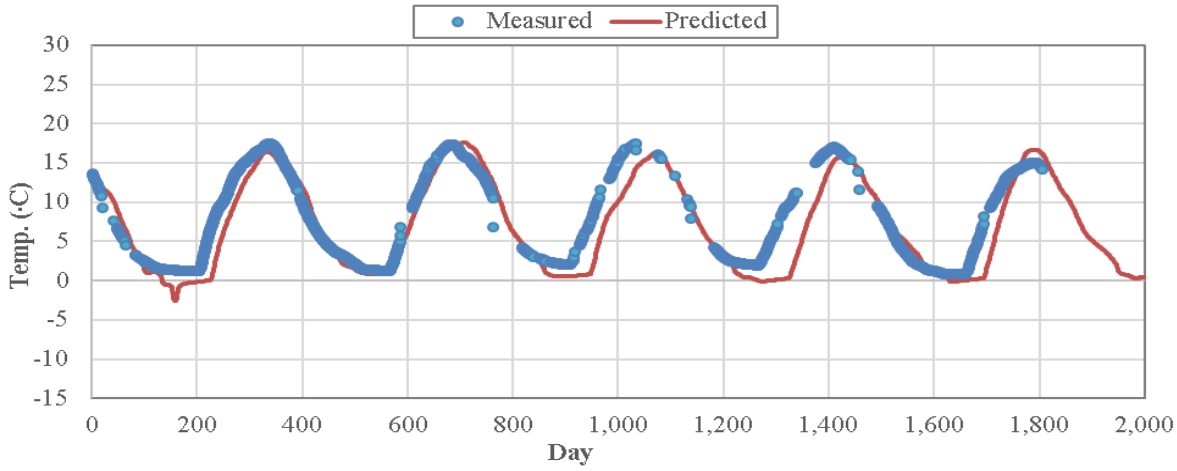

Figure 8-6: The measured and predicted temperatures – CS at depth 2.5 m below the surface

Comparing the results at depth 2.5 m below the surface indicates that the predicted temperature values remained around zero for a longer time compared to the measured values at site. While at this depth, the predicted values reach a slightly lower temperature (almost -3.5˚C). Similar to the observation in CS, there is a better agreement in predicted and measured temperature values at depth 2.5 below the surface of the B.Ash section than at the shallower depths.

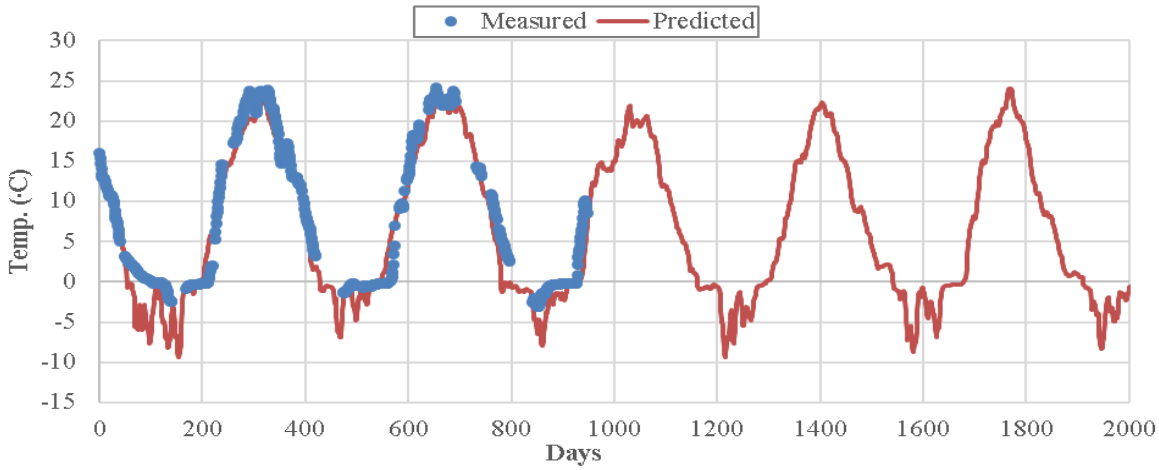

Figure 8-7: The measured and predicted temperatures – B.Ash at depth 1.7 m below the surface

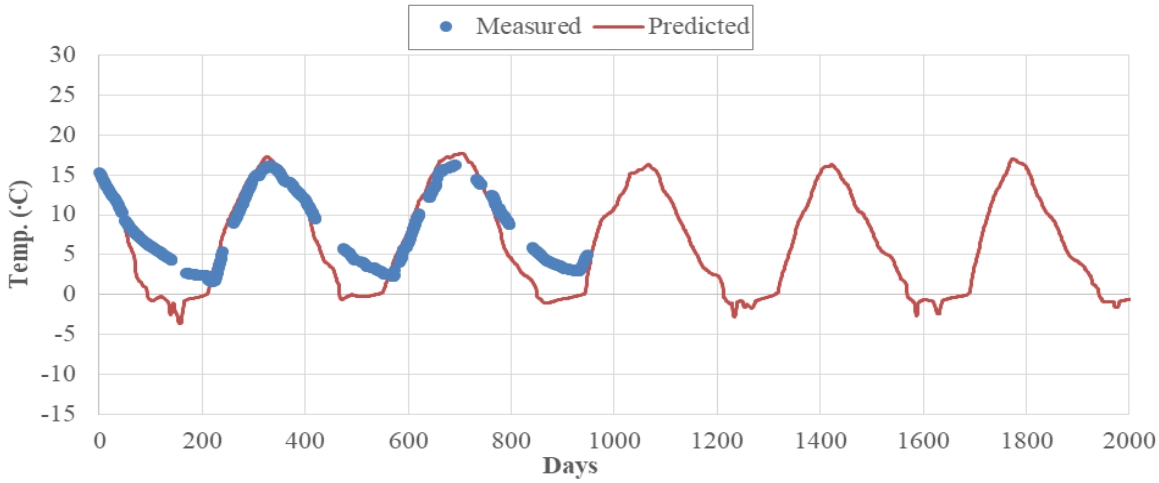

Figure 8-8: The measured and predicted temperatures – B.Ash at depth 2.5 m below the surface

Figures 8-9 to 8-11 show the measured and predicted temperature fluctuation at different depths of the Poly-10 section. As previously demonstrated, the insulated sections experience more fluctuation in temperature at depths above the insulation layers (GBC and HMA). Similarly, the

predicted temperature of the Poly-10 section in the GBC layer shows higher fluctuation compared to the CS.

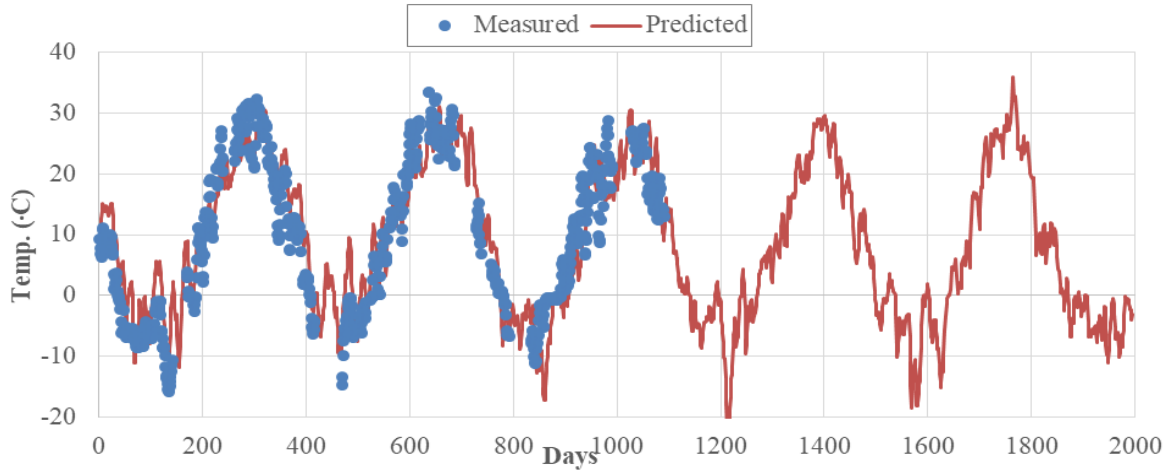

Figure 8-9: The measured and predicted temperaturse – Poly-10 at depth 0.7 m below the surface

Figure 8-10 and 8-11 show the temperature fluctuation for depth 1.7 m and 2.5 m below the surface, inside the subgrade layer of the Poly-10 section. As expected, the temperature fluctuation at these depths is low and similar to the CS and B.Ash sections, and there is an acceptable agreement between the measured and predicted temperature.

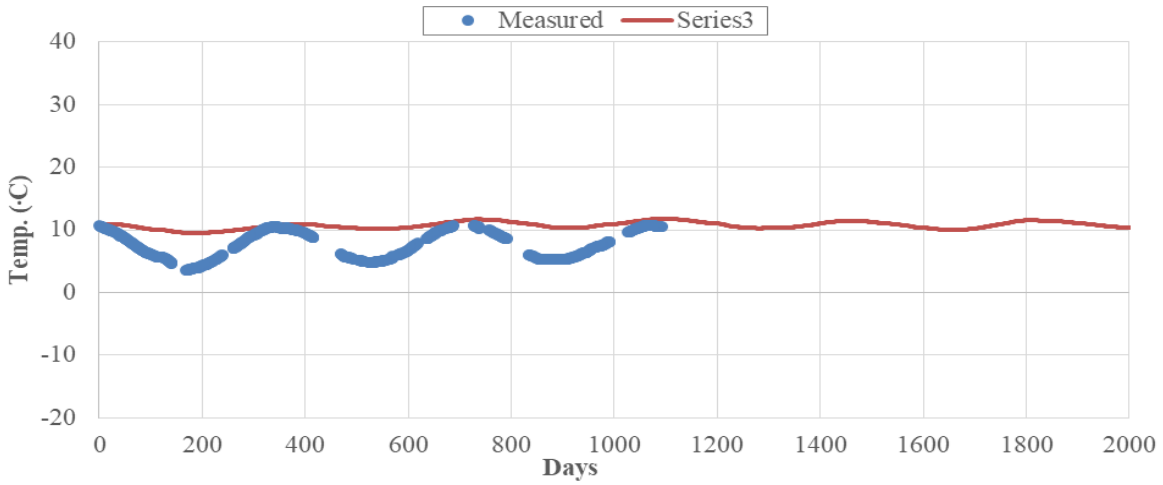

Figure 8-10: The measured and predicted temperatures – Poly-10 at depth 1.7 m below the surface

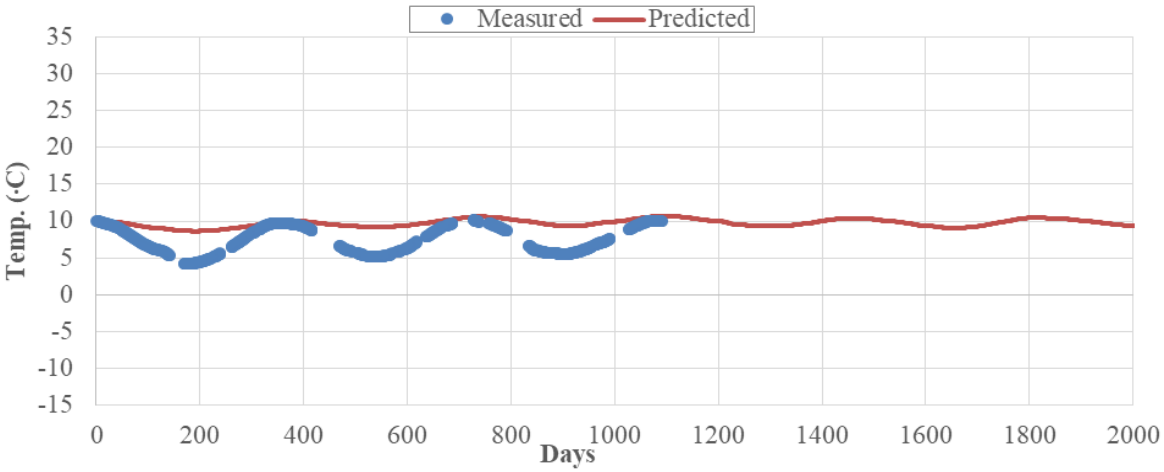

Figure 8-11: The measured and predicted temperatures – Poly-10 at depth 2.7 m below the surface

8.2.2. Surface temperature

One of the influential factors on pavement structural response to a load is the dynamic modulus of the HMA. This characteristic of HMA is affected by frequency of the applied load and temperature of the asphalt layer. The frequency of the load is governed by the speed of vehicles passing the road and their tire pressure (Huang, 2004). Hence, as at IRRF, the surface layer (HMA) is similar for all the sections. When a vehicle passes the road, the different temperature of HMA can be the only factor affecting the HMA response. It was previously proven that heat accumulation above the insulation results in higher surface temperature during summer and lower temperature during winter time (Dore and Zubeck, 2009). The difference in surface temperature of the different sections of IRRF leads to variation in HMA dynamic modulus; hence, a different pavement response. This section of the study aims to use the predicted temperature at surface of the different sections of IRRF and investigate its effect on variation of HMA dynamic modulus. Figure 8-12 shows the measured temperature in mid-depth HMA layer in CS along with the predicted values of HMA temperature at the same level for different sections of IRRF.

There is an agreement between the overall trend of measured and predicted temperatures. In contrast with what expected, the predicted temperature of the B.Ash and Poly-10 sections are lower in summer and higher in winter than the CS. In addition, higher fluctuation is observed for the predicted temperature compared to the predicted values of the CS.

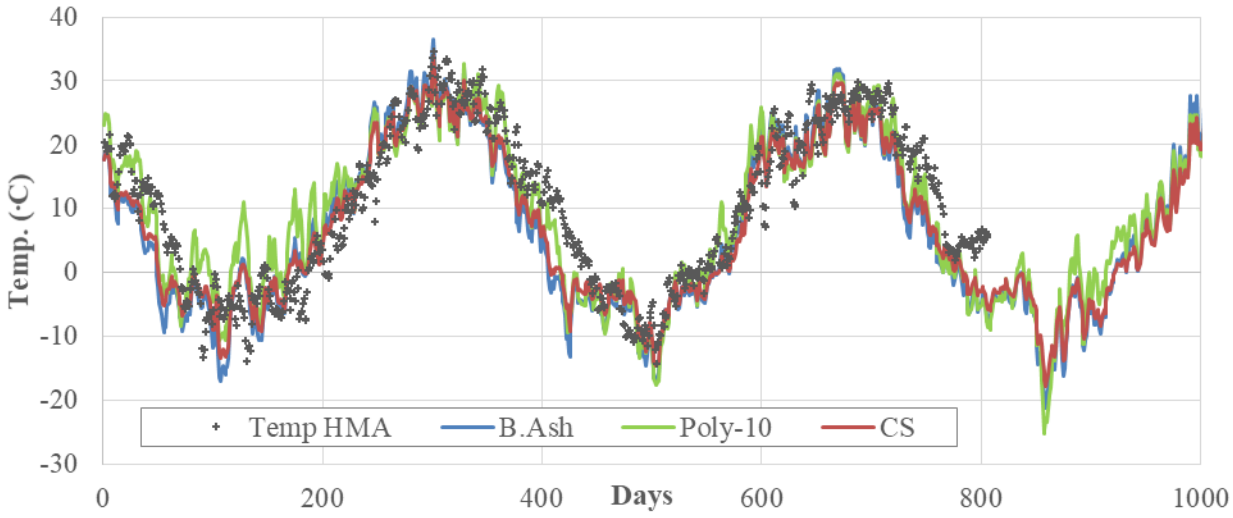

Figure 8-12: The measured and predicted HMA temperatures of different sections

8.2.3. Dynamic modulus of HMA

Based on the predicted temperature in Figure 8-11, the average, maximum, and minimum seasonal temperatures of different sections of IRRF are calculated and the results are presented in Table 8-3. Using the shift factor and dynamic modulus test performed in the laboratory, the dynamic modulus (M_r^*) of HMA is predicted for each temperature (Shafiee et al., 2015).

Comparing the M_r^* value based on the average predicted and measured temperatures at mid-depth of CS indicates that the prediction resulted in having less than 20 percent difference in dynamic modules. The result is consistent in fall and winter, having less than a 10 percent difference when using the minimum predicted temperature. However, the peak values of temperature in spring and summer are under predicted for CS, which leads to a predicted M_r^* of 145 percent higher than that resulting from the measured temperature. It is an important deficiency as the spring-thaw season, considering the subgrade resilient modulus drop, plays an important role in performance evaluation of the pavement.

As there was not any thermometer in the HMA layer of the insulated sections, the predicted temperature of these sections were compared with the predicted values of CS. However, the difference cannot be a direct indicator of the more or less accurate prediction of temperature as the temperature of the insulated sections at the surface will be different from the conventional ones. The same comparison for M_r^* may not result in a highest accuracy evaluation, but as all of them are the predicted values, the comparison provides a base for performance evaluation.

Based on the M_r^* values presented in Table 8-3, the performance of the pavement will be highly affected by using polystyrene with 10 cm thickness compared with using bottom ash material. The significance is shown by an average 4 percent lower M_r^* over the year for Poly-10 sections compared to the average M_r^* values of the predicted one in CS. The data did not show a significant difference between the predicted M_r^* values of the CS and B.Ash sections on a year round average. However, the M_r^* values loss in spring in the B.Ash section is as high as 7 percent, which can be significant as this is the season for thaw weakening of the subgrade as well. The same deficiency was observed during the spring season for the Poly-10 section with a loss of approximate 11 percent of M_r^* values.

Table 8-3: Average seasonal temperature and M_r^* comparison of different sections of IRRF

	Average HMA Temp. (·C)				M_r^* Difference		
	Measured	Predicted					
Season	CS	CS	B.Ash	Poly-10	CS	B.Ash	Poly-10
Fall	8.9	3.8	2.2	6.2	24%	5%	-8%
Winter	-5.0	-4.4	-5.1	-2.2	-1%	2%	-6%
Spring	11.2	11.9	13.4	14.1	-4%	-7%	-11%
Summer	24.9	21.6	21.5	22.7	22%	1%	-5%
Average	9.99	8.22	7.98	10.18	8%	0%	-4%

8.3. CONCLUSIONS

The study attempted to evaluate the accuracy of current software in modeling the temperature regime in the pavement, especially the ones comprised of insulation layers, using the inputs obtained from the laboratory and literature. The result of modeling is compared against the site observations to evaluate accuracy. An acceptable agreement existed between the predicted and measured temperature regime in the pavement of all sections. The agreement was more pronounced in deeper layers as they were least affected by the ambient temperature. The difference in the GBC layer of the CS and Poly-10 sections reached as high as 15·C and 7·C.

Then variation in temperature of the HMA layer of different sections was investigated and compared against the measured temperature of HMA in CS. The effect of temperature variation on the dynamic modulus of HMA was investigated. The results indicted the possibility of an average drop of 11% and 8% in the HMA dynamic modulus during spring for the Poly-10 and B.Ash sections, respectively.

8.4. REFERENCES

ASTM Standard C136-06. (2006). *Standard Test Method for Sieve Analysis of Fine and Coarse Aggregates*. ASTM International, West Conshohocken, PA.

Batenipour, H. (2012). *Understanding the performance of highway embankments on degraded permafrost*. University of Manitoba (Canada

Braley, W. A., & Zarling, J. P. (1991). MUT1D: user-friendly one-dimensional thermal model. In *Cold Regions Engineering*(pp. 1-10). ASCE.

Darrow, M. M. (2010). Measurement of temperature and soil properties for finite element model verification. *Institute of Northern Engineering, Fairbanks, AK*.

Dow Building Solutions. http://dow-styrofoam.custhelp.com/app/answers/detail/a_id/721. Accessed Jul. 1, 2016

Flynn, D. (2015). Field and numerical studies of an instrumented highway embankment in degrading permafrost.

GeoStudio (2012), GeoSlope International, Calgary, Alberta.

Guy Doré and H. K. Zubeck, (2009). *Cold Regions Pavement Engineering* (1st edition). New York: McGraw-Hill Professional.

Huang, Y. H. (2004). Pavement analysis and design.

http://www.climate.weatheroffice.ec.gc.ca , Accessed Jul. 1, 2016

Krahn, J. (2004). *Thermal modeling with TEMP/W: an engineering methodology*.

N. Tavafzadeh, S. Nassiri, M. Shafiee and A. Bayat. (2014). "Using Field Data to Evaluate Bottom Ash as Pavement Insulation Layer." *Transportation Research Record: Journal of the Transportation Research Board 2433,* 39-47.

Riche, F., & Schneebeli, M. (2013). Thermal conductivity of snow measured by three independent methods and anisotropy considerations. *The Cryosphere*, *7*(1), 217-227.

Rieger, S. (2013). *The genesis and classification of cold soils*. Elsevier.

Shafiee, M. H., Hashemian, L., & Bayat, A. (2015). *Seasonal analysis of flexible pavement response to falling weight deflectometer*. International Journal of Pavement Research and Technology, 8(5), 346-352.

The City of Edmonton Transportation. (2012). *Roadway Design Standard Construction Specifications* (2012 edition).

Toogood, J. A. (1976). Deep soil temperatures at Edmonton. *Canadian Journal of Soil Science*, *56*(4), 505-506.

9. MOISTURE MEASUREMENT AT IRRF

9.1. ABSTRACT

The following chapter investigates the moisture variation in different pavement layers of IRRF sections. The chapter presents the laboratory procedure for calibrating the time domain reflectometer (TDR) probes. Then the developed formula is used to evaluate and assess the data collected using the TDR probes at site. The variation in moisture data was connected to an ambient temperature and freezing index. Then, the resilient modulus formula from literature and laboratory were used to calculate the subgrade resilient modulus. The values were compared against the back-calculated resilient modulus from FWD presented in previous chapters of this thesis.

9.2. INTRODUCTION

The environmental conditions such as precipitation, variation in ambient temperature, and depth to the water level causes seasonal variation in the moisture content of the unbound layers which leads to fluctuation in resilient modulus of different layers of pavement (Models, 2000). Moisture variation and its dependent state variable in pavement materials, known as matric suction in unsaturated soil mechanics (Krahn and Fredlund, 1972), have a significant effect on the resilient modulus and permanent deformation of pavement materials (Carlos et al., 2011). Damage due to freezing occurs when frost penetrates the subgrade soil, increasing matric suction in the freezing zone; water then moves toward the freezing front and ice lenses form. Ice lenses in fine soils continually expand by attracting moisture from the underlying shallow water table, resulting in frost heave at the pavement surface (Dore and Zubeck, 2009). Frost heave can negatively impact the performance and ride quality of the road. When thawing occurs in the following spring, ice lenses melt, water content increases in the subgrade soil, and consequently the strength of the subgrade soil decreases, leading to structural damage, differential settlements, and damage to the pavement structure when exposed to heavy traffic loads.

The main objective of this section is to provide the state of moisture change at different layers of IRRF. The objective is followed by interpreting the TDRs moisture reading and finally the water content fluctuation in pavement during the monitoring period.

9.3. PROCEDURE OF CALIBRATION OF TDR

For measuring water content of soil in IRRF project, the CS650 Water Content Reflectometer was used which measures the volumetric water content, electrical conductivity, dielectric permittivity, and temperature of soils. The probe has two 30 cm length parallel rods connected at the head together. Table 1 shows the probe physical characteristics (Campbell Scientific Canada, 2011).

Table 9-1: The characteristics of TDR CS 650

Rods	Probe Head
300 mm long	L 85 mm
32 mm spacing	W 63 mm
3.2 mm diameter	D 18 mm

Figure 9-1: TDR CS 650 used at IRRF

For measuring the volumetric water content of the soil, the TDR has a differential emitter-coupled logic (ECL) oscillator which emits an electromagnetic wave through the pros media surrounded the rods. The velocity of the wave propagation depends on the dielectric permittivity (K) of porous media. Increasing the water content causes decreasing the propagation velocity or increasing the time required for the electromagnetic wave to travel from one rod to the other one. This dependency resulted in naming the probe as Time Domain Reflectometer (TDR). (Campbell Scientific Canada, 2011)

The quality of TDR measurement is affected by electrical conductivity (EC) of the surrounding area (Campbell Scientific Canada, 2011). Hence, whatever changes the EC of soil (for instance ions, temperature) can also affect the TDR measurements result. For this reason, it essential to calibrate the TDRs for specific soil and compaction and temperature. The following chapter explains the steps taken to find a proper equation for correcting the moisture content measurement of subgrade and GBC material.

Laboratory preparation of sample:

In the laboratory a soil sample having the following dimensions was prepared. The dimension of the container was 40 cm deep with a diameter of 28.7 cm. The specific dimensions of the container were necessary in order to have an appropriate cover of soil around the rods (10 cm) to eliminate the effect of other surroundings (air).

Soil was compacted in a way that the thickness of each layer remained at about 4 cm after compaction, so 10-lift of compacted soil was required to fill the container. Each lift had an average weight of 4.65 kg. Using a marker, horizontal lines were marked inside each container at 4 cm from the bottom (Figure 9-2). The energy required for soil compaction was calculated using the following equation:

$$E = \frac{(\text{number of blow}) * (\text{number of layers}) * (\text{weight of hammer}) * (\text{height of drop})}{\text{total sample volume}} = 591.3 \times 10^3 \qquad \text{Equation 9-1}$$

where E is required energy for compaction ($KN.\,m/m^3$), number of layers is equal to 10, weigh of hammer was 24.4 N, height of drop was 304.8 mm, and total volume was 25,865 cm3. Then the number of drops was calculated as high as 210 for each layer.

After finishing compaction, the TDR was inserted into the container in a way to keep the TDR rods parallel (Figure 9-2). After compaction of each layer, the moisture content of the layer was measured by taking a sample. The overall moisture content of the sample was calculated by taking an average over the moisture of each layer sample. The container weighed almost 50 kg after compaction. A similar procedure was performed for different moisture content.

Figure 9-2: The procedure of TDR calibration

9.3.1. Temperature dependency

Temperature has two distinct effects on TDR measurement. The first one is temperature influence on the operation of the probe electronics which is less than 2% for the range of -10 to 70°C. The second temperature impact is that changes occur in the dielectric permittivity of soil due to temperature change, which results from the high dependency of permittivity of water to temperature. The K of water changes from a value of 88 at 0 °C to 64 at 70 °C. Since water is the

main contributor to the K of soil, variation of temperature leads to considerable changes in the K of soil and directly affects the moisture measurement performed by TDR.

To eliminate the temperature dependency, the compacted sample was put in a refrigerator. The temperature was changed between 25 to 2 °C. The temperature range was selected based on the temperature change observed at site and was selected in a way to be far enough from the freezing point, at which moisture freezes and the TDR value changes dramatically.

The thermocouples were put at 5 cm below the surface, mid-depth, and 5 cm above the bottom of the sample to make sure the temperature was constant through the sample. The thermocouples had blue wires (Figure 9-3).

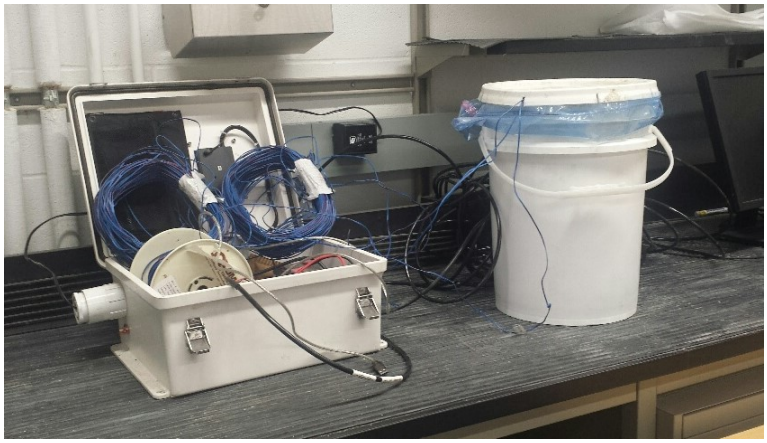

Figure 9-3 The thermocouples at different depths

The result of EC measured versus temperature for one of the tests is plotted in Figure 9-1. The correlation is linear with an R-square as high as 99.5%. The temperatures were compared to 21°C or, in other words, 21°C was chosen as a base point for comparing the EC.

The result indicated considering 21°C as the reference temperature; the temperature dependency may be eliminated using the following formula.

$$VWC_{21} = VWC/(0.0084(T - 21) + 0.9936) \quad \text{Equation 9-2}$$

Where, the WVC is the volumetric water content (m3/m3) and T is the temperature of the sample (°C) reported by TDR.

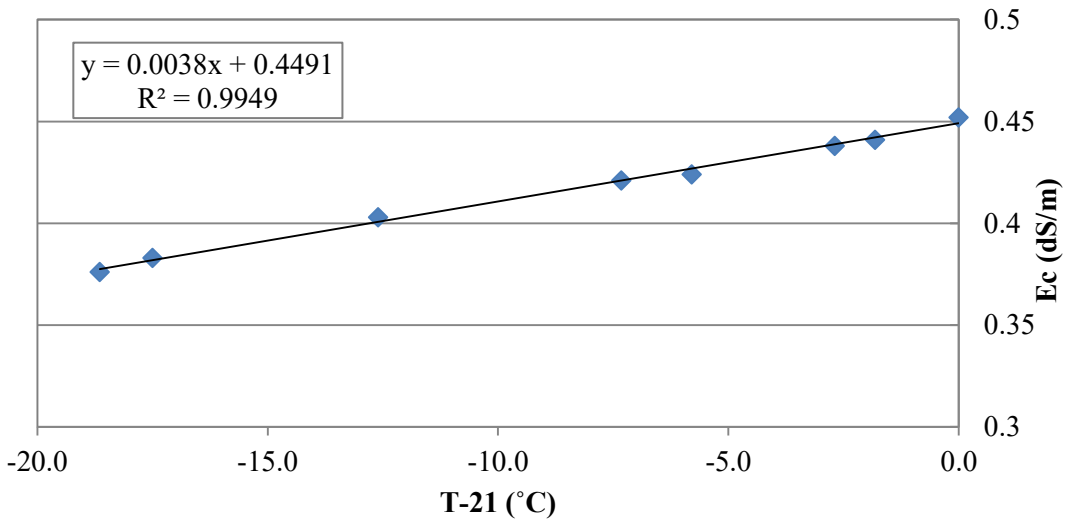

Figure 9-4 The sample result of temperature dependency test

9.3.2. Soil type/compaction calibration

As mentioned in previous sections, the TDR has to be calibrated based on the soil type and the compaction of the soil. This test was performed for both subgrade and GBC material. During the calibration process, the TDR response to moisture changes was measured and plotted in Figure 9-5 (a and b).

For each moisture content, the dry density was calculated based on the weight soil in the container, and moisture content was measured using samples taken after compaction of each soil layer.

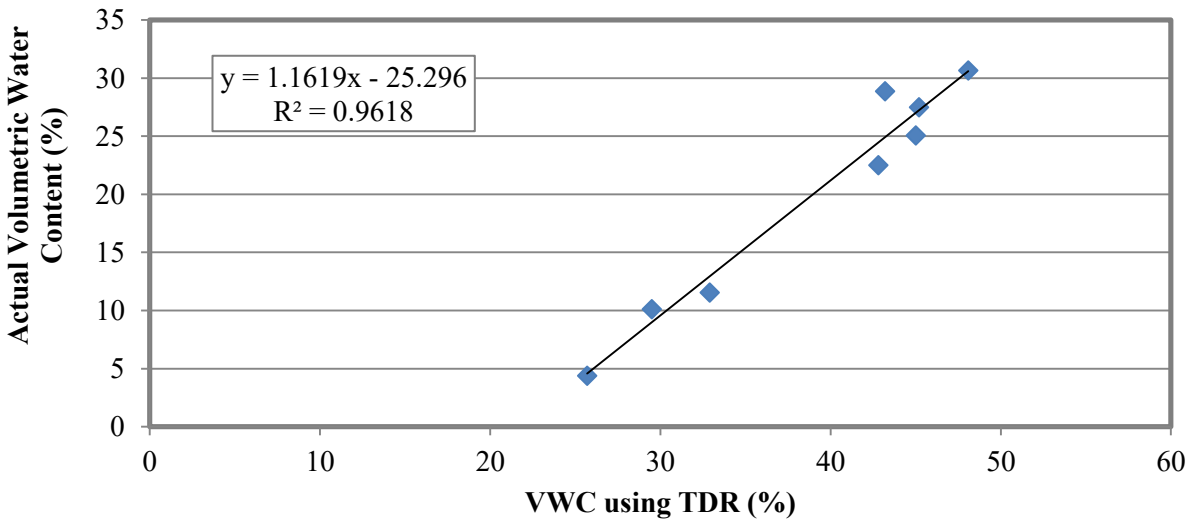

a. VWC versus the Gravimetric water content measured using subgrade samples

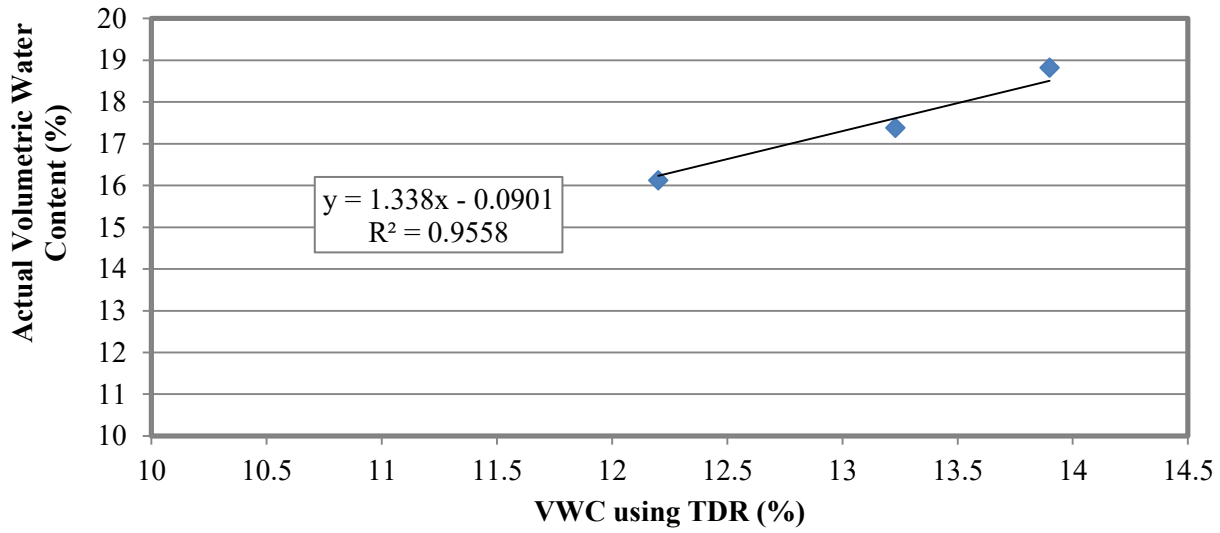

b. VWC versus the Gravimetric water content measured using GBC samples

Figure 9-5: VWC measured by TDR versus the Gravimetric water content

9.4. MOISTURE DATA COLLECTED AT IRRF

Using the calibration equation developed in previous sections, the data collected at site is translated into reliable meaningful format. It is important to consider that the TDRs are able to show the unfrozen volumetric water content (UVWC) since the frozen water is dielectric constant; and in the case of temperatures below zero having a proper condition for freezing, the TDRs show a drop in moisture content which actually reflects the unfrozen portion of water existing in the porous media (Campbell Scientific Canada, 2011). A sharp decline in UVWC is an indicator of frost occurrence, and small changes can be correlated to intake or discharge of water in the system.

Figure 9-7 and 9-8 demonstrate the temperature and moisture variation in the GBC layer during the monitoring period. During winter, a sharp drop in moisture content is observed, which is a sign of frost occurrence in this layer is. During winter, the moisture was frozen in the GBC layer. As soon as spring set in, the moisture started melting. The whole process of melting occurs in a short period of time. For instance, during the first spring, the moisture melted in this layer from 27 to 30 March 2013, (only three days). After a sharp increase of moisture in this layer during spring, there was a period in which the extra moisture accumulated in soil and required time to drain out of the system. It takes a couple of weeks until the extra water is discharged from the system even for the GBC layer, which is designed to discharge the water in a minimum time. For instance, the thaw weakening period, when the moisture is still accumulated in the GBC layer, took until the end of

June 2013. Which means that the extra water drained out of the system in almost three months. It is interesting that the moisture reached an equilibrium lower than its initial value in this layer.

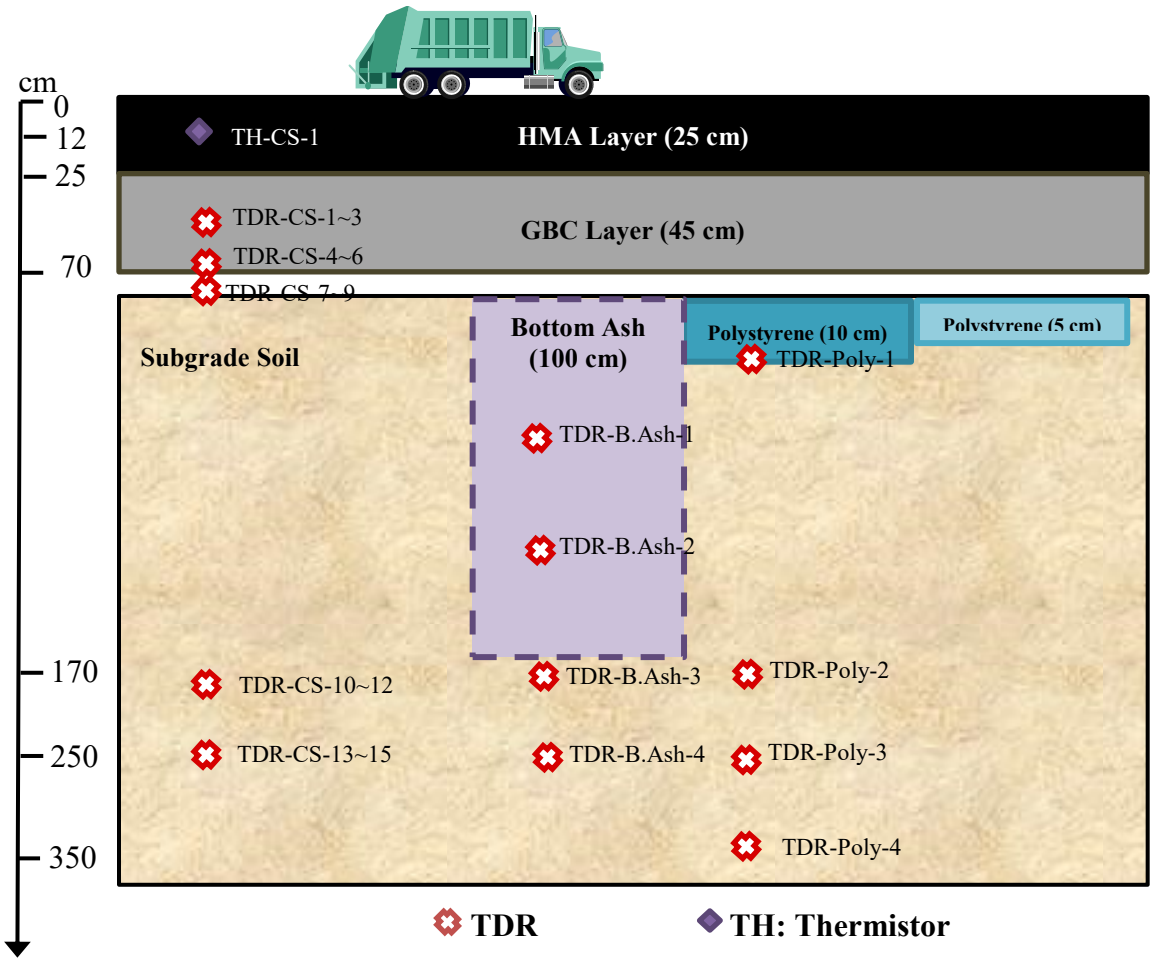

Figure 9-6 Cross sections and as-built depth of thermistors and moisture probes

The initial value of VWC in GBC of depth 0.4 m was about 17.9 percent while the equilibrium value of VWC is 15.0 percent. The trend of decline in moisture value at the equilibrium point continued in the next year. In summer 2014, the moisture level reached about 14 percent and this value continued to remain the same for the next years during summer. A decline in the pick VWC right after the thawing occurrence was also observed. While in the first spring, the maximum VWC observed was as high as 18.9 percent, the value decreased gradually over the years and reached 15.8 percent in spring time of 2016. During the laboratory compaction of the GBC layer, it was also observed that the optimum moisture content for compacting the GBC was in a way that could

be during the compaction process. The VWC of GBC at both depths (0.4 m and 0.55 m) followed the same trend.

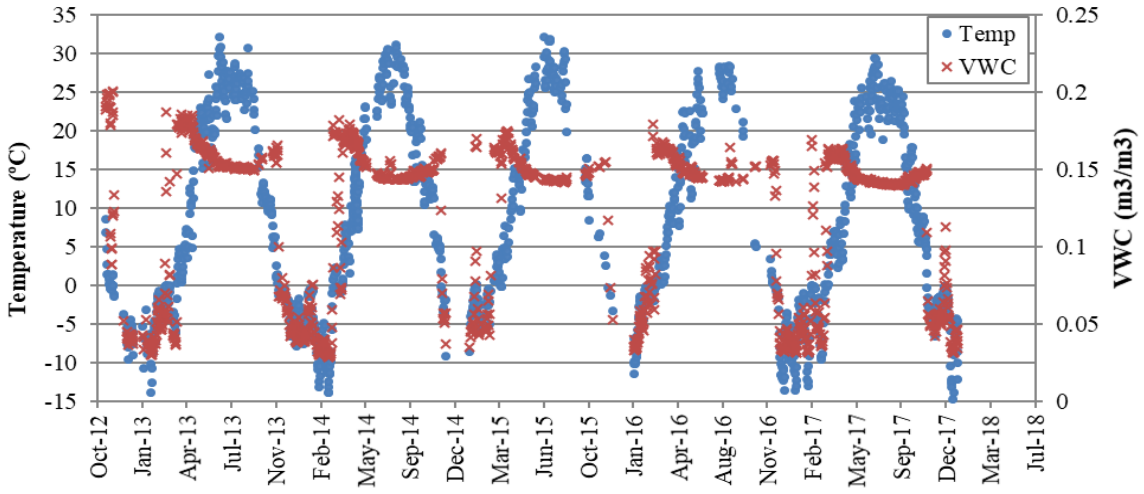

Figure 9-7: UVWC at depth 0.4 m below the surface in GBC of CS (TDR-CS-1)

Figure 9-9 to 9-11 depict the VWC in subgrade of CS. The moisture content at different depths of subgrade layers started at the optimum and like the GBC layer a sharp declined occurred after the winter set in. Similar to the GBC layer, a declining trend of moisture content was observed within years. The VWC started at a depth of 0.75 m below the surface changed from the value of 31.2 percent in the first fall and dropped to a value of 30.0 percent within four years of data monitoring. However, at depth 1.75 m below the surface, the patterns and values remained approximately similar during the monitoring period. At this depth, the equilibrium value of VWC in summer was as high as approximately 29.0 percent during the monitoring period.

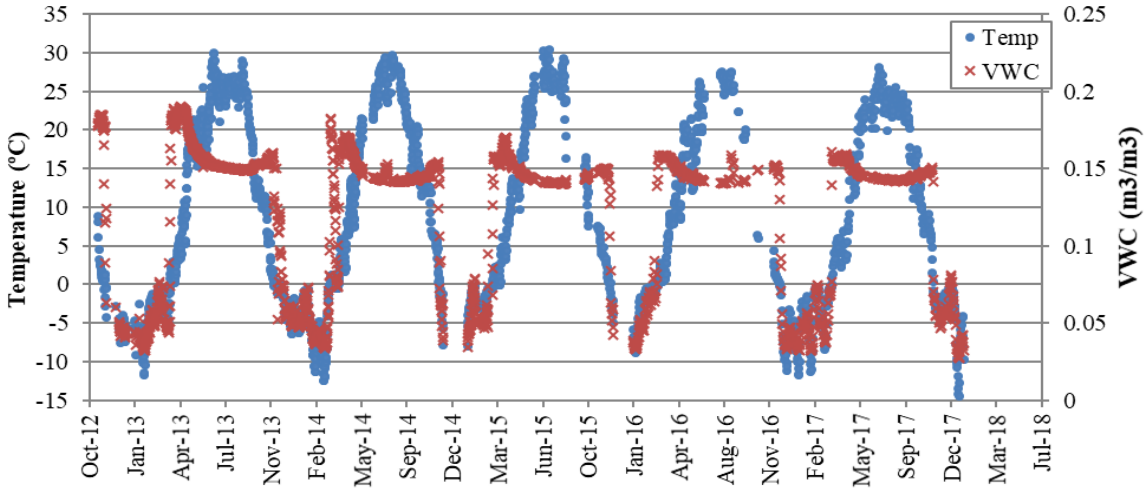

Figure 9-8: UVWC at depth 0.55 m below the surface in GBC of CS (TDR-CS-4)

The peak value of moisture accumulation in the subgrade layer in spring also changed over the years at both depths. Figure 9-11 shows that the freezing and thawing occurred with delay in deeper locations and the length of the winter is smaller. Table 9-2 presents the peak value observed in winter and summer and winter duration at depth of 0.7 and 1.7 m below the surface of CS along with air freezing index (FI) of each year. The prolonged winter in 2012-2013, which is clear from the highest amount of FI, led to the highest moisture accumulation at both depths and longer winter duration compared to any other year. The decreasing amount of moisture accumulation after the spring-thaw occurrence followed the same trend of FI deduction over the years. The only exception is the moisture accumulation at depth 0.7 m below the surface where the VWC is lower than the following years.

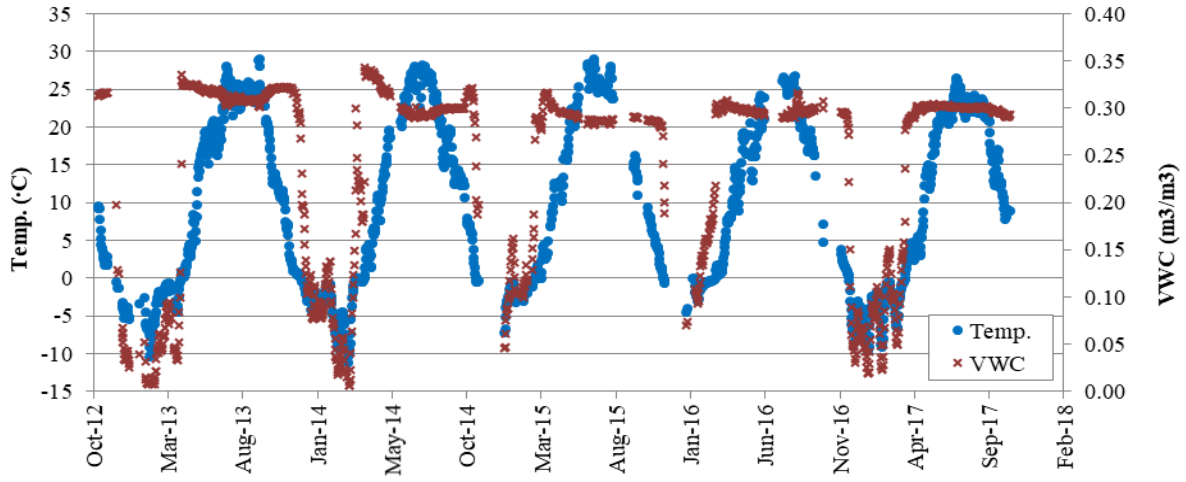

Figure 9-9: UVWC at depth 0.75 m below the surface in Subgrade of CS (TDR-CS-8)

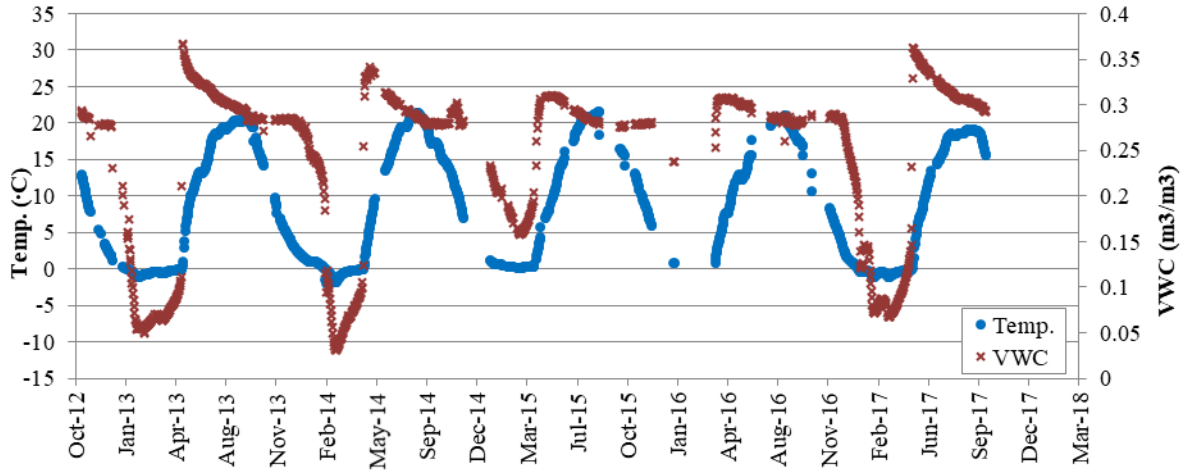

Figure 9-10: UVWC at depth 1.7 m below the surface in Subgrade of CS (TDR-CS-11)

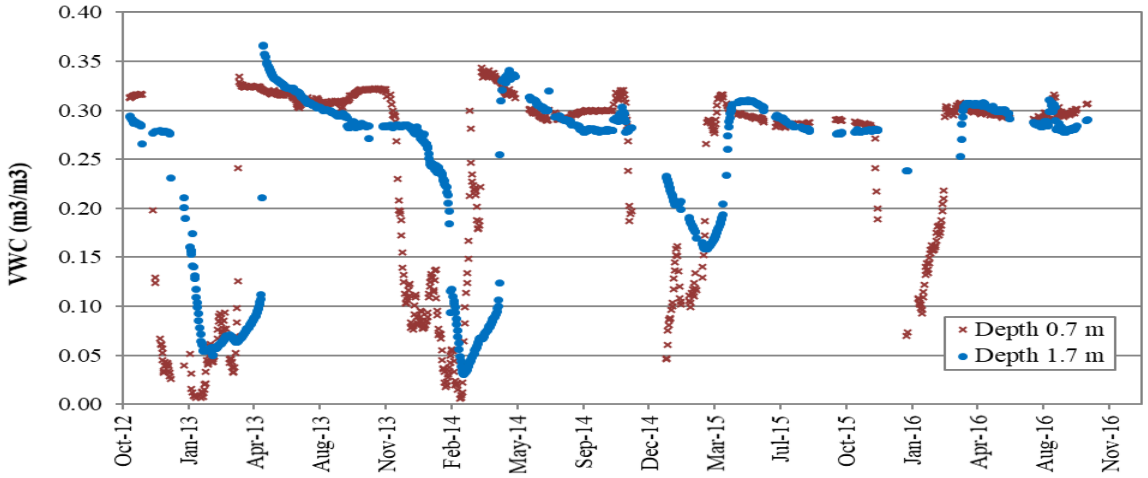

Figure 9-11: UVWC at different depth of Subgrade of CS

Table 9-2: Winter Length, VWC and Freezing Index of Each Year

Year	Winter Length		Pick VWC (m3/m3)		FI	TI
	Depth 0.7 m	Depth 1.7 m	Winter	Summer	(°C.days)	(°C.days)
2012-2013	130	112	0.32	0.366	1,308	368
2013-2014	127	76	0.34	0.334	1,141	352
2014-2015	125	62	0.31	0.31	865	567
2015-2016	103	52	0.30	0.30	600	306

Figure 9-12 and 9-13 show the UVWC at depth 1.75 m and 2.5 m below the surface in the subgrade layer of the B.Ash section. The temperature data shows that the temperature in the subgrade of this section never went below zero. However, there are moisture variations measured at depth 1.75 m below the surface (Figure 9-12), which cannot be interpreted by temperature changes. It seems the variation was a result of an inherent problem in the measurement system. At depth 2.5 m below the surface, as expected, no frost was observed and the moisture remained constant through the monitoring period.

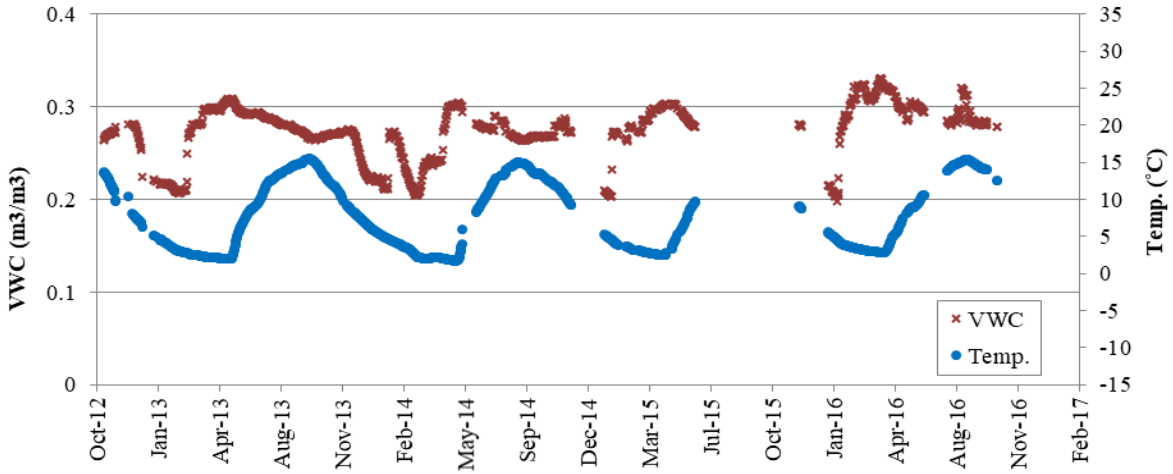

Figure 9-12: UVWC at depth 1.75 m below the surface in Subgrade of B.Ash (TDR-BA-3)

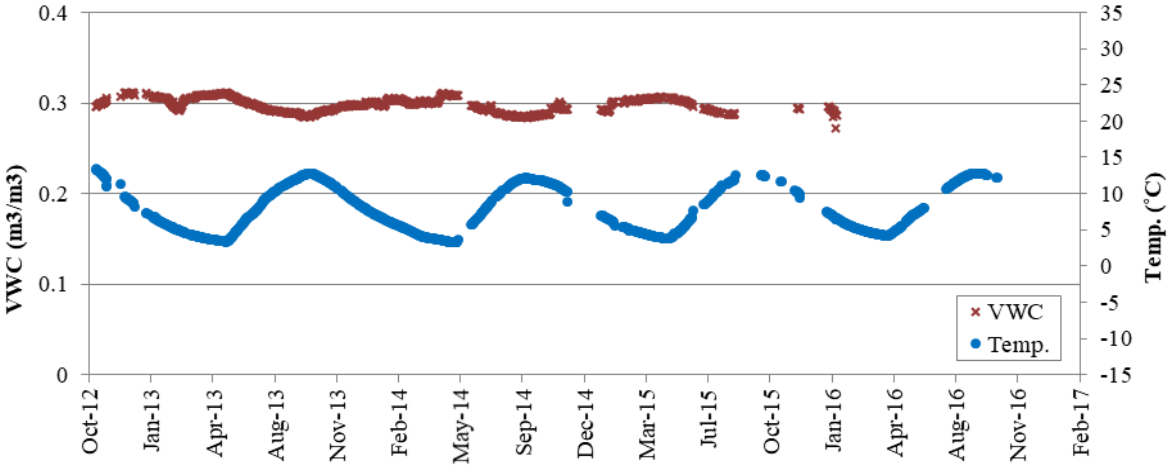

Figure 9-13: UVWC at depth 2.7 m below the surface in subgrade of B.Ash (TDR-BA-4)

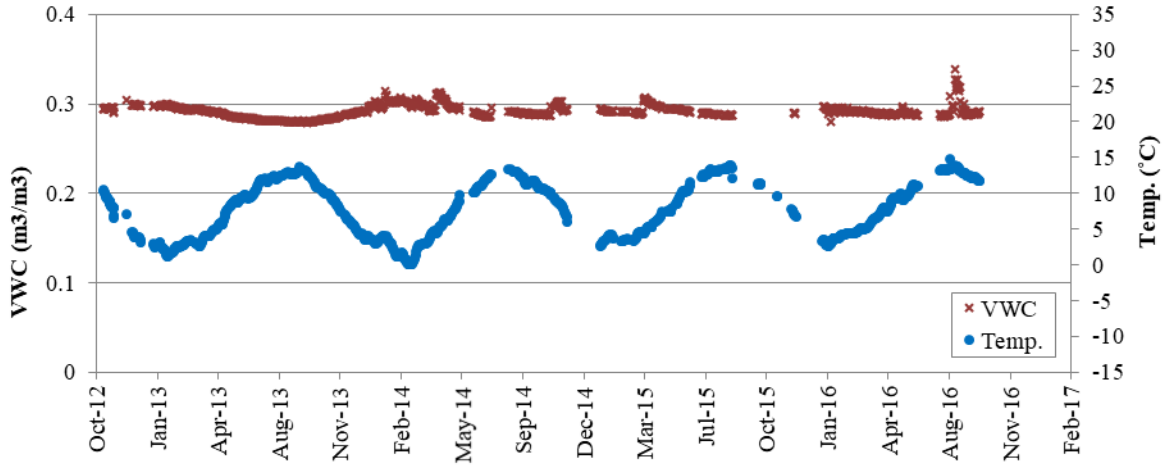

Figure 9-14: UVWC at depth 0.8 m below the surface in subgrade of Poly-10 (TDR-Poly-1)

Figures 9-14 and 9-15 plotted the moisture and temperature variation in subgrade layer of the Poly-10 section. Since the temperature always remained above zero during the monitoring period at both depth of this section, the variation in moisture content is minimum.

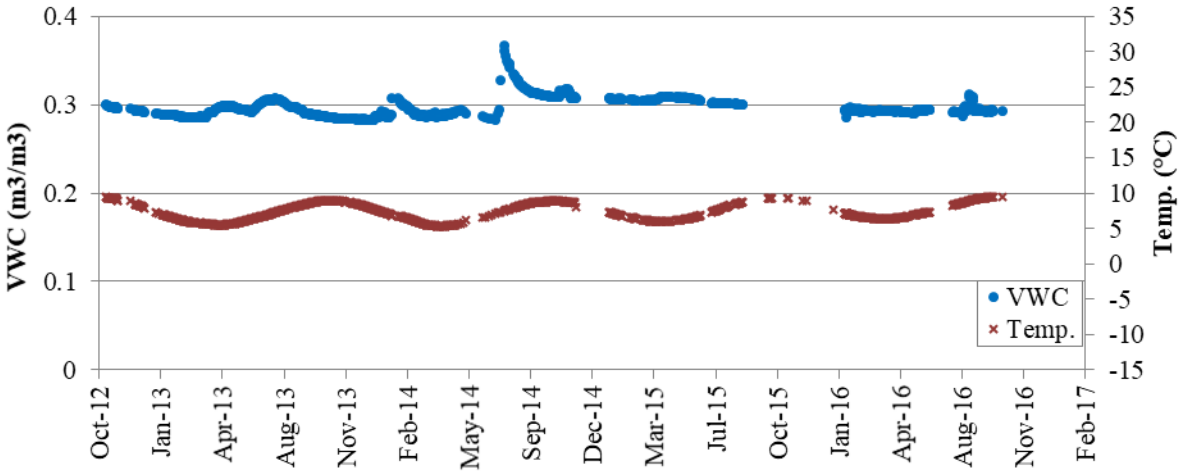

Figure 9-15: UVWC at depth 1.7 m below the surface in subgrade of Poly-10 (TDR-Poly-2)

9.5. SUMMARY AND CONCLUSION

This chapter summarized the procedure for calibrating the sensors used on an IRRF test road to collect the data related to moisture. The calibration procedure resulted in two different formula for translating the data collected at site to the real values of moisture in subgrade and GBC material. The value of VWC of subgrade and GBC material at different sections were also presented in this chapter.

9.6. REFERENCES

ASTM Designation: D6433-11 (2011). Standard Practice for Roads and Parking Lots Pavement Condition Index Surveys, ASTM International.

Campbell Scientific Canada (2011) "Instruction manual :CS650 and CS655 Water Content Reflectometers".

Cary Carlos E., and Claudia E. Zapata. (2011). "Resilient modulus for unsaturated unbound materials." *Road Materials and Pavement Design 12*, no. 3, 615-638.

Doré, G., and Zubeck, H. K. (2009). *Cold Regions Pavement Engineering*. 1st ed. New York: McGraw-Hill Professional.

Krahn, J., and D. G. Fredlund. (1972), "On Total, Matric and Osmotic Suction", *The Emergence of Unsaturated Soil Mechanics*, 35.

Models, Moisture-summary O F Predictive. (2000). "Guide for Mechanistic-Empirical Design Moisture-Summary of Predictive Models," no. June.

10. CONCLUSION AND RECOMMENDATIONS

This study has been developed to conduct state-of-the-art research on the effect of using waste/recycled materials such as bottom ash as insulation layers on IRRF test roads. These roads have three insulated sections that consist of bottom ash (100 cm) and two different thicknesses of polystyrene boards (5 cm and 10 cm), while the adjacent conventional section is considered the control section (CS). The following statements can be concluded from the study:

- Higher R-value of the Polystyrene boards outperformed the Bottom Ash layer as insulation by decreasing the frost depth by at least 40 percent in comparison to the Control Section. The Bottom Ash displayed a 28-percent reduction in frost depth. The subgrade temperature in the Bottom Ash and Polystyrene sections never dropped below zero; however, frost penetrated 1.4 m in the subgrade of the Control Section, which remained frozen for four months. Based on the conducted observational study in chapter 3, one can conclude that Bottom Ash as a recycled material can effectively reduce frost penetration into the subgrade.
- Based on the result of the FWD test, it can be concluded that although the polystyrene layers effectively reduced frost depth and protected the subgrade soil, they also lowered structural capacity during the non-freeze-thaw season, which is almost one third of the year. The section containing the bottom ash layer performed almost the same as the conventional section.
- The study presented in chapter 5 showed that, polystyrene sections outperformed the B.Ash section by exhibiting the lowest variation in resilient modulus. However, the polystyrene layers may decrease the load bearing capacity of the section by half that of the CS. Increasing the thickness of the polystyrene layer from 5 to 10 cm almost doubled the structural capacity lost, which should be considered when optimizing insulation layer thickness in design procedures. Although the B.Ash section undergoes freeze-thaw effects, the ratio of resilient modulus of this section never dropped below 0.94 during the recovering period, while this ratio in the CS dropped to 0.86. Overall, the bottom ash layer did not notably change the load bearing capacity of the section.
- The long-term performance evaluation of the pavement sections in chapter 6 indicated that, the B.Ash section performed similarly to the CS in terms of viscoelastic behavior, and performed considerably better than the CS in terms of fatigue cracking risk. However, the polystyrene

sections were more prone to damage, especially during the summer when the HMA temperature was more than 25°C.

- The capital cost comparison of the pavements comprised of insulation layers in chapter 7 illustrated that, the Bottom ash is a reliable cost effective solution for damage mitigation in construction of pavement in cold regions if the source of material is available. However, when the frost penetration exceed 3.7 m, the capital cost of construction of roads using polystyrene is less than of that of Bottom ash material
- Geo-studio is a powerful finite element software for modeling the temperature and moisture regime in the pavement especially in warm seasons, if the material property of different pavement layers are defined properly. However, the finite element modeling presented in chapter 8 did not result in a good agreement with field observation of the HMA temperature. Based on what is presented in chapter 3, the insulation layers cause trapping the heat on the upper portion of the pavement and lead to higher temperature fluctuation in the HMA layer. However, the predicted temperature of the insulated sections experienced lower fluctuation compared to CS, which results in a noticeable HMA dynamic modulus difference compared to what was expected from site investigation.
- The overall increased demand to more sustainable roads leads to use waste/recycle material in pavement construction. The need has to be investigated by engineers who require experimental studies comprised of long-term pavement performance monitoring, especially in regions with severe weather conditions. Therefore, in the interest of future research, the following recommendations are proposed:
- Examine a wider range of insulation material under different thicknesses of HMA and GBC. This evaluation is essential especially for thin HMA pavements.
- Evaluate the pavement performance under heavier axle loads, also perform stress and strain measurements at various depths of insulated pavement to measure actual response and incorporate the results in design methods. Application of HWD (High Weight Defelectometer) can be an essential part of future work.
- Improve the modeling approaches to enhance the prediction for temperature on top of the pavement layer and gain a better understanding of the effect of using insulation material on HMA modulus change especially during critical spring-thaw period.

- Investigate icing formation on the pavement, especially in the case of using insulation material with high R-Value near the surface of the pavement.
- Verify the predicted long-term performance, which are currently presented based on the short-term responses evaluation by conducting long term scheduled surface distress survey.
- Develop numerical models to incorporate the predicated temperature and moisture variations in design of insulated pavements.
- Conduct a long term monitoring to quantify the cost of pavement maintenance and rehabilitation and combine the cost with the capital cost of the project to evaluate the total cost effectiveness of using insulation material.

BIBLIOGRAPHY

AASHTO TP79-09 (2009). Determining the Dynamic Modulus and Flow Number for Hot Mix Asphalt (HMA) Using the Asphalt Mixture Performance Tester (AMPT). American Association of State Highway and Transportation Official.

Ahmed, Z., Marukic, I., Zaghloul, S., & Vitillo, N. (2005). Validation of enhanced integrated climatic model predictions with New Jersey seasonal monitoring data. *Transportation Research Record: Journal of the Transportation Research Board*, (1913), 148-161.

"Alberta Recycling." http://www.albertarecycling.ca/RecyclingMain.aspx?id=84 Accessed Jan. 1, 2013.

Alberta Transportation and Utilities. (1997). *Pavement Design Manual*.

Alberta Utilities Commission. http://www.auc.ab.ca/applications/decisions/Decisions/2012/2012-027.pdf, Accessed Jul. 1, 2014.

Asphalt Institute. (1982) Research and Development of the Asphalt Institute's Thickness Design Manual (MS-1), 9th edition. Research Report 82–2.

ASTM Designation: D6433-11 (2011). Standard Practice for Roads and Parking Lots Pavement Condition Index Surveys, ASTM International.

ASTM Standard C136-06 (2006). Standard Test Method for Sieve Analysis of Fine and Coarse Aggregates. ASTM International, West Conshohocken, PA.

ASTM Standard D698. (2012) *Standard Test Methods for Laboratory Compaction Characteristics of Soil Using Standard Effort*. ASTM International, West Conshohocken, PA.

ARA, Inc., (2004). ERES Consultant Division. "*Guide for Mechanistic–Empirical Design of New and Rehabilitated Pavement Structures*". Final report, NCHRP Project 1-37A. Transportation Research Board of the National Academies, Washington, D.C. http://www.trb.org/mepdg/guide.htm.

Batenipour, H. (2012). *Understanding the performance of highway embankments on degraded permafrost*. University of Manitoba (Canada

Braley, W. A., & Zarling, J. P. (1991). MUT1D: user-friendly one-dimensional thermal model. In *Cold Regions Engineering* (pp. 1-10). ASCE.

Birgisson, B., Ovik, J., & Newcomb, D. (2000). Analytical predictions of seasonal variations in flexible pavements: Minnesota Road Research Project site. *Transportation Research Record: Journal of the Transportation Research Board*, (1730), 81-90.

Campbell Scientific Canada (2011) "Instruction manual: CS650 and CS655 Water Content Reflectometers".

Cary, C.and Zapata C.E.. (2011), "*Resilient Modulus for Unsaturated Unbound Materials*", Road Materials and Pavement Design, (12.3), 615-638.

Chomton G.and Valayer P.J. (1972) Applied Rheology of Asphalt Mixes Practical Application. In Proceedings of Third International Conference on the Structural Design of Asphalt Pavements, London.

Côté, J., and Konrad, J. M. (2005). Thermal conductivity of base-course materials. *Canadian Geotechnical Journal*, (42-1), 61–78.

Darrow, M. M. (2010) Measurement of temperature and soil properties for finite element model verification. *Institute of Northern Engineering, Fairbanks, AK*.

Division.Xu, B., R. Ranjithan, S., & R.Kim, Y. (2002) New Condition Assessment Procedure for Asphalt Pavement Layers, Using Falling Weight Deflectometer Deflections. In *Transportation Research Record: Journal of the Transportation Research Board, No. 1806*, Transportation Research Board of the National Academies, Washington, DC, pp. 57–69.

Deblois, K., Bilodeau J., and Dore G. (2010) Use of Falling Weight Deflectometer Time History Data for the Analysis of Seasonal Variation in Pavement Response. *Canadian Journal of Civil Engineering* 37.9, pp 1224-1231.DOI:10.1139/L10-069.

Dore, G., Konrad J.M., Roy M., and Rioux N. (1995) Use of Alternative Materials in Pavement Frost Protection: Material Characteristics and Performance Modeling. In *Transportation Research Record: Journal of the Transportation Research Board, No. 1481*, Transportation Research Board of the National Academies, Washington, D.C., pp. 63–74.

Doré, G., and Zubeck, H. K. (2009). "*Cold Regions Pavement Engineering"*. 1st ed. New

York: McGraw-Hill Professional.

Dow Building Solutions. (2016). <http://dow-styrofoam.custhelp.com/app/answers/detail /a_id/11273/kw/styrofoam%20r-value> (Mar. 1, 2016)

Dysli, M., Lunardini, V., & Stenberg, L. (1997). Related effects on frost action: Freezing and solar radiation indices. *Ground freezing*, *97*, 3-23.

Eaton, R. A., Roberts, R. J., & Humphrey, D. N. (1994). Gravel Road Test Sections Insulated with Scrap Tire Chips: Construction and the First Year's Results (No. CRREL-SR-94-21). *Cold Regions Research and Engineering Lab Hanover NH*. Environment Canada. http://weather.gc.ca/canada_e.html, Accessed Jan. 1, 2013.

Edgar, T., R. Mathis, and Potter, C. (2015). Injection of Structural Polymer Foam to Control Highway Frost Heave. Airfield and Highway Pavements. 873–884.

Environment Canada. *Canadian Weather*. http://weather.gc.ca/canada_e.html Accessed Jan. 1, 2014.

Esch, D.C. (1972). Control of Permafrost Degradation Beneath a Roadway by Subgrade Insulation *, Alaska Department of Transportation and Public Facilities*, Juneau, Alaska.

Flynn, D. (2015). Field and numerical studies of an instrumented highway embankment in degrading permafrost.

GeoStudio (2012), GeoSlope International, Calgary, Alberta.

Gandahl, R. (1982). The Use of Plastic Foam Insulation in Roads. In *4th Canadian Permafrost Conference, Calgary, Alberta , March 2*, 570–76. Calgary, Alberta, march 1981.

Gilpin, R. R. (1980). A Model for the Prediction of Ice Lensing and Frost Heave in Soils. *Water Resources Research*, (16)5, 918–930.

Ghuzlan, K.A. and Carpenter S.H. (2006) Fatigue Damage Analysis in Asphalt Concrete Mixtures Using the Dissipated Energy Approach. *Canadian Journal of Civil Engineering*, Vol. 33, No. 7, pp. 890–901.

Havukanen, J. (1983). "The utilization of compacted coal ash in earth works." In *Proceedings of the eighth European conference on soil mechanics and foundation engineering*, vol. 2, 773-776.

Havukainen, J. (1987). The Utilization of Coal ash in Earth Works. In *Advances in Mining Science and Technology, Vol. 2: Reclamation, Treatment and Utilization of Coal Mining Wastes*, Amsterdam: Elsevier, 245-252.

Hendrickson, C., and Au, T. (1989). *Project Management for Construction: Fundamental Concepts for Owners, Engineers, Architects and Builders.* Prentice Hall.

Hein, D. K., and F. W. Jung. (1994). "Seasonal variations in pavement strength." In *fourth International Conference, Bearing Capacity of Roads and Airfields*, vol. 1.

Holt, A., Sullivan, S., and Hein, D. K. (2011). Life Cycle Cost Analysis of Municipal Pavements in Southern and Eastern Ontario. *Presented at the 2011 Annual Conference and Exhibition of the Transportation Association of Canada*, Edmonton, AB.

http://www.climate.weatheroffice.ec.gc.ca , Accessed Jul. 1, 2016

Huang, Y. H. (2004). Pavement analysis and design. Englewood Cliffs, N.J., Prentice-Hall, ©1993

Huang, W. (1990) The Use of bottom ash in Highway Embankment and Pavement Construction, PhD, Purdue University.

Huang, Y., Bird, R. N., and Heidrich, O. (2015). A review of the use of recycled solid waste materials in asphalt pavements. *Resources, Conservation and Recycling*, (52)1), 58–73.

Kim, Y. R., B. Xu, and Kim Y. (2000) A New Backcalculation Procedure Based on Dispersion Analysis of FWD Time-History Deflections and Surface Wave Measurements Using Artificial Neural Networks. In *Nondestructive Testing of Pavements and Backcalculation of Moduli*: *Third Volume*. ASTM International.

Klein, R., N. Nestle, R. Niessner, and T. Baumann. (2003) Numerical Modeling of the Generation and Transport of Heat in a Bottom Ash Monofill. Journal of Hazardous Materials, Vol. 100, No. 1–3, 147–162.

Krahn, J., and Fredlund D. G. (1972), On Total, Matric and Osmotic Suction, *The Emergence of Unsaturated Soil Mechanics*, 35.

Krahn, J. (2004). *Thermal modeling with TEMP/W: an engineering methodology*.

Liang, R., Al-Akhras K., and Rabab'ah S. (2006). Field Monitoring of Moisture Variations Under Flexible Pavement. *Transportation Research Record* 1967 (1): 160–72. doi:10.3141/1967-16.

Myhre, O. (1994). Bearing Capacity and Performance of Pavement Structures Insulated with Polystyrene Boards. *In 4th International Conference, Bearing Capacity of Roads and AirfieldsFHWA, U of Minnesota*, Army Corps of Engineers, NRC Canada, FAA (Vol. 2).

Nixon, D., Eng, P., & Lewycky, E. D. (2011). Edmonton Experience with Bottom ash and Other Insulating Materials for Mitigation of Frost Heave Induced Damage. In *Annual Conference of the Transportation Association of Canada , Edmonton, Alberta, September 11-14*. Edmonton, Alberta.

Oosterbaan, M. D., and Leonards G. A. (1965). Use of Insulating Layer to Attenuate Frost Action in Highway Pavements. Highway Research Record (101).

Penner, Edward. (1967). Experimental pavement structures insulated with a polyurethane and extruded polystyrene foam. *Physics of Snow and Ice: proceedings*. 1311-1322.

Popik M.and Tighe . (2005). The Effect of Seasonal Variations on the Resilient Modulus of Unbound Materials. In *Proceedings of Annual Conference of Transportation Association of Canada*, Calgary, Alberta, 3-5.

Qi, J., Ma, W., & Song, C. (2008), Influence of Freeze–Thaw on Engineering Properties of a Silty Soil, *Cold Regions Science and Technology*, 53(3), 397-404.Quintero, N. (2007). "Validation of the Enhanced Integrated Climatic Model (EICM) for the Ohio SHRP Test Road at U.S. 23." *M.S. Thesis Submitted to the Russ College of Engineering and Technology of Ohio University*,November.

Rajaei, P., and Baladi, G. (2015).Frost Heave: A Semi-Empirical Model Based on Field Data. *16th International Conference on Cold Regions Engineering*, 382–393.

Redles, T. A., Ali, A. W., Mehta, Y. A., & Cleary, D. (2018) Estimating Fatigue Endurance Limits of Flexible Airfield Pavements. International Journal of Pavement Engineering. 19(6). pp. 534-542.

Riche, F., & Schneebeli, M. (2013). Thermal conductivity of snow measured by three independent methods and anisotropy considerations. *The Cryosphere*, *7*(1), 217-227.

Rieger, S. (1983). *The Genesis and Classification of Cold Soils.* Academic Press, New York.

Rieke, R.D., Vinson T.S. and Mageau D.W. (1983). The Role of Specific Surface Area and Related Index Properties in the Frost Heave Susceptibility of Soils. *Proceedings of the Fourth International Conference on Permafrost*, National Academies Press, Washington, D.C., 1066–1071.

RS Means. (2017). <https://www.rsmeans.com/products/online.aspx> (Mar. 1, 2015)

Saarelainen, S. (1996). Pavement Design Applying Allowable Frost Heave. *Proceedings of the Eighth International Conference on Cold Regions Engineering*, ASCE Press, Reston, VA.

Sakulich A. R., (2011) Reinforced geopolymer composites for enhanced material greenness and durability. *Sustainable Cities and Society*, (1)4, 195–210.

Salour, F., & Erlingsson, S. (2013). Investigation of a pavement structural behaviour during spring thaw using falling weight deflectometer. *Road Materials and Pavement Design 14*, no. 1, 141-158.

Sarkar, R., and Dawson, A. R. (2015). Economic assessment of use of pond ash in pavements. *International Journal of Pavement Engineering*, 1–17.

Schmalzer, P.N. (2006). *Long-Term Pavement Performance Program Manual for Falling Weight Deflectometer Measurements*. Federal Highway Administration, Office of Research, Development and Technology, Turner-Fairbank Highway Research Center.

Schmalzer, Peter N. (2006). *Long-Term Pavement Performance Program Manual for Falling Weight Deflectometer Measurements*. Federal Highway Administration, Office of Research, Development and Technology, Turner-Fairbank Highway Research Center.

Shafiee, M.H., Hashemian L., and Bayat A. (2015) Seasonal Analysis of Flexible Pavement Response to Falling Weight Deflectometer." *International Journal of Pavement Research and Technology* 8, no. 5: 346-352.

Shen, S., & Carpenter, S. H. (2007) Dissipated Energy Concepts for HMA Performance: Fatigue and Healing. Technical Report of Research Supported by the Cooperative Agreement DOT 05-C-AT-UIUC-COE.St-Laurent, D. (1995) *Évaluation Structurale de Chaussées Souples dans un Contexte Climatique Nordique*. Universite Laval.

St-Laurent, D., and Roy, M. (1995). Évaluation structurale des chausses souples dansun contexte climatique nordique : une étude avec le FWD [Structural evaluation of flexible pavements in a northern context: A study using the FWD]. *Proceedings of the 30th Annual Conference of AQTR, Association Québécoise du Transport et des Routes*. Quebec, Canada.

Steurer, P. M. (1989) Methods used to create an estimate of the 100-year return period of the air-freezing index. Frost-protected shallow foundation development program—Phase II final report: Appendix A. Rep. Prepared for the Society of the Plastics Industry, NAHB Research Center, Upper Marlboro, MD, 7 pp.

Stubstad, R.N. (2002) LTPP Data Analysis: Feasibility of Using FWD Deflection Data to Characterize Pavement Construction Quality. *National Cooperative Highway Research Program Web Document 52. National Cooperative Highway Research Program*, Washington, DC.

Tatarniuk, C., Lewycky, D. (2011). A Case Study on the Performance of High Load Polystyrene as Roadway Insulation in Edmonton , Alberta , Canada. In *2011 Conference and Exhibition of the Transportation Association of Canada, September 11, Edmonton, Alberta*. Edmonton, Alberta.

Tavafzadeh, N., Nassiri S., Shafiee M.H., and Bayat A. (2014) Using Field Data to Evaluate Bottom Ash as Pavement Insulation Layer. In *Transportation Research Record: Journal of the Transportation Research Board, No. 2433*, Transportation Research Board of the National Academies, Washington, D.C., pp. 39–47.

Tavafzadeh, N., Hashemian L, and Bayat A. (2016) The Effect of Insulation Layers on Pavement Strength During Non-Freeze-Thaw Season. *International Journal of Pavement Engineering*, in press.

Tavafzadeh, N., Hashemian L, and Bayat A. (2016) The Effect of Seasonal Variation on Load Bearing Capacity of Pavements Comprised of Insulation Layers. In *Transportation Research Record: Journal of the Transportation Research Board of the National Academies*, Washington, D.C., DOI: 10.3141/2579-10.

The City of Edmonton Transportation. Roadway — Design Standard — Construction Specifications, 2012 Edition, http://www.edmonton.ca/city_government/documents/RoadsTraffic/Volume_2_-_Roadways_May_2012.pdf, Accessed March 1, 2015.

Tompson, M.R., Dempsey, B.J., Hill, H., and Vogel, J. (1988) Characterizing Temperature Effects for Pavement Analysis and Design. Transportation Research Record, No. 1121, Journal of the Transportation Board of the National Academy, Washington, D.C., 14–22.

Toogood, J. A. (1976). Deep soil temperatures at Edmonton. *Canadian Journal of Soil Science*, *56*(4), 505-506.

Transportation Officials. (1993). *AASHTO Guide for Design of Pavement Structures*. Vol. 1. AASHTO.

Uzarowski, L., Rizvi, R., Krzewinski, T. G., Ulring, J. D., and Maher, M. L.J. (2013). Runway Pavement Rehabilitation Design and Construction in Remote Areas in the North-Case Study.*ISCORD 2013: Planning for Sustainable Cold Regions*, 585–596.

Van Dijk W/, (1975) Practical Fatigue Characterization of Bituminous Mixes. *Proceedings of the Association of Asphalt Paving Technologists (AAPT)*, vol. 44, p. 388.

Van Dijk W. and Visser W. (1977) The Energy Approach to Fatigue for Pavement Design. *Proceedings of the Association of Asphalt Paving Technologists (AAPT)*. vol. 46, pp. 1-40.

Von Quintus, H., and Killingsworth B. (1998) *Analyses Relating to Pavement Material Characterizations and Their Effects on Pavement Performance*. No. FHWA-RD-97-085.

Widyatmoko, I., C. Ellis, and J.M. Read. (1999) The Application of the Dissipated Energy Method for Assessing the Performance of Polymer-Modified Bituminous Mixtures. *Materials and Structures*, Vol. 32, No. 4, pp. 304–310.

Wyman, J. H., Braley, G. A., & Stevens, R. I. (1985) *Field Evaluation of FHWA Vehicle Classification Categories*. *Executive Summary (No. 8405) Maine Department of Transportation, Bureau of Highways, Materials and Research*

Xu, B., Ranjithan, R.S., Kim, R. Y. (2002). New Condition Assessment Procedure for Asphalt Pavement Layers, Using Falling Weight Deflectometer Deflections. *Transportation Research Record 1806*, Transportation Research Board, Washington, DC, 57-69.

Young, F. D. (1965). Experimental foamed plastic base course. *Highway Research Record*, (101).

Yang, Shu-Rong, Wei-Hsing Huang, and Yu-Tsung Tai. (2005), Variation of Resilient Modulus with Soil Suction for Compacted Subgrade Soils. *Transportation Research Record: Journal of the Transportation Research Board,* (1913), 99-106.

Zapata, C. E., Andrei, D., Witczak, M. W., & Houston, W. N. (2007). Incorporation of Environmental Effects in Pavement Design. *Road Materials and Pavement Design* 8 (4): 667–93. doi:10.1080/14680629.2007.9690094.Zapata, Ce, and Houston W.. (2008). Calibration and Validation of the Enhanced Integrated Climatic Model for Pavement Design. (Vol. 602) *Transportation Research Record*

Zhi, W., S. Yu, M. Wei, and Jilin Q. (2005) Evaluation of EPS Application to Embankment of Qinghai–Tibetan Railway. *Cold Regions Science and Technology*, Vol. 41, No. 3, pp. 235–247.

APPENDIX 1. PAVEMENT VISUAL INSPECTION

Pavement visual inspection was run in years 2015-2016 and 2018 based on ASTM Designation: D6433-11 (2011). The quantity of each type of distress is recorded and summarized in Table A1. There were mainly two kinds of road distress found during the pavement survey, raveling and longitudinal cracking. The distresses were interpreted and assigned as either medium (M) or high (H) depending on their severity.

Table A1: Summary of Visual inspection

Year	2015		2016		2018	
Station	Cracking (m)	Raveling (m^2)	Cracking (m)	Raveling (m^2)	Cracking (m)	Raveling (m^2)
CS	-	4 (M)	-	4 (M)	-	4 (M)
B.ASh	0.056 (M)	0.159 (H)	0.056 (M)	0.159 (M)	0.056 (M)	0.159 (M)
Poly-10	-	-	-	-	-	-
Poly-5	-	-	-	-	-	-

As indicated in Table A1, the severity of the distress and the length of the longitudinal cracking observed in the B.Ash section did not change within the three years of monitoring. Figure A1 shows the severity of raveling and transverse cracking. Based on the observation and required calculations, the PCI of all sections are higher than 75, which categorized them as satisfactory to good condition.

2015 2016 2018

a) Raveling

2016 2018

b) Longitudinal Cracking

Figure A1: Raveling and Longitudinal Cracking for three years of monitoring

References:

ASTM Designation: D6433-11 (2011). Standard Practice for Roads and Parking Lots Pavement Condition Index Surveys, ASTM International.